2009

Therapeutic Strategies Aimed to Facilitate Axonal Regeneration and Functional Recovery Following Traumatic Spinal Cord Injury

Woon Chow
Virginia Commonwealth University

School of Medicine
Virginia Commonwealth University

This is to certify that the dissertation prepared by Woon Nam Chow entitled THERAPEUTIC STRATEGIES AIMED TO FACILITATE AXONAL REGENERATION AND FUNCTIONAL RECOVERY FOLLOWING TRAUMATIC SPINAL CORD INJURY has been approved by his or her committee as satisfactory completion of the dissertation requirement for the degree of Doctorate of Philosophy

Raymond J. Colello, D.Phil., Department of Anatomy and Neurobiology, School of Medicine

John W. Bigbee, Ph.D., Department of Anatomy and Neurobiology, School of Medicine

John A. DeSimone, Ph.D., Department of Physiology and Biophysics, School of Medicine

David G. Simpson, Ph.D., Department of Anatomy and Neurobiology, School of Medicine

Dong Sun, M.D., Ph.D., Department of Neurosurgery, School of Medicine

Jerome F. Strauss III, M.D., Ph.D., Dean, School of Medicine

F. Douglas Boudinot, Ph.D., Dean, Graduate School

September 15, 2009

THERAPEUTIC STRATEGIES AIMED

TO FACILITATE AXONAL REGENERATION AND FUNCTIONAL RECOVERY

FOLLOWING TRAUMATIC SPINAL CORD INJURY

A dissertation submitted in partial fulfillment of the requirements for the degree of Doctorate of Philosophy at Virginia Commonwealth University.

by

WOON NAM CHOW
B.S., Biomedical Engineering, Virginia Commonwealth University, 2003
B.S., Physics, Virginia Commonwealth University, 2003

Director: RAYMOND J. COLELLO, D.PHIL.
ASSOCIATE PROFESSOR, ANATOMY AND NEUROBIOLOGY

Virginia Commonwealth University

Richmond, Virginia
May 2011

Table of Contents

Page

List of Tables.....v

List of Figures.....vii

List of Abbreviations.....viii

Chapter

1 Traumatic Spinal Cord Injury: the Epidemiological, Anatomical, and Pathological

Dissertation Synopsis.....1

Introduction.....2

Epidemiological Statistics.....3

Spinal Cord Anatomy.....4

Spinal Cord Injury Pathological and Clinical Classification.....5

The Obstacles to Successfully Treating Spinal Cord Injury.....9

Cyst Formation.....10

Chondroitin Sulfate Proteoglycans.....12

Neurotrophins.....14

Reactive Astrogliosis and Gliotic Scar Formation.....17

Edema and Inflammation.....19

Summary.....23

Page

2 Evaluating Neuronal and Glial Growth on Electrospun Polarized Matrices

Introduction.....30

Materials and Methods.....33

Results.....38

Discussion.....42

3 Evaluating the Incorporation of Nerve Growth Factor and Chondroitinase ABC into an Electrospun Scaffold by Utilizing an Alginate Delivery System

Introduction.....56

Materials and Methods.....58

Results.....64

Discussion.....66

4 Preliminary Tests of Implanting Electrospun Matrices in a Rat Spinal Cord Transection Model

Introduction.....82

Materials and Methods.....83

Preliminary Results.....85

Page

5 Chronicling the Injury-Induced Proliferative Response at the Spinal Cord Injury Lesion Site and Attenuating the Response with X-Irradiation

Introduction....91

Materials and Methods....93

Results....97

Discussion....99

6 Concluding Statement....101

Appendix

FTY720 Reduces Inflammation and Promotes Functional Recovery after Spinal Cord Injury

Introduction....116

Materials and Methods....118

Results....123

Discussion....128

References....150

List of Figures

Page

Figure 1.1.....24

Figure 1.2.....26

Figure 1.3.....28

Figure 2.1.....44

Figure 2.2.....46

Figure 2.3.....48

Figure 2.4.....50

Figure 2.5.....52

Figure 2.6.....54

Figure 3.1.....72

Figure 3.2.....74

Figure 3.3.....76

Figure 3.4.....78

Figure 3.5.....80

Figure 4.1.....87

Figure 4.2.....89

Page

Figure 5.1.....101

Figure 5.2.....103

Figure 5.3.....105

Figure 5.4.....107

Figure A.1.....134

Figure A.2.....136

Figure A.3.....138

Figure A.4.....140

Figure A.5.....142

Figure A.6.....144

List of Tables

Page

Table 6.1.....114

Table A.1.....146

Table A.2.....148

List of Abbreviations

2D FFT	2-dimensional fast fourier transform
7-AAD	7-aminoactinomycin D
ANOVA	analysis of variance
BBB	Basso-Beattie-Bresnahan
BDNF	brain-derived neurotrophic factor
BrdU	bromodeoxyuridine
BSA	bovine serum albumin
cAMP	cyclic adenosine monophosphate
ChABC	chondroitinase ABC
CNS	central nervous system
CSPG	chondroitin sulfate proteoglycans
DAPI	4',6-diamidino-2-phenylindole
DC	direct current
DMSO	dimethyl sulfoxide
DRG	dorsal root ganglion
E16	embryonic day 16
EAE	experimental autoimmune encephalomyelitis
EC	eriochrome cyanine

ECM	extracellular matrix
FBS	fetal bovine serum
GAG	glycosaminoglycan
GFAP	glial fibrillary acidic protein
HFIP	1,1,1,3,3,3-hexafluoro-2-propanol
IGF-1	insulin-like growth factor 1
IL	interleukin
OPC	oligodendrocyte progenitor cells
P3	postnatal day 3
PBS	phosphate buffered saline
PDS	polydioxanone
MASCIS	multicenter animal spinal cord injury study
MS	multiple sclerosis
NGF	nerve growth factor
NT-3	neurotrophin-3
NT-4	neurotrophin-4
p75NTR	p75 neurotrophin receptor
S1P	spingosine-1-phosphate
SCI	spinal cord injury
SEM	scanning electron microscopy

SVZ	subventricular zone
T8	thoracic level 8
TNF	tumor necrosis factor
Trk	tropomyosin receptor kinase
UTI	urinary tract infection

Abstract

THERAPEUTIC STRATEGIES AIMED

TO FACILITATE AXONAL REGENERATION AND FUNCTIONAL RECOVERY

FOLLOWING TRAUMATIC SPINAL CORD INJURY

By Woon Chow, B.S., B.S.

A dissertation submitted in partial fulfillment of the requirements for the degree of Doctorate of Philosophy at Virginia Commonwealth University.

Virginia Commonwealth University, 2011

Major Director: Raymond Colello, D.Phil.
Associate Professor, Anatomy and Neurobiology

Traumatic spinal cord injury (SCI) is a physically debilitating, emotionally devastating, financially costly, and life-changing condition that afflicts more than 1,000,000 people in the United States alone. Owing to the characteristic neuropathology and low regenerative capacity of the central nervous system, many victims of SCI are left permanently paralyzed. Though the tissue damage caused by the initial insult almost certainly cannot be reversed, intensive research in recent years to elucidate the cellular and molecular events that follows has provided new grounds for optimism. Accordingly,

in this dissertation, we present a number of potential treatment strategies aimed to address some of these pathological sequelae seen post-SCI so as to facilitate the regeneration of axons and the recovery of physiological functions.

After the initial traumatic insult, a prominent and lasting injury-induced proliferative response occur and results in the development of a gliotic scar that isolates the lesion from the surrounding viable tissue. Although this process aids to prevent the spread of uncontrolled tissue damage, the scar nevertheless acts as a physical barrier to axonal regeneration. Furthermore, cells within the scar are a major source of axon growth-inhibitory molecules such as chondroitin sulfate proteoglycans (CSPG) and thus the scar acts concomitantly as a biochemical barrier. Concurrent to all this, inflammatory cells infiltrate the lesion and promote cell death through immunologic activation. Neuronal survival is also threatened from the lack of neurotrophic support caused by axonal severance. Finally, the pathology culminates in the formation of a fluid-filled cyst, which represents a gap that further hinders axonal regrowth.

Since regeneration cannot physically occur in the presence of a cavity, we, by employing electrospinning techniques, generated a biocompatible matrix implant that can bridge and direct axonal elongation across the fluid-filled cyst. Given the complex array and scope of pathological sequelae post-SCI, it is generally recognized that a multifaceted approach is required to successfully treat SCI. In view of this, we presented novel approaches by which successful tried and true therapeutic strategies are combined

to generate an enhanced matrix. An enzyme as well as a growth factor was incorporated into our matrix implants in order to respectively neutralize CSPGs and provide neurotrophic support. Using *in vitro* assays, we were able to demonstrate excellent protein bioactivity after incorporation. *In vivo* experimentation of these enhanced matrices is now ongoing. To address the injury-induced proliferative response, which represents an on-ramp off-ramp obstacle that prevents axonal regeneration onto our matrix implant, we showed how X-irradiation can be utilized to moderate this response by killing dividing cells so as to facilitate a more efficient penetration of regrowing axons into and beyond the gliotic scar. Finally, we demonstrate how a novel pharmacologic agent FTY720 can be used to attenuate the inflammatory response by preventing lymphocytic egress from lymphoid tissues.

Collectively, these ideas and experimental results represent novel therapeutic strategies that can be combined in order to bring about meaningful functional recovery after SCI.

Chapter 1

Traumatic Spinal Cord Injury: the Epidemiological, Anatomical, and Pathological

Dissertation Synopsis

This dissertation investigates potential therapies that are directed at various therapeutic obstacles after traumatic spinal cord injury (SCI). In Chapter 1, we discuss what is currently known about SCI, specifically the causes and classifications, pathology and associated therapeutic challenges. In each of the following chapters, the discussion is then narrowed on a particular obstacle and a potential therapeutic strategy that addresses the obstacle. Chapter 2 describes electrospinning and how that can be used to fabricate biocompatible implantable matrices to bridge the fluid-filled cyst. The electrospinning discussion is expanded in Chapter 3 when we describe how these matrices can be supplemented with a neurotrophin and an axon growth-inhibitor neutralizing enzyme. Chapter 4 describes a preliminary study in which these enhanced matrices were implanted into a rat model of SCI. Chapter 5 focuses on the injury-induced proliferative response and the potential of using X-irradiation to moderate this reaction. These studies,

along with some concluding remarks, are summarized in Chapter 6. In the appendix, we detail a potential pharmacologic intervention to suppress the inflammatory response.

Introduction

Traumatic injury to the spinal cord results in the severing of axons and cell death, leading ultimately to the disruption of communication pathways between the brain and distal targets and resulting in paralysis and loss of sensation. A myriad of complex cellular and biochemical events follow the initial insult, which often further damages the cord parenchyma and reduces the permissiveness of the microenvironment to axonal regeneration. Specifically, inflammatory cells infiltrate the lesion area and release toxic substrates, driving viable neurons and glia alike into apoptosis. Glial cells at the border of the lesion epicenter react to the injury by hypertrophying and proliferating to form scar-like barriers and upregulating their expression of various axon growth-inhibitory compounds. Concurrently, parenchymal destruction leads to the formation of a fluid-filled cyst, resulting in a physical gap that further complicates the prospect of regeneration. In short, the cellular and biochemical responses following SCI are numerous, complex, and possess certain elements of destruction. Thus, potential treatments for SCI were generally unavailable until the last few decades. And though little can be done to reverse the initial insult, through our increasing understanding of the pathology seen after SCI, new potential treatment strategies that target specific therapeutic obstacles can be devised and combined to bring about meaningful functional recovery.

In this introductory chapter, we first present some general information about SCI including statistics, basic anatomy, and classifications before proceeding to discuss individually each of the major therapeutic obstacles that confront researchers and clinicians. Later, in the remaining chapters, we shall describe our ideas and the investigations of these ideas for addressing each of these obstacles.

Epidemiological Statistics

The prevalence of SCI in the U.S. is often cited by the literature and various special interest groups to be from a conservative number of 200,000 (Berkowitz, 1998) to a higher estimation of 450,000 cases (National Spinal Cord Injury Association). Incidence is estimated to be approximately 11,000 cases each year (Berkowitz, 1998). However, a recent 2009 report from a project led by researchers at the University of New Mexico's Center for Development and Disability suggests that there may be a gross underestimation of SCI prevalence in this country (Christopher & Dana Reeves Foundation). The project, which included exhaustive surveys conducted on more than 33,000 randomly sampled households, estimated that there may be an upward of 1,275,000 people, or approximately 0.4%, of the U.S. population, currently living with SCI. According to this newly generated report, more than 82% of the SCI cases were caused by trauma, with 28% of the cases resulting from occupational accidents, 24% from motor vehicle accidents, 16% from sport-related injuries, 9% from falls, 4% from violence-related injuries, and 1% from natural disaster-related injuries. Paraplegia is documented in about 43% of SCI cases while quadriplegia in about 56%. Of those

reported being paralyzed due to a SCI, 61% were males. Currently, SCI costs the U.S. health care system approximately $40.5 billion annually, a four-fold increase from the estimated cost of 9.7 billion in 1998. The considerable annual costs of living with SCI coupled with the overwhelming physical and emotional hardship suffered by both the patient and family make SCI an important public health concern that is worthy of finding a cure.

Spinal Cord Anatomy

Enclosed within and protected by the bony vertebral column in the spinal canal, the human spinal cord is a long, thin, soft, ovoid-shaped bundle of nervous tissue that extends inferiorly from the medulla oblongata at the level of the foramen magnum to typically the upper lumbar vertebral level. Considered to be a part of the central nervous system (CNS) along with the brain, the spinal cord is similarly ensheathed by the three meninges, which include the outer dura mater, the arachnoid mater, and the innermost pia mater. Cerebrospinal fluid is found in the subarachnoid space as in the brain as well as in the central canal, the adult remnant of the neural tube. The peripherally located white matter of the spinal cord contains ascending and descending neural tracts of axons that act as signal transmission conduits between the brain and the rest of the body. Damage to these tracts in a SCI causes a majority of the symptoms seen post-injury. The centrally located gray matter contains neuronal cell bodies that are involved with motor control, reflexive loops, and central pattern generation. Enlargements, which are portions of increased girth due to the greater amount of tissue needed to innervate the limbs, are

found at the cervical and lumbar levels. In general across mammalian species, the more dorsal aspect of the cord contains tissue that are associated with afferent, or sensory, inputs and the more ventral aspect contains tissue that are associated with efferent, or motor, outputs.

The anatomy of the spinal cord and its surrounding structures plays a considerable role in explaining the favored level of injury in SCI. SCI generally occur at the level of the cervical and lumbar cord, which is attributable to the presence of the enlargements at these locations. Due to the compact physical space between the cord and the spinal canal at these vertebral levels, the spinal cord can easily be trapped and compressed if there is any orthopedic involvement when trauma occurs. In contrast, mid-thoracic cord injuries are quite rare, since a small but significant space cushion exists between the cord and bone.

Spinal Cord Injury Pathological and Clinical Classification

Pathological Classification

Spinal cord trauma can be a result of any or the combination of the following: application of pressure such as stretching or squeezing, bruising, tearing, or crushing. The manner by which the spinal cord is injured has considerable influence on the prognosis as well as the therapeutic strategies involved. Accordingly, a pathological classification, initially devised by Bunge et al. (1993), relates the manner by which the cord is injured to the gross appearance and histology of the cord seen at autopsies. The four groups included in this classification are solid cord injuries, contusion/cavitation

injuries, laceration injuries, and massive compression injuries, with each of these types corresponding respectively to the manner of injury stated above.

Solid Cord Injuries

Solid cord injuries are SCI in which no gross defects are seen. Grossly, the cord appears normal, with no softening, bruising, discoloration, or a compromise of the meninges. However, histologically, sections show a loss of normal architecture, demonstrating the occurrence of damage (Figure 1.1B). Solid cord injuries are rare and are only involved in about 10% of SCI cases. The cause of solid cord injuries is still unclear, though inflammation is thought to play a major role in the development of these injuries. It is suggested perhaps that a slight application of pressure on the cord, such as stretching or squeezing, which in itself is relatively harmless to cord tissue, is enough to trigger an inflammatory cascade. The ensuing inflammation, as an insidious component of secondary injury, damages spinal cord tissue. (Primary injury is the initial insult.)

Frequently, minor cases of SCI may not initially present with any clinical findings and only later does the patient begin to exhibit symptoms of a SCI. This very fact supports the general notion that perhaps much of the tissue damage sustained after a primary SCI insult, especially in cases where cord anatomy was not drastically altered, is due to secondary injury. Accordingly, the many notable potential therapeutic strategies to SCI and traumatic brain injury alike seen in the literature often target a component of secondary injury.

Contusion/Cavitation Injuries

The second type, contusion/cavitation injuries, is the most common and is involved in more than half of all traumatic SCI cases. Also known as percussive SCI, these injuries are usually caused by a dislocated vertebra or displaced discs and ligaments compressing and subsequently bruising the cord. Grossly, there is no disruption of the pial surface despite the fact that often there are areas of hemorrhage in the central grey matter. These areas eventually undergo liquefactive necrosis and the debris is subsequently cleared by inflammatory cells, ultimately resulting in the classical formation of a fluid-filled cyst (Figure 1.1C). Concurrently, a prominent reactive astrogliotic reaction around the lesion site ultimately develops into a gliotic scar surrounding the cyst.

Laceration Injuries

The third type, laceration injuries, account for about 20% of SCI cases. Often, these injuries are a result of broken fragments of vertebra cutting the cord. Gun-shot and stab wounds are also responsible. In contrast to contusion/cavitation injuries, rupturing in the pial membrane is apparent (Figure 1.1D). As a consequence, extra-medullary fibroblasts migrate into the lesion site, deposit a substantial quantity of collagen, and ultimately form a mesenchymal scar. The prognosis of laceration injuries is often poor since the dense scarring characteristically blocks any attempts of axonal regrowth or rewiring. Minor functional improvements can often be seen in SCI patients post-trauma as the injury stabilizes, but this rarely occurs in laceration SCI.

Massive Compression Injuries

Finally, in massive compression injuries, the cord is essentially crushed, usually from extensive orthopedic trauma. The pathological evolution of these lesions is similar to that of laceration injuries due to the pial disruption. Accordingly, considerable fibrosis and dural adhesion typically results (Figure 1.1E). Less than a 20% of traumatic SCI cases are classified as massive compression injuries.

Most SCI cases can be classed as one of these four types. However, some injuries, especially multi-level ones, may involve more than one of these pathologies. Outwardly, this pathological categorization scheme seems somewhat overly simplified, but nevertheless helpful when prognosticating the progression of a SCI.

Clinical Classification

In contrast to the pathological classification, a clinical classification of SCI is based on the functional implications post-injury. In general, SCI can be classified as complete, incomplete, or discomplete. Complete injuries usually involve trauma so severe that there is total paralysis and sensation loss below the level of the lesion. This clinical type frequently implies a total cord transection, which is an exceptionally uncommon event. In contrast, incomplete injuries signify that some physiological function is preserved below the injury level. The implication here is that the cord has not been completely severed. In many cases of incomplete injury, the cord is generally anatomically intact but the injury has caused disruption in some but not all the neural tracts. Finally, discomplete injuries appear to be clinically complete but

neurophysiologically incomplete. Patients with this type of injury are completely paralyzed below the lesion, but they exhibit some brain influence on spinal cord function. This presentation of SCI has not been fully explained and the cause is still unclear. Generally, once a SCI patient is stable after admission, he or she often undergoes extensive testing to determine the completeness as well as the physiological level of injury. This evaluation includes assessing the three major afferent and efferent spinal cord pathways, specifically the dorsal column tracts with pinpricks and the spinothalamic tracts with light touches at all dermatomes plus the corticospinal tracts with muscle strength tests on all major muscle groups.

These classifications convey the varieties and range of clinical and pathological consequences after SCI. Accordingly, SCI treatment strategies must be tailored to the specific injury type.

The Obstacles to Successfully Treating Spinal Cord Injury

In this project, we were most interested in furthering our understanding of and testing improved potential therapies for contusion/cavitation typed SCI since as aforementioned, they are the most common cases clinically. In the following sections, the therapeutic obstacles to successfully treating this percussive type of SCI are discussed. These obstacles, as well as our therapeutic ideas for addressing them, are revisited in the remaining chapters individually.

In short, percussive injury to the cord in both humans and animal models results in a pathological cascade of cellular and molecular events that culminate in the

characteristic formation of a fluid-filled cyst enclosed by a cellular wall made by the proliferation of glial cells and subsequent scarring (Balentine, 1978; Wozniewicz et al., 1983; Kakulas, 1984; Bresnahan et al., 1991; Bunge et al., 1993; Ito et al., 1997; Norenburg et al., 2004). The cyst forms a physical gap within the cord parenchyma, preventing axons from crossing the lesion to reach downstream targets. The gliotic scar, formed by the hypertrophy and hyperplasia of various cells in and around the lesion, presents a physical as well as biochemical barrier due to the increased cellular expression of compounds that inhibit growth cone migration (Lemons et al., 1999; Morgenstern et al., 2002). In addition to these pathological hallmarks, inflammation, mentioned previously as a component of secondary injury, plays an insidious role in the promotion of cellular apoptosis, exacerbating the damage initially sustained by the primary insult (Anderson et al., 1985; Blight, 1992). Furthermore, the loss of trophic support exacerbates neuronal cell death. These SCI pathological features of scar development, inflammation, cavity formation, molecular inhibitors, and loss of trophic support are now discussed in greater detail.

Cyst Formation

Though cystic formations generally occur late in the pathologic evolution of the SCI lesion, we initiate our discussion with this topic since they represent the single most prominent obstacle to axonal regeneration. Customarily found in contusion/cavitation injuries, fluid-filled cysts typically form at injury epicenters weeks to months following SCI (Balentine, 1978; Norenburg et al., 2004). Cysts may have a singular, multiple, or

multiloculated presentation and a wall of gliotic scarring, deposited during the lesion-isolation process, surrounds the cysts. The cysts are essentially the end products of debris clean-up at the lesion site and they represent the final healed state of a CNS injury. Similar to cysts in that they are fluid filled, syrinxes, differ in that they possess a thicker and denser gliotic wall due to increased pressure in the cavity. Syrinxes may exacerbate existing neurological deficits since adjacent cord parenchyma may be compress as the cavity increase in size. Cavity formations are yet another obstacle in successfully treating SCIs. Due to the lack of a solid substrate, this pathological endpoint represents a physical gap that prevents regenerating axons from crossing to reach their downstream targets.

To this end, in Chapter 2, we show how electrospinning was utilized to fabricate a bridging matrix. Recognizing that an ideal bridging scaffold would be biocompatible, durable, porous, and directional such that it can spatially guide regrowing axons, we generated via electrospinning a matrix that possess all of these properties and demonstrated their excellent neurite-guiding ability *in vitro*. Furthermore, in Chapter 3, in preparation for the assessment of these matrices *in vivo*, we show how we refined the electrospinning process by adopting an air-gap spinning system so as to generate implantable 3-dimensional cylindrical structures possessing the same qualities that are capable of filling the gap left within the damaged cord. A preliminary test of these matrices in an animal model of SCI is presented in Chapter 4.

Chondroitin Sulfate Proteoglycans

After SCI, glial cells within the scar and in the surrounding lesion zone proliferate and hypertrophy to form the gliotic scar. In addition, these cells upregulate their expression of CSPGs (Lemons et al., 1999). CSPGs are well-known inhibitors of axonal regeneration (McKeon et al., 1995; Canning et al., 1996; Gopalakrishnan et al., 2008; Yang and Schnaar, 2008).

Chondroitin sulfate is simply a sulfated glycosaminoglycan (GAG), which is a long unbranched polysaccharide consisting of a variable number of repeating disaccharide units. One or more of these chains are often found attached to a core protein via a serine residue as part of a proteoglycan. Depending on the core protein to which the GAG chain is attached, the entire molecule is called by a distinctive name. Examples of CSPG molecules include aggecan, brevican, neurocan, phosphacan, versican, and NG2. The pattern of sulfation can be rather complex as each disaccharide possesses four possible positions for group attachment and the diseaccharide may be unsulfated or sulfated in 1, 2, or 3 positions. For this reason, there can be a very large number of sulfation motifs which defines the individual binding site.

CSPGs are expressed almost ubiquitously and are found in the ECM of most tissues. In addition to their structural role in the ECM, these molecules are important regulators in various biological processes involving cellular recognition, migration, and signaling (Brittis et al., 1992; Sheng et al., 2005). In certain tissues, they provide very specific functions. For example, CSPGs are a major component of cartilage and by virtue of their numerous tightly packed and highly negatively charged sulfate groups, generate

the electrostatic repulsion that provides much of the compression resistance. In the nervous system, they contribute to the regulation of various CNS developmental processes, acting as a stop signal to neuronal and axonal growth cone migration (Powell et al., 1997; Cortes et al., 2009).

Upon injury to the CNS, there is a general massive upregulation of CSPGs at the lesion site and surrounding areas (Lemons et al., 1999). Although this expression usually peaks during the first week post-injury, levels of CSPG usually stay high as the gliotic scar matures (Tang et al., 2003). The production of a certain CSPG is attributable generally to a particular cell type. Brevican and phosphacan are mainly products of astrocytes whereas versican and NG2 are almost exclusively expressed by oligodendrocyte progenitor cells (OPC) (McKeon et al., 1999; Asher et al., 2002; Bouslama-Oueghlani et al., 2005). Neurocan is produced by both astrocytes and OPCs (Asher et al., 2000).

The exact mechanism by which CSPGs inhibit the regeneration of axon is still unclear. Substantial evidence suggests that the sulfated GAG chains are the elements responsible. Nevertheless, it is well-recognized that successful SCI therapies include an element that targets these nefarious molecules so as to neutralize their axon growth-inhibitory property. *In vitro* experimentation by various research groups with the bacterial enzyme chondroitinase ABC (ChABC), which cleaves the GAG chains, have shown a drastic reduction of the inhibitory activity of CSPGs (Iaci et al., 2007; Massey et al., 2008). Furthermore, recent *in vivo* studies using ChABC demonstrated enhanced axonal sprouting and neuroplasticity as well as improved functional recovery (Bradbury

et al., 2002; Caggiano et al., 2005; Huang et al., 2006; Tester and Howland, 2007). In view of these successes by others, in Chpater 3, we show how we integrate ChABC into our implantable electrospun matrices as well as present data from *in vitro* assays that demonstrate the extent to which the enzyme remained bioactive.

Neurotrophins

Neurotrophic factors, or neurotrophins, are small, secreted peptides that act on cells in the nervous system via specific receptors that activate intracellular signaling cascades to promote cell survival, growth, and differentiation (Markus et al., 2003). In general, neurons projecting axons via specific tracts within the spinal cord respond to one particular neurotrophin or a collection of factors.

The nerve growth factor (NGF) family of neurotrophins includes the four related peptides that share structural and sequence homology: NGF, brain-derived neurotrophic factor (BDNF), neurotrophin-3 (NT-3), and neurotrophin-4 (NT-4). These factors can bind to two entirely distinct classes of receptors. The first known targets, Trk (tropomyosin receptor kinase) receptors are a family of tyrosine protein kinase receptors that mediates high affinity binding. Each of the Trk receptor members bind only with specific neurotrophins. TrkA receptors, which are expressed by sympathetic, trigeminal, and dorsal root ganglion neurons as well as by cholinergic neurons of the striatum and basal forebrain, specifically recognize NGF (Barbacid, 2004). TrkB receptors are activated primarily though their binding with BDNF and NT-4. The principal targets of NT-3 are TrkC receptors, which have been shown to be expressed on developing

corticospinal neurons (Chen et al., 1996, Namiki et al., 2000; Iarikov et al., 2007). In some cellular contexts, NT-3 is also able to bind TrkA and TrkB, though with less efficiency. Activation of the Trk class of receptors results in the prototypical function of neurotrophins, namely the promotion of cell survival and growth. The second known target (though first discovered) of neurotrophins is the p75 neurotrophin receptor (p75NTR), a member of the tumor necrosis receptor superfamily. In contrast to the Trk family, all four mentioned neurotrophins are able to bind to p75NTR, although with much less but similar affinity. The specific role of p75NTR is not entirely clear. Due to their low affinity for the neurotrophins, some have suggested that p75NTR may act to take up excess concentrations and affecting neurons in a manner beyond survival and growth in such occasions. The p75NTR is known to be highly expressed in certain developing neurons as well as in axotomized adult neurons, which suggests a physiological role in mediating the higher neurotrophin expression by the local glial cell population seen after trauma. It has been demonstrated that p75NTR increases both the binding affinity and specificity for Trk receptor. This is especially evident with NGF in that both p75NTR and TrkA are required for the efficient generation of high affinity binding sites (Esposito et al., 2001). However, other studies have point to the role of p75NTR as a pro-apoptotic mediator. Cells expressing P75NTR in the absence of Trk receptors may be driven to programmed cell death in the presence of a neurotrophin rather than surviving (Teng et al., 2005). Another interesting observation related to SCI is the relationship between the p75NTR and Nogo-66 receptor. The Nogo-66 receptor, with its downstream Rho kinase pathway, is responsible for mediating the inhibitory

effects on axonal growth of three notorious myelin-associated glycoproteins, specifically Nogo-A, myelin-associated glycoprotein and oligodendrocyte-myelin glycoprotein (Liu et al., 2002; Xie and Zheng, 2008). The p75NTR receptor act as a co-receptor to the Nogo receptor complex and when p75NTR was knocked out in mice, outgrowth inhibition of axons was no longer observed (Wang et al., 2002; Wong et al., 2002). In short, though the meaning of the association between P75NTR and Trk, with some seemingly synergistic and others antagonistic effects, is still quite controversial, it is apparent that there are independent and dependent roles and actions of these two types of receptors.

After ligand binding, the high affinity Trk receptors undergo dimerization and autophosphorylates tyrosine residues in their cytoplasmic domains. The neurotrophins and its activated Trk receptors are subsequently internalized through clathrin-coated pits and conveyed retrogradely up the axon toward the neuronal soma. This endocytosis and subsequent vesticular transport serves to bring the activated signal close to certain organelles, such as the nucleus, where the signal can be acted upon to bring about specific cellular responses by way of gene transcription. Signaling in the neuronal cell body controls the more global cellular functions of survival, proliferation, and differientation (Jacobson et al., 1997). In contrast, local signaling is also known to occur and has been shown to regulate growth cone motility (Thoenen and Barde, 1980). In one study, Gallo et al. was able to demonstrate that the TrkA receptor mediated growth cone turning toward a localized source of NGF (1997). The molecular mechanisms by which neurotrophins regulate growth cone motility are not well understood. However, recently

acquired experimental evidence suggests that these Trk-dependent actions may converge downstream with the abovementioned Rho kinase pathway and that a local accumulation of actin filaments may result from an increase in intracellular calcium concentration (Gehler et al., 2004).

In general, neurons in the CNS obtain their trophic support from the target tissue to which their axons project and this secretion of neurotrophins by the target tissue prevents the associated neuron from initiating apoptosis. Thus, a low maintenance level of neurotrophins is required to ensure neuronal survival. Upon axotomy after SCI, the disconnected neurons no longer receive a survival signal and may be driven into programmed cell death. However, studies have shown that exogenous introduction of neurotrophins after CNS injury rescues these axotomized neurons, ensuring cell survival and in many cases cause enhanced axonal regrowth (Namiki et al., 2000; Mitsui et al., 2005; Blesch and Tuszynski, 2007). Accordingly, also in Chapter 3, we describe the incorporation of NGF into our implantable electrospun matrices by way of alginate microspheres and present data from *in vitro* assays that demonstrate the extent to which the growth factor remained bioactive when incorporated.

Reactive Astrogliosis and Gliotic Scar Formation

In human percussive SCI, the reactive astrogliotic, or gemistocytic, response is characterized by cellular hypertrophy and injury-induced proliferation, which ultimately results in a gliotic scar that is classically seen around the boundary of the lesion epicenter (Figure 1.2). This outcome brings about a number of neuroprotective benefits. As a new

glia limitans forms, reactive gliotic processes interdigitate and become linked by tight junctions. This functions to isolate the SCI lesion containing necrotic tissue debris from viable tissue in the periphery, resulting in the reestablishment of the integrity of the CNS microenvironment within and aiding to prevent a further spread of cellular destruction (Norenburg et al., 2004). Astrocytes within the developing gliotic scar are known to play a homeostatic role in restoring extracellular ionic balance and uptaking of the excess excitatory neurotransmitters and other toxic metabolites that may have accumulated in the lesion and the surrounding cord tissue (Davies et al., 2006; White and Jakeman, 2008). Furthermore, as the gliotic scar forms, reactive astrocytes often extensively remodel the extracellular matrix (ECM) and lay down abundant deposits of basal membrane. Analogous to wound contracture after skin injuries, this basal membrane can contract to bring together opposite margins of the lesion, shrinking the lesion as debris is cleared out. In addition, the gliotic scar provides a cellular scaffold for inwardly migrating epithelial cells to revascularize the lesion site.

In contrast to the above benefits, the scar has been implicated in blocking axonal regeneration physically as well as biochemically via the expression of chondroitin sulfate proteoglycans (CSPG) and other inhibitory factors. First causally suggested by Ramón y Cajal (1928), subsequent experimental results readily confirms that though regenerating CNS axons sprout growth cones, axonal regrowth and growth cone migration invariably stop at the gliotic scar border (Reier et al., 1986). The cause of the physical barrier is still unclear. Though the gliotic scar is sealed sufficiently to prevent the spread of damage peripherally from the lesion epicenter, many studies have shown that astrocytic processes

and their associated tight junctions do not create a physical impediment (Norenburg et al., 2004). However, there is a possibility that the basal membrane is capable of obstructing axonal regrowth due to its contractile properties, resulting in its dense architecture. Consequently, success in inducing regenerating axons to regrow past the scar to seek distal targets requires a physical alteration of the scar to some extent.

In view of the inability of regenerating axons to penetrate the scar to reach our implantable electrospun matrix scaffold and off on the opposite side, in Chapter 5, we present a potential non-invasive therapy in which single-dose X-irradiation is used to moderate the injury-induced proliferative response so as to increase the spatial separation between reactive cells, which may create small gaps to facilitate regeneration at the on-ramp and off-ramp sites adjacent to the matrix. The attenuation of cellular proliferation needs not be extreme since gliotic scarring nevertheless confers important neuroprotective benefits.

Edema and Inflammation

Edema is often the first gross sign following SCI that can be detected, usually radiographically. This edema is probably due to the vascular changes, namely vasodilation and hyperemia, which occur early on in the injury response (Sharma et al., 1993). Specifically, a breakdown of the blood-spinal cord barrier, loss of cerebral autoregulation, and the consequent increased permeability of capillaries results in an exudation of plasma fluid into the extracellular space. This vasogenic edema can cause an ischemia that may possibly be due to the increased hydrostatic pressure in the region.

In contrast to the brain, the spinal cord has a thicker and perhaps more rigid pial-glial zone, which can exacerbate this ischemic mechanism. This ischemia can in turn cause a buildup of undesirable metabolites and excitatory neurotransmitters, causing more neurons in the vicinity to die (Stiefel et al., 2005). Research completed at this institution has shown that perhaps more significant than vasogenic edema is the cytotoxic edema that may be caused by these events (Marmarou et al., 2006). This mostly occurs in astrocytes, especially those with astrocytic end-feet adjacent to capillaries (Bullock et al., 1991).

The basis for the increased permeability of the blood-spinal cord barrier is attributed generally to a host of secreted factors. It is well-established that expressions of pro-inflammatory cytokines such as Interleukin (IL)-1, IL-3, and IL-6 as well as their associated receptors are strongly upregulated post-injury. In addition, various complement components and tumor necrosis factor (TNF) were also observed to be increased in their expression. These and a number of other factors, such as various matrix metalloproteinases, may be responsible for the enhancement of vascular permeability and the subsequent infiltration of immune cells. Furthermore, the sustained elevations of particularly TNFα and IL-1β may cause neuronal and oligodendroglial cell death (Lee et al., 2000; Hermann et al., 2001; Cai et al., 2003). Accordingly, blocking TNFα and IL-1β have shown to be neuroprotective in various models of CNS trauma (Nesic et al., 2001; Genovese et al., 2006). Though it is recognized that cytokines play an important and seemingly destructive role in mediating the inflammatory reaction

following SCI, the full extent of involvement by these various pro-inflammatory factors on the secondary degenerative processes remains unclear.

As mentioned, the cytokine mediated vascular changes attract inflammatory cells into the lesion site (Trivedi et al., 2006). As shown in animal studies, compared to post-traumatic inflammation in brain injuries, SCI tends to elicit a more prominent cellular immune response (Schnell et al., 1999a). Following identical laceration injuries delivered to mouse brain and spinal cord, higher numbers of neutrophils and activated macrophages were shown to be recruited to the SCI lesion site and their extent of infiltration was more profound. In a subsequent study by the same group, similar results were obtained when non-traumatic injections of pro-inflammatory cytokines into the two different tissues—neutrophil and macrophage recruitment was always greater in the spinal cord (Schnell et al., 1999b). Anatomical and molecular variabilities between the brain and spinal cord may account for these regional differences in inflammatory reactions (Tveten, 1976a, b). Nevertheless, these results demonstrate that knowledge and data gleaned from studying CNS inflammation in the brain cannot be applied to SCI without further examination.

After injury to the cord parenchyma, blood monocytes, granulocytes, and lymphocytes readily migrate across the permeable blood-spinal cord barrier. It has been demonstrated numerous times that immune cell infiltration into the SCI lesion site largely contributes to the secondary injury process and may considerably expands lesion volume (Dusart and Schwab, 1994; Blight et al., 1995; Glaser et al., 2004). The earliest arrival of neutrophils usually occurs within 12 h with ED1 immunoreactive macrophages appearing

soon after (Carlson et al., 1998; Norenburg et al., 2004). These cells phagocytose cellular and myelin debris and begin the intensive clean-up process that may continue for the next 3 to 5 d. By day 3, numerous fat-laden macrophages occupy the lesion site. Though the process of debris removal in itself is beneficial, many researchers have suggested that a number of elements may perhaps be neurotoxic. Neutrophils release a potent cocktail of reactive oxygen species and enzymes intended for a bacterial invasion. It is almost certain that neutrophils confer no meaningful neuroprotection in the CNS post-injury given their foremost function as bactericidal cells.

Lymphocytes, in particular the T cell, have been implicated in promoting cellular apoptosis following the release of neural self-antigens and the resulting activation of immunological cascades after CNS injury (Popovich et al., 1996; Gonzalez et al., 2003; Ankeny et al., 2006). In experimental trials, injection of activated T cells from SCI rats alone has shown to cause CNS injury in naïve animals (Popovich et al., 1996). Consequently, one element of a successful SCI therapy must include a means to modulate the inflammatory response so as to reduce cell death and preserve the enduring viable tissue parenchyma surrounding the lesion site.

Accordingly, in the appendix, we present a potential pharmacologic therapy that aims to induce lymphopenia following SCI. By preventing lymphocytic egress from lymph nodes, we show the extent to which fingolimod, commonly known as FTY720, preserves cord white matter, improves bladder function, and enhances functional recovery.

Summary

Figure 1.3 illustrates and summarizes the major therapeutic challenges posed by SCI that we have just now discussed. Given the multitude and the variety of obstacles, SCI is a costly, debilitating, and life-changing medical condition that will require a combination of approaches to successfully treat. In the following chapters, we will present our ideas and the investigations of these ideas for addressing each of these key challenges.

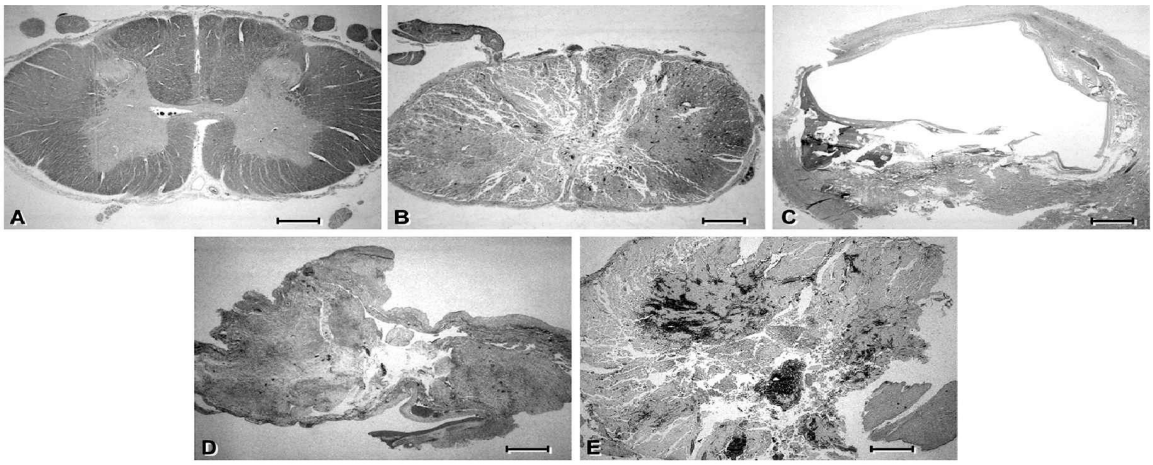

Figure 1.1. (A) Cross sectional histology of a normal human spinal cord at the cervical level. (B) Cords in solid cord injuries display a loss of the normal tissue architecture. (C) Cystic formation in cord parenchyma in contusion/cavitation injuries. (D) Pia is penetrated in laceration injuries. (E) Massive compression injuries generally results in the pulpification of cord tissue and extensive hemorrhage. Scale Bars (A to E) = 2 mm. Adapted from Norenberg et al. (2004).

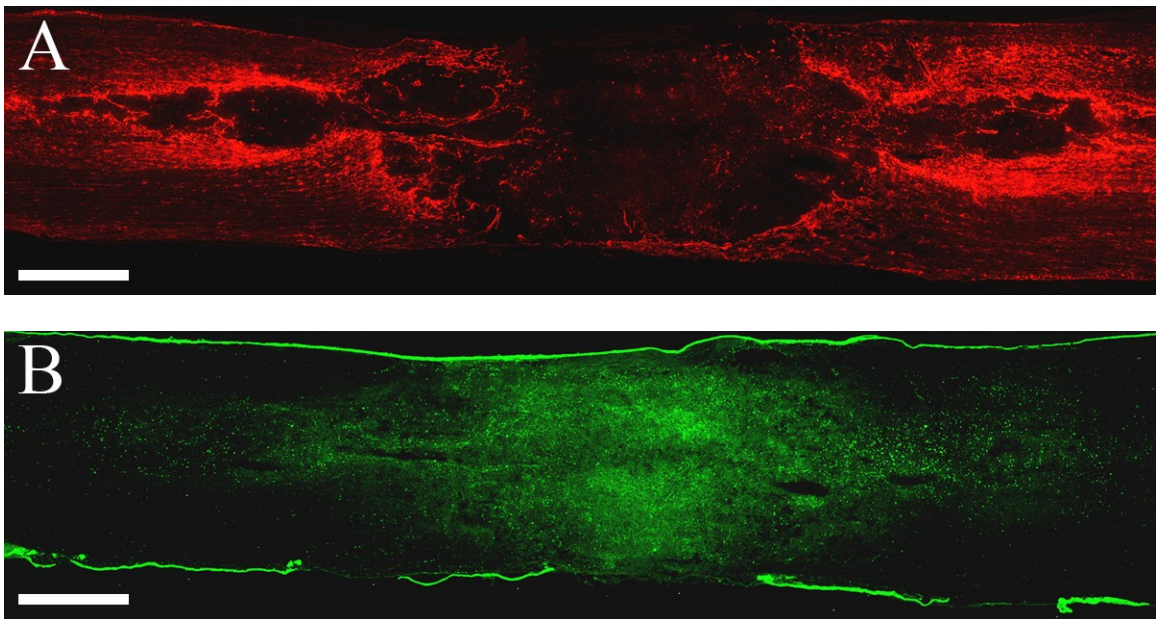

Figure 1.2. (A) Longitudinal sections of a rat spinal cord, which received a contusion injury 14 d earlier, immunolabeled for GFAP (red). Gliotic scarring is readily seen by the high intensity of labeling around the edge of the developing cyst located at the lesion epicenter. (B) The same section immunolabeled for bromodeoxyuridine (green), a proliferation marker. Scale Bars (A and B) = 1 mm.

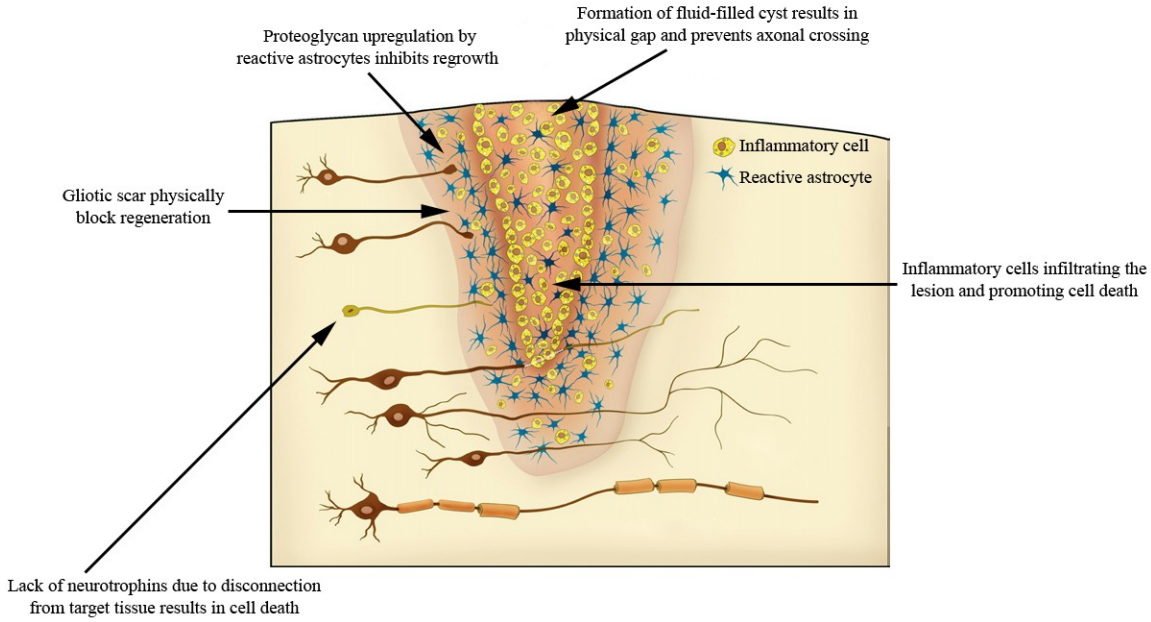

Figure 1.3. A cartoon illustrating the various therapeutic challenges posed by contusion/cavitation SCI. Adapted from Fitch and Silver (2008).

Chapter 2

Evaluating Neuronal and Glial Growth on Electrospun Polarized Matrices

Introduction

Percussive injury to the spinal cord, in both human insults and animal models, results in the liquefactive necrosis of the tissue in and around the lesion site. Commonly, a fluid-filled cyst is the final consequence of this process. Because of the lack of a solid substrate, this late-stage pathological endpoint presents a physical gap which impedes axonal regeneration and functional recovery after spinal cord injury (SCI). Though other therapeutic obstacles exist post-SCI, the cystic formation represents a single most formidable challenge to axonal regrowth.

To guide regenerating axons across this cavity, several research groups have investigated the use of bridging materials that include substrates derived from either stem cells (McDonald et al., 1999; Akiyama et al., 2002), support cells (Xu et al., 1995; Li et al., 1997), autologous grafts (von Wild and Brunelli, 2003; Houle et al., 2006), embryonic grafts (Reier et al., 1986), natural substances (Marchand et al., 1993), or

synthetic substances (Tsai et al., 2004; Wen and Tresco, 2006). Many of these approaches have shown promise in attracting regenerating axons onto the prosthetic bridge. However, documented cases of axons traversing these conduits to reach the intact tissue on the opposite margin of the lesion area are rare. Consequently, successes in inducing axonal regeneration have not translated into appreciable recovery of function. Nevertheless, despite the failure of significant axonal regrowth on existing bridges, advances in generating conduits for growth across lesioned areas must be made to successfully restore function after SCI.

In a simplified view, an ideal bridging neural conduit would be made from a biocompatible material that contains either channels or fibers that spatially guide regenerating axons. Since damage to the spinal cord induces necrosis that frequently affects multiple fiber tract systems, this bridge should fill the extent of the cyst area. Additionally, it should have a level of porosity that allows the inward migration and incorporation of supportive cells as well as the traversing axons. Finally, the ideal bridge should have the capacity to deliver signaling factors in a controlled manner to aid in the attraction, directional growth, and viability of traversing regenerating axons. One technique that has the capacity to generate such an ideal bridging prosthesis is electrospinning. Similar in concept to electrospraying, electrospinning uses a high-voltage electric field to generate extremely fine fibers that are deposited on a grounded collector to form a nonwoven mat (Bowlin et al., 2002). Chemically, these mats can be electrospun from either extracellular matrix (ECM) proteins or synthetic polymers, both of which can be spun alone or in combination with other growth-promoting factors.

Physical properties of these matrices, such as fiber diameter, porosity and alignment can also be controlled (Fridrikh et al., 2003). In the field of tissue engineering, the application of this technique has resulted in the generation of several biocompatible substrates such as growth-promoting dermal implants, cardiac patches, and synthetic vessels (Stitzel et al., 2001; Sun et al., 2005). For example, studies show that interstitial fibroblasts and endothelial cells migrate readily into an implanted electrospun collagen matrix from surrounding tissue (Telemeco et al., 2005). Once there, these cells proliferate and actively remodel this biological substrate, resulting in accelerated wound repair with less contracture. More recently, electrospinning has been used to generate growth matrices for cortical stem cells (Yang et al., 2005). Collectively, these studies indicate the potential utility of electrospining to create biocompatible substrates for use in injury repair.

In the study presented in this chapter, we examined the potential use of electrospinning to engineer a polarized matrix for axonal guidance. This matrix, which was spun from the resorbable suture material, polydioxanone (PDS), was tested for biocompatility with cells of neuronal and glial origin, and the growth dynamics of these cells on the matrix were assessed in cell culture studies. These experiments demonstrate that both the directionality and exuberance of axonal growth are controlled significantly by the physical and chemical properties of the underlying electrospun substrate. Controlling these two parameters of axonal growth are prerequisites to establishing a successful strategy for bridging lesioned areas in SCI.

Materials and Methods

Electrospinning

Electrospun matrices were fabricated from the PDS II violet monofilament surgical suture (Ethicon) as described previously (Boland et al., 2005). Briefly, for each matrix, 150 mg of 10% weight/volume of cut PDS filament was dissolved overnight in the solvent 1,1,1,3,3,3-hexafluoro-2-propanol. The solution was then transferred to a 5-ml syringe tipped with an 18-gauge blunt-end needle (Kontes) and the syringe mounted onto a syringe pump set at a delivery rate of approximately 30 ml/hr. The needle was connected via a wire outfitted with an alligator clip to the positive output lead of a high voltage direct current (DC) power supply (Spellman CZE1000R) set to 22 kV. The grounded rectangular mandrel, with a cross-section of 10 × 3 mm, was placed 20 cm from the needle (Figure 2.1). An electric field was generated across the nozzle and the grounded mandrel, inducing a jet of solution to be drawn out from the syringe and resulted in the deposition of a solid fiber core onto the rotating mandrel (Taylor, 1964). By varying the rotation rate of the mandrel, as determined by a calibrated digital stroboscope (Shimpo Instruments DT-311A), aligned and random fibers with diameters of 2 to 3 mm could be generated (Figure 2.2). Specifically, a faster rotation rate of 5000 rpm was used to spin matrices of aligned fibers (aligned matrices) whereas a slower rotation rate of approximately 10 rpm or less generated randomly oriented fibers (random matrices). Additionally, an even distribution of the fibers on the mandrel was achieved by allowing the mandrel assembly to translate (0.5 Hz).

Scanning electron microscopy

To prepare the matrices for scanning electron microscopy (SEM), 1-mm squares of both aligned and random matrices were cut from the electrospun mat and sputter-coated in gold. Photomicrographs (750 ×) were taken of random areas in each matrix, digitized with a flatbed scanner, and analyzed for fiber alignment using 2-dimensional fast Fourier transform (2D FFT).

2-Dimensional Fast Fourier Transform Alignment Analysis

As previously described by this laboratory (Alexander et al., 2006), utilizing the FFT function of the ImageJ image processing software, an image containing a graphical representation of the frequency content was generated from a digitized, square, grayscale image of the elements to be analyzed. Pixel intensities and the distribution of the intensities (frequency content) of this output image correlate to the directional content of the original image. Pixel intensities were summed along a radius from the center to the edge of the image to quantify the relative contribution of objects oriented in that direction. This summing was repeated at 1° increments around the image and the 360 summations were plotted. In this manner, a 2D FFT of an image containing randomly oriented elements results in relatively constant pixel intensities independent of direction. Theoretically, a radial summation of this type of data set should be represented as a flat line; however, because of edge effects associated with square images, an undulating plot with four small, symmetrical peaks results. In contrast, a 2D FFT of an image that has elements that are aligned preferentially would result in higher pixel intensities along the

aligned direction. Accordingly, when the radial summations are plotted, two peaks, representing the two angles (180° apart) associated with the aligned elements in an image are generally seen (Ayres et al., 2006, 2008).

Dorsal Root Ganglia Isolation and Culture

In this study, the potential of aligned matrices to influence the growth dynamics of extending dorsal root ganglion (DRG) neurites was tested. A set of random matrices was used as controls. In accordance with the Virginia Commonwealth University Institutional Animal Care and Use Committee, DRGs were dissected from embryonic day 16 (E16) Sprague Dawley rats as described previously (Sharma and Bigbee, 1998). Briefly, following removal from the uterus, the developing spinal cord from each embryo was exposed anteriorly. The entire cord was dissected from its rostral end and placed in Leibovitz L-15 media with 10% fetal bovine serum (FBS). The attached DRGs were then plucked off with fine tip forceps.

Circles of aligned and random matrices of 8-mm in diameter were sterilized in 100% ethanol, rinsed in Hank's balanced salt solution, and secured on the bottom of a 35-mm diameter Petri dish using hypodermic needles. Using a dissection microscope, several DRGs were micropipetted onto each matrix and pinned in place with 0.15-mm diameter minuten pins (Austerlitz). Cultures were incubated at 37°C with a 95% air/5% CO^2 gas mix in Eagle's minimum essential medium with glutamine supplemented with 10% glucose, 5% FBS and 0.01% 2.5 S nerve growth factor. The medium was changed every 2 d, alternating between the above medium and medium containing the antimitotic

agent, 5-fluorodeoxyuridine (10^{-5} M), which limits the proliferation of Schwann cells in DRG cultures (Wood, 1976). Following a 10-d incubation, the cultures were fixed in 4% paraformaldehyde in 0.1 M phosphate-buffered saline (PBS). Following fixation, DRG cultures were immunostained for the β-tubulin neuronal marker TuJ1 (Covance). Cultures were first blocked for 30 min in a solution consisting of PBS with 10% FBS and 0.3% Triton X-100, incubated for 2 h in a 1:500 dilution of TuJ1 mouse primary antibody in PBS and visualized with a 1:200 dilution of Alexa Fluor 488 goat anti-mouse secondary antibodies (Invitrogen) in PBS. Subsequently, 6 × digital, wide-field, fluorescence images of the DRG and its neuritic outgrowth were obtained using an Olympus BX51 microscope. For this study, DRGs were pinned on at least six matrices (three aligned and three random) and the experiment was repeated at least three times.

Astrocytic isolation and culture

In this study, the potential of aligned matrices to influence growth dynamics of astrocytes was tested. A set of random matrices was used as control. In accordance with the Virginia Commonwealth University Institutional Animal Care and Use Committee, rat primary astrocytes were isolated using methods described previously (McCarthy and de Vellis, 1980). Isolated postnatal day 3 (P3) rat cortices were minced and dissociated mechanically and enzymatically. Cells were seeded into T-75 poly-L-lysine-coated tissue culture flasks that contained Dulbecco's modified Eagle medium/Ham's F-12 medium, 10% FBS, and 1% antibiotic-antimycotic agent, and allowed to proliferate until the population reached confluency. During this time, media changes were made every 3

to 4 d. To purify the resulting mixed glia culture upon confluency, cultures were shaken overnight in an incubator to remove non-adherent cells. Two cycles of treatment with the selective replication inhibitor cytosine arabinoside were carried out subsequently to further purify the astrocytic population.

Circles of aligned and random matrices were placed into 10-mm diameter culture wells and seeded with enzymatically dissociated astrocytes at a concentration of 10^4 cells/ml. Cultures were incubated for 7 d in the astrocyte media described above and fixed using 4% paraformaldehyde. Following fixation, astrocyte cultures were immunostained for the astrocytic marker, glial fibrillary acidic protein (GFAP) (DAKO). Cultures were incubated for 2 h in a 1:1000 dilution of the GFAP rabbit primary antibody in PBS and visualized with a 1:200 dilution of Alexa Fluor 568 goat anti-rabbit secondary antibodies (Invitrogen) in PBS. Images of astrocytes grown on aligned and random matrices were obtained with a Leica TCS-SP2 AOBS confocal microscope. For this study, astrocytes were seeded on at least six matrices (three aligned and three random) and the experiment repeated at least three times.

Astrocytes-Dorsal Root Ganglia Co-culture

To test the extent to which astrocytes affect the growth of DRG neurites on electrospun PDS matrices, DRGs were co-cultured with astrocytes that were first seeded on matrices as outlined above. Specifically, astrocytes were grown on either aligned or random matrices for 10 d until confluent. DRGs were then pipetted onto these astrocyte-seeded matrices, pinned down and cultured for an additional 10 days.

Immunocytochemistry was performed using a primary antibody cocktail of GFAP and TuJ1, and confocal images obtained for analysis. To determine the length of DRG neuritic outgrowth on aligned matrices with and without astrocytes, a distance measurement was made from the center of the DRG to the furthest extent of overall neuritic outgrowth. Student's t-test was used to determine statistical significance. For this study, astrocytes and DRGs were seeded and pinned respectively on at least six matrices (three aligned and three random) and the experiment repeated at least three times.

Results

Using the apparatus shown in Figure 2.1, PDS was electrospun onto a mandrel with a rotation speed of either 5000 rpm or approximately 10 rpm to fabricate matrices containing fibers with varying degrees of alignment. SEM was then used to visualize the extent to which a mandrel speed of 5000 rpm generates aligned fibers (aligned matrix) and a mandrel speed of approximately 10 rpm generates randomly orientated fibers (random matrix). Although the difference in fiber alignment between the two types of matrices was evident at the SEM level (Figure 2.2A and D), a more objective determination of alignment was desirable to establish whether fiber alignment was significantly different. To achieve this, we employed a 2D FFT methodology. Such an approach quantitatively analyzes the extent to which the population of fibers in the matrix is aligned with respect to each other, thereby establishing a general direction of alignment of the entire fiber population. After executing the algorithm on a converted grayscale

SEM image cropped down to a square (Figure 2.2A and D), the immediate output of a 2D FFT is a frequency spectrum (Figure 2.2B and E). The distribution of the pixels in the frequency spectrum can be used to evaluate fiber alignment in an original data image. A data image containing random elements produces a frequency spectrum with pixels distributed about the center in a symmetrical distribution (Figure 2.2B). Conversely, a data image containing aligned elements produces a frequency spectrum with pixels distributed in an elongated ellipse (Figure 2.2E). Figure 2.2C and F are graphs of a 2D FFT analysis on representative images of a random and aligned matrix, respectively. The height and width of the peaks indicate the uniformity of fiber alignment. The axis of distribution of the pixels in the frequency spectrum reports the principal axis of orientation (Ayres et al., 2006, 2008). Fibers electrospun at a high mandrel speed were displayed graphically as having a dominant orientation toward a specific direction (approximately 180°, or a vertical orientation, in this case), thereby indicating a significant degree of alignment for the general fiber population. In contrast, for a random matrix, the presence of four small symmetrical peaks (associated with edge artifact) indicates that there is no preferential alignment. Moreover, the degree of fiber alignment in both types of matrices is consistent between electrospun samples fabricated for this study and those used in subsequent experiments.

After confirming the matrix alignment, DRGs were pinned to matrices, cultured for 10 d, fixed and immunolabeled for the TuJ1 neuronal marker. Representative, low-power, fluorescent images of the DRGs on aligned and random matrices showed different patterns of neuritic outgrowth (Figure 2.3). On a random matrix, neurites grew radially

outward from the ganglion without preference to any specific direction, generating a round, spokes-of-a-wheel appearance (Figure 2.3A). In contrast, on an aligned matrix, most neurites grew preferentially along a particular axis (Figure 2.3B). Using reflectance confocal microscopy, it was confirmed that this axis of growth was in the same orientation as the underlying fibers of the matrix (data not shown). Although a few neurites were not oriented initially to the direction of the underlying matrix, most eventually turned and continued their extension in the direction of the underlying fibers. Additionally, neurites growing in the direction of the underlying matrix grew faster than those growing perpendicular to the aligned fiber axis or on random matrix.

An observation that is not apparent in these images but evident in cultures grown for extended periods is that neurites began to show signs of cellular deterioration, such as the presence of membrane blebbing and vesiculation (Figure 2.6A). These changes are common in neurons grown *in vitro* for extended periods in the absence of supportive or ECM substrata. Considering this and the fact that the matrices are generated from a resorbable material (PDS) that dissolves with time, we hypothesized that a glial substrate might provide a more stable, supportive interface between the resorbable matrix and the outgrowing neurites. Accordingly, astrocytes purified from P3 rat cortices were seeded onto aligned and random matrices and grown for 7 d. Subsequently, the matrices were fixed and immunolabeled for the astrocytic marker GFAP. Confocal images of astrocytes grown on both types of matrices show that these cells grew readily on electrospun PDS (Figure 2.4). However, astrocytes grown on a random matrix extend processes that are positioned more randomly (Figure 2.4A and C). This is in striking contrast to astrocytes

grown on an aligned matrix (Figure 2.4B and C), for which process extension mirrors the orientation of the underlying fibers.

To test the extent to which astrocytes might improve the growth of DRG neurites on electrospun PDS matrices, DRGs were grown on matrices pre-seeded with astrocytes. First, dissociated astrocytes were seeded on aligned and random matrices and incubated for 10 d before DRGs were pinned onto the astrocyte-seeded matrices and incubated for 10 d. Subsequently, the matrices were fixed and dual-immunolabeled for TuJ1 and GFAP. Following 20 d of growth, astrocytes seeded on both matrices extended longer processes than after only 7 d of growth (Figure 2.5A and C). Moreover, astrocytic processes were aligned to match the orientation of the underlying PDS fibers within each matrix, which is consistent with a shorter culture period. DRGs grown on a substrate of randomly-oriented astrocytes grew radially outward from the ganglion without preference to any specific direction (Figure 2.5A and B). Conversely, DRGs grown on a substrate of aligned astrocytes (Figure 2.5C and D) displayed a similar alignment and extended longer processes than when grown on a glia-free matrix (Figure 2.5F). Many of the neurites on the aligned, astrocyte-seeded matrices reached the border of the matrix and continued growing on its opposite side. In both cases (aligned and random), processes changed direction readily to grow along astrocytic processes (Figure 2.5E). Moreover, DRGs grown on either seeded matrix displayed less fasciculated outgrowth than observed on PDS matrices alone and appeared to be more robust, as evidenced by the lack of vesiculations and membrane blebbing (Figure 2.6).

Discussion

In this study, we have examined the potential use of electrospinning to engineer a polarized matrix for axonal guidance. By varying the rate of rotation of the mandrel, matrices containing aligned fibers and randomly oriented fibers were fabricated from PDS. The degree of fiber alignment was determined visually by SEM and quantified by 2D FFT analysis. Both neurons and astrocytes were grown separately and in combination on these matrices to assess biocompatibility and growth dynamics. Specifically, when E16 DRGs were placed on these matrices and allowed to grow for 10 d, the direction of the projecting neurites matched the orientation of the underlying PDS fiber population. Moreover, on aligned matrices, the length of neuritic outgrowth exceeded that seen on random matrices. After 10 d in culture, however, neurites began to exhibit evidence of necrosis. In view of this, we tested the extent to which cortical astrocytes are compatible with these matrices and whether their presence affects DRG growth. When seeded on these PDS matrices, astrocytes grew robustly and the orientation of process outgrowth matched that of the underlying matrix. When DRGs were grown on these glial substrates, they exhibited no evidence of necrosis and their neurites aligned with astrocytes and displayed longer process outgrowth than on aligned PDS matrix alone. Collectively, these experiments demonstrate the potential for electrospinning to generate an aligned matrix that influences both the directionality and dynamics of DRG neuritic growth.

In addition to generating an aligned matrix to influence the directionality of neuritic outgrowth, the process of electrospinning can be manipulated further to generate

matrices with additional characteristics that mimic more closely the *in vivo* environment of the central nervous system (CNS). Specifically, ECM molecules such as collagen and elastin remain biologically active when electrospun into matrices (Boland et al., 2004). These experiments provide evidence that viable ECM molecules in the CNS can also be electrospun into matrices to influence neuritic outgrowth. In our study, however, we elected to use the synthetic molecule PDS as the solute for electrospinning because of its proven biocompatibility, which is indicated by its inability to elicit an immune response, and its structural stability in biological tissue. These characteristics prevent the matrix from being remodeled in a manner that compromises its fiber polarity within a short time frame, which is relevant when considering the use of this matrix to bridge lesioned areas of the CNS. Specifically, the alignment of the fibers in the matrix will remain stable, allowing regenerating axons sufficient time to cross the lesion into healthy target tissue. Moreover, by seeding the PDS matrix with astrocytes, we have generated a cellular bridge that retains alignment stability while providing crucial trophic support. In the next two chapters, further modifications to the electrospinning process to generate a scaffold that may be able to counter the inhibitory compounds seen after SCI as well as the testing of these superior matrices are discussed.

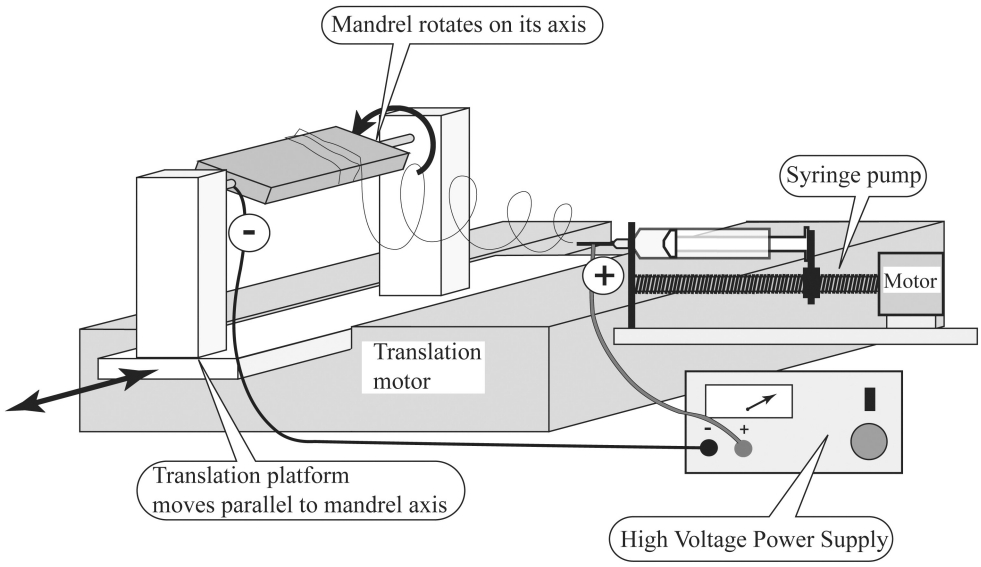

Figure 2.1. The electrospinning apparatus. Key system components include a solution reservoir (syringe), nozzle (18-gauge, blunted, metallic needle), high-voltage DC power supply, and grounded target (rotating mandrel).

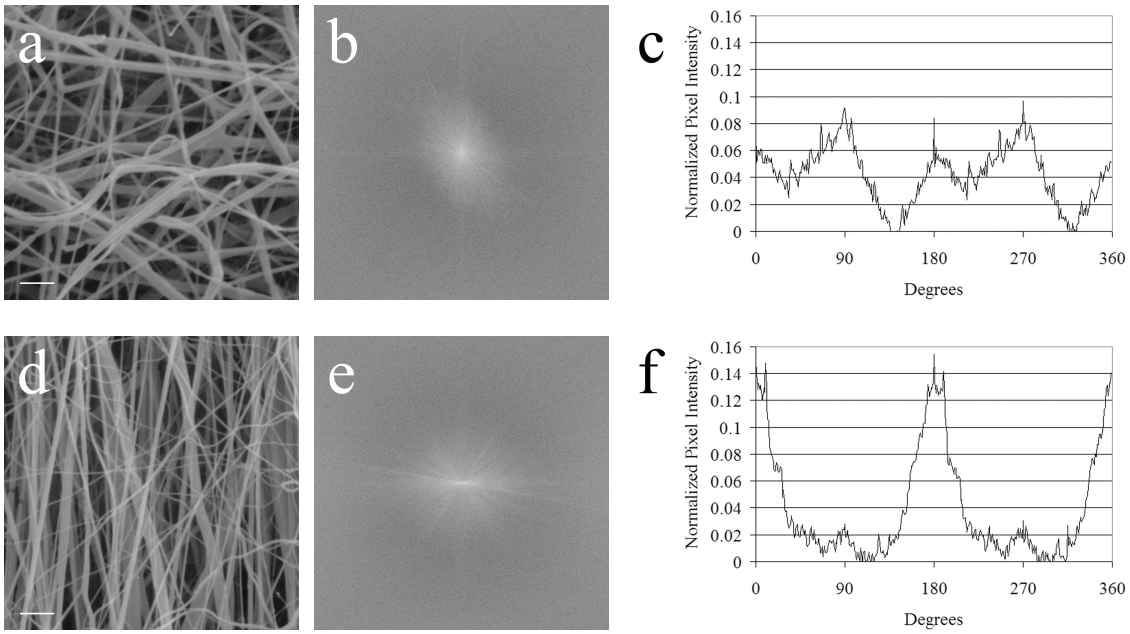

Figure 2.2. Generation of aligned and randomly oriented PDS matrix fibers. (A) SEM shows more randomly oriented fibers in a representative random matrix, generated by using a slower mandrel rotation speed (approximately 10 rpm). (B) Raw output of the 2D FFT alignment analysis of a random matrix. The more radially symmetrical silhouette of the 2D FFT is consistent with fibers that are oriented in random directions. (C) Radial plot of the summations of relative pixel intensity at a radius versus the angle (°). The periodicity of the graph is caused by the inherent symmetry of the raw 2D FFT output. The smaller, broader peaks reflect a more random distribution of directionality. (D) SEM showing more consistently oriented fibers in a representative aligned matrix that is generated using a mandrel rotation speed of 5000 rpm. (E) Raw output of the 2D FFT alignment analysis of an aligned matrix. The slender profile of the silhouette indicates fiber alignment. (F) A taller, narrower peak at approximately 180° indicates the general direction in which the fiber population is oriented. Scale bars (A and B) = 10 μm.

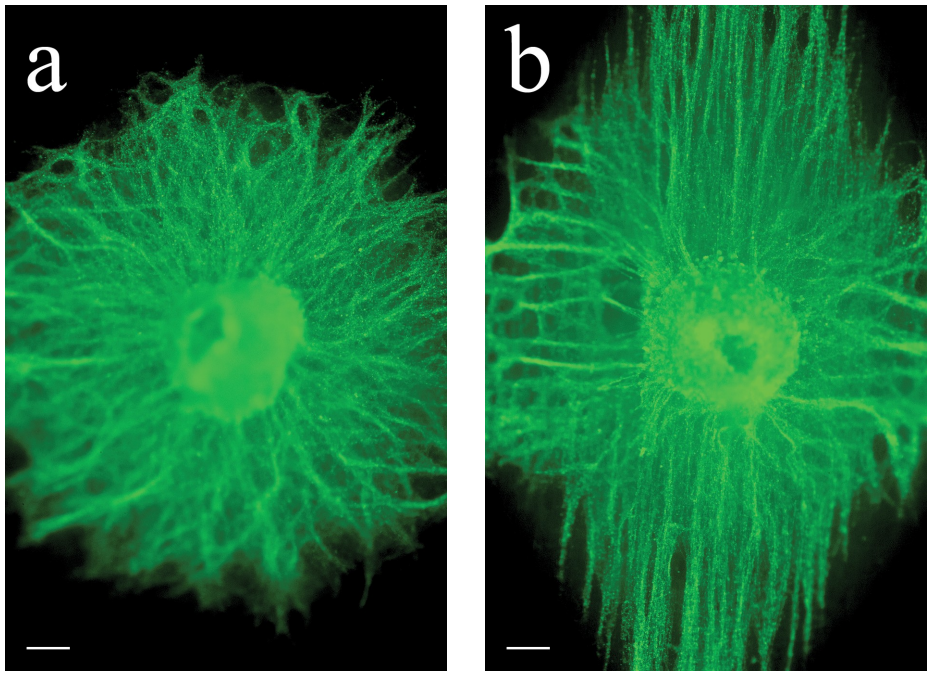

Figure 2.3. Fiber alignment of the electrospun matrix is conferred to pinned DRGs. Low-power, wide-field, fluorescent image of a representative DRG immunostained for TuJ1 (green) on matrix fixed 10 d after pinning. (A) DRG on a random matrix fixed 10 d after pinning. DRG neurites grown on a random matrix displayed a tortuous growth pattern that reflects the underlying matrix. (B) In contrast to DRG grown on a random matrix, neurites grew preferentially in one direction (vertical in this image) that reflects the orientation of the underlying matrix fibers. Scale bars (A and B) = 200 μm.

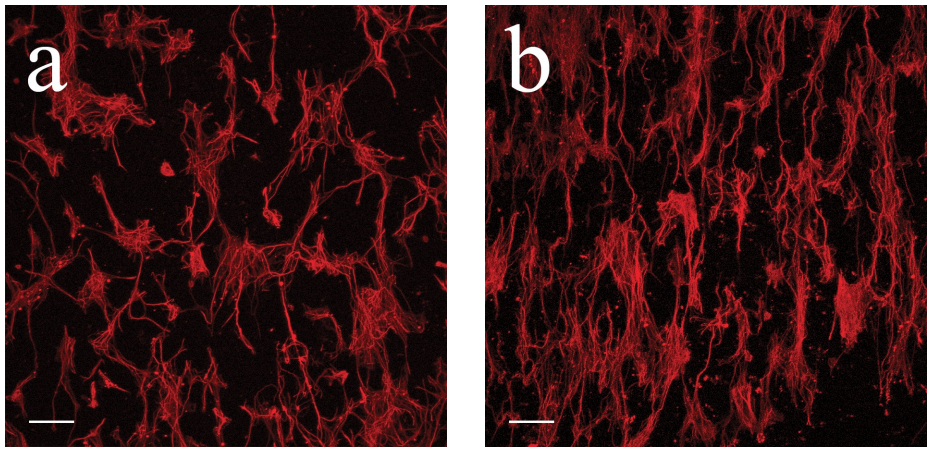

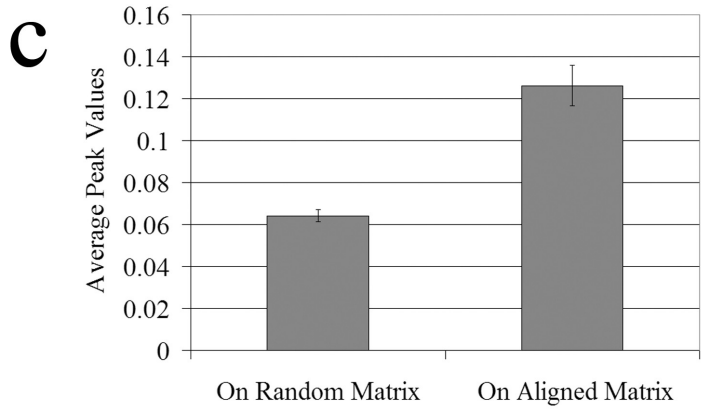

Figure 2.4. Fiber alignment of the matrix is conferred onto seeded astrocytes. Confocal images of astrocytes, immunostained with GFAP (red), grown on a random (A) or aligned matrix (B) for 7 d after seeding. In both instances, the orientation of the underlying matrix fibers is conferred to the astrocytic processes. (C) The average peak value of the 2D FFT analysis (radial plot) on astrocytes seeded on matrices. Astrocytic process alignment on random and aligned matrices is statistically different ($p = 0.004$). Scale bars (A and B) = 100 μm.

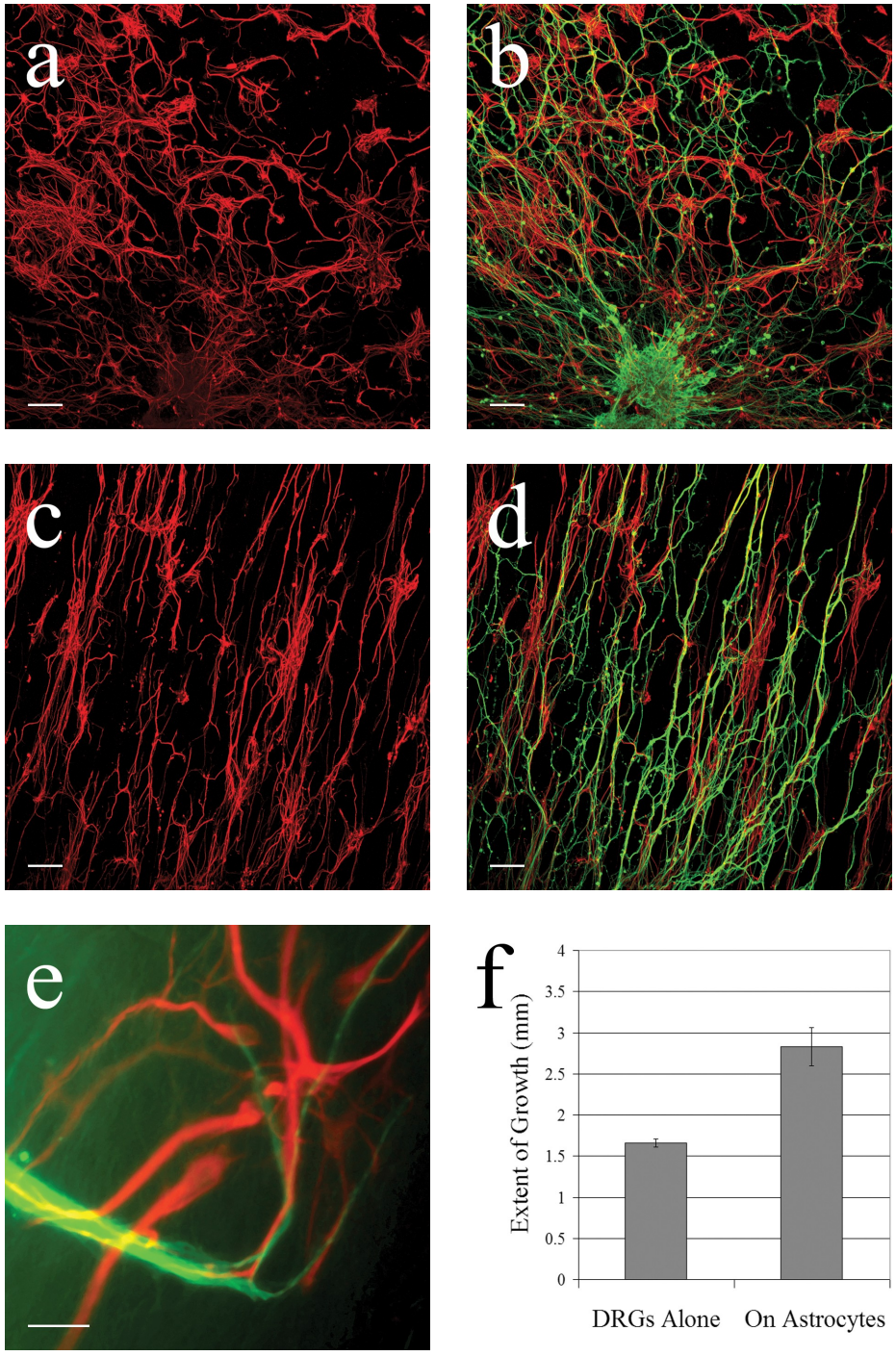

Figure 2.5. Aligned astrocytes influence the directionality and length of DRG neuritic outgrowth (A to D). Confocal images showing DRG neurites (green) grown on astrocytes (red) seeded on either random (A and B) or aligned (C and D) matrices. In the presence of randomly oriented astrocytes (B), the orientation of the neurites is radial, growing out from the ganglion in all directions, whereas neurites grown on an aligned astrocyte-seeded matrix (D) display a similar alignment. (E) High-power, wide-field, fluorescent image showing that neurites change direction to grow along astrocytic processes. (F) The length of DRG neuritic outgrowth on aligned matrices with or without seeded astrocytes. Outgrowth is significantly longer ($p = 0.008$) when grown on astrocyte-seeded matrices. Scale bars (A to D) = 100 µm. Scale bar (E) = 30 µm.

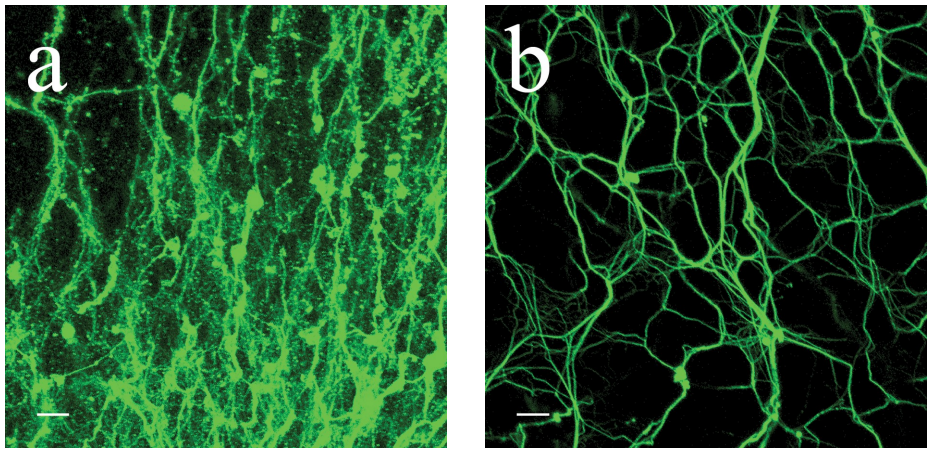

Figure 2.6. DRGs on astrocyte-seeded matrices grew more robustly, as evidenced by lack of vesiculation and fasciculation. DRGs grown for 10 days on (A) a PDS matrix alone in the absence of astrocytes and (B) on an astrocyte-seeded PDS matrix. Astrocytes cannot be visualized because of the filter selection for this fluorescent image. Scale bars (A and B) = 10 μm.

Chapter 3

Evaluating the Incorporation of Nerve Growth Factor and Chondroitinase ABC into an Electrospun Scaffold by Utilizing an Alginate Delivery System

Introduction

One of the many obstacles to spinal cord injury (SCI) repair following trauma is the formation of a cyst that impedes axonal regeneration. Accordingly, as described in the previous chapter, we examined the potential use of electrospinning to engineer an implantable polarized matrix for axonal guidance. Briefly, in a series of *in vitro* studies, we found that matrix alignment can be conferred to extending neurites, demonstrating the potential for electrospinning to generate an aligned matrix that can be implanted into the cyst so as to guide regenerating axons post-SCI.

However, many other obstacles hinder axonal regrowth in addition to the cyst. As previously described, astrocytes within the SCI lesion site proliferate, hypertrophy, and begin to express chondroitin sulfate proteoglycans (CSPG), which represent potent inhibitors to axonal regeneration. At the neuronal level, axotomy of motor and sensory

neurons results in the loss of neurotrophic support by target tissue, furthering the extent of neuronal cell death. Additionally, the presence of myelin debris, as a result of oligodendrocyte death, acts as a potent inhibitor to axonal regeneration. Collectively, these cellular responses to SCI represent major impediments to axonal regeneration. Mono-therapies that address each of these obstacles to regeneration individually have resulted in only limited axonal regrowth and functional recovery. To date, no single intervention has been devised to collectively address all of these obstacles to regeneration after SCI.

In view of this, we hypothesized that our previously tested electrospun matrix can be supplemented with compounds that can promote neuronal survival and neutralize the growth-inhibitory proteins associated with gliotic scar. One crucial criterion for optimizing axonal regeneration following SCI is to promote the survival of neurons whose axons have been severed. It is well-known that neurotrophic factors are produced in the central nervous system (CNS) following trauma (Dougherty et al., 2000; Krenz and Weaver, 2000). Their presence mitigates injury-induced neuronal cell death and promotes axonal plasticity and regeneration (Bregman et al., 1999; Zhou et al., 2003). Furthermore, both *in vitro* and *in vivo* studies have begun to establish the extent to which particular trophic factors stimulate axonal regeneration of the varying descending motor tracts and ascending sensory systems of the spinal cord. For example, one particular neurotrophic factor, nerve growth factor (NGF), is essential for the growth and survival of several populations of sensory neurons that project axons through the spinal cord (Tuszynski et al., 1994; Acosta et al., 2001). Accordingly, in a series of *in vitro* dorsal

root ganglion (DRG) bioassays, NGF was incorporated into electrospun matrices with the use of an alginate delivery system and the extent to which NGF remains bioactive was assessed.

In addition, we sought to investigate the extent to which we could incorporate other proteins into the matrix that could facilitate axonal regeneration. Specifically, it is well-documented that following CNS injury astrocytes become reactive and begin to express CSPGs, which are well-known inhibitors to axonal regrowth. Many *in vitro* and *in vivo* studies have established that the enzyme chondroitinase ABC (ChABC) is capable of inactivating the inhibitory functions of these proteins. Accordingly, in another series of *in vitro* bioassays, ChABC was incorporated into electrospun and the extent to which the enzyme remains bioactive was assessed.

Materials and Methods

Generation of Alginate Microspheres

Found in the cell walls of certain brown algae and seaweeds, alginate is a viscous gum that is used in many industrial, food processing, and biomedical applications as a waterproofing, thickening, or detoxification agent. Its apparent ease of gelation and biocompatibility can be exploited, providing a delivery vehicle for NGF in our study. Specifically, almost any protein of interest can be encapsulated in alginate microspheres and dried and upon hydration, release their content in a sustained manner (Noushi et al., 2005).

Alginate microspheres were generated by electrospraying technique. A solution of 0.05-mg/ml sodium alginate and 0.05-mg/ml protease-free bovine serum albumin (BSA) (used as a carrier) was first produced and subsequently the solute of interest in the quantity of interest was added to 1 ml of this solution. The solution was then loaded into a 5-ml syringe tipped with an 18-gauge blunt-end needle (Kontes) and the syringe installed onto a vertically mounted syringe driver such that the needle was pointed down (Figure 3.1). The needle was connected to the anode of a high voltage direct current (DC) power supply (Spellman CZE1000R) via a wire outfitted with an alligator clip. A metal plate, which was connected to the cathode, was placed beneath the syringe driver. A 150-mm glass Petri dish filled with 2% calcium chloride solution was placed on the metal plate to facilitate collection of the alginate microsphere. Upon switching on the power supply, the resulting electric field induced the formation of a fine aerosol mist of alginate and upon contact with the calcium chloride solution, microsphere formation takes place. Microspheres were collected and washed by centrifugation in a 2% calcium chloride solution supplement with 10% isopropanol and finally pelleted and the supernate removed. To further dry the alginate, the remaining sediment is diluted 1:4 in 1,1,1,3,3,3-hexafluoro-2-propanol (HFIP) by volume and the mixture is placed in a syringe. At this point, the HFIP, being the densest liquid in the mixture will settle to the bottom and it is subsequently dispensed, leaving the semi-dry alginate microspheres in an interface layer just above. After dispensing the bulk of the HFIP, the tri-layered mixture is deposited in another container and by way of yet another syringe and fine hypodermic needle, the bottommost and topmost layers are removed to a greatest extent possible

without disturbing the middle layer containing the microspheres. Finally, the remaining middle layer is frozen in liquid nitrogen and subsequently lyophilized. The alginate is ready for use after rehydration.

Although the collection rate is incredibly difficult to measure and a 100% collection cannot be assumed, it is estimated that conservatively that we collect at least 50% of the microspheres that can potentially form. With that in mind, 5 µg of NGF (Invitrogen) was incorporated into the alginate microspheres such that when microspheres were allocated to individual cultures, the amount of NGF contained in the microspheres would have the same order of magnitude as compared to the amount contained in DRG culture media. In contrast, control microspheres were generated with 5 µg of protease-free BSA.

Dorsal Root Ganglia Isolation

DRGs were isolated from embryonic day 16 (E16) Sprague Dawley embryos as described previously in Chapter 2. Briefly, embryos were removed from the uterus of a gravid rat and dissected open anteriorly to expose the developing spinal cord. The entire cord was then dissected free from its rostral end and placed in Leibovitz L-15 media with 10% fetal bovine serum (FBS). The attached DRGs were then plucked off with fine tip forceps.

Nerve Growth Factor Bioassay

To test the effectiveness of using alginate to deliver NGF, dissected DRGs were placed into poly-L-lysine-coated wells of a 48-well plate. Each batch of alginate microspheres were rehydrated in culture media. Assuming 50% collection, as previously discussed, a volume of media containing a desired quantity of NGF, which is incorporated in the microspheres, can be calculated. After ensuring a uniform distribution of the microspheres, a calculated volume containing microspheres having a desired quantity of NGF that would ultimately provide a concentration of 0.3 μg/ml in the culture was transferred into Transwell membrane inserts and the inserts were placed in wells containing DRGs. In normal DRG culturing conditions, a concentration of 0.1 μg/ml is used. Since the microspheres do not release their contents all at once, a higher starting concentration was desired. Microspheres containing BSA were similarly deployed to act as controls. Incubation media consisted of Eagle's minimum essential medium with glutamine supplemented with 10% glucose and 5% FBS. Additional negative and positive controls were set up by incubating DRGs with NGF-free and NGF-containing media, respectively. A schematic of the experimental setup is shown in Figure 3.3. This assay was performed three times per animal with populations of E16 rat DRGs from four different animals.

To visualize the DRGs, the cultures were first fixed in 4% paraformaldehyde and subsequently immunolabeled for the β-tubulin neuronal marker TuJ1 (Covance) as previously described in Chapter 2.

To quantify the extent of growth exhibited by the DRG cultures, the area occupied by the DRG neuritic processes was measured. Wide-field fluorescence images of the DRGs were obtained and loaded into Adobe Photoshop. Using the "contrast" tool, the contrast of the image is increased such that the colored pixels depicting neuritic processes reach maximum color intensity. These pixels were then counted and since each pixel has an equivalent area, an actual area can be estimated without bias.

Electrospinning

As before, polydioxanone (PDS) was again used to fabricate matrices in this study. However, instead of using a rotating grounded mandrel, an air-gap electrospinning system was adopted. Air-gap electrospinning utilizes two separate fixed grounded posts in which the solution jet whips back and forth between the grounds, resulting in the deposition of fibers between the posts. The rationale for migrating to this system is that this methodology offers superior fiber alignment. In addition, this system allows for the spinning of 3-dimensional cylinders, which is required when these matrices are ultimately tested in animal models of SCI.

Briefly, for each matrix, a PDS filament was dissolved in the solvent HFIP at a concentration of 125 mg/ml and the solution was deposited in a syringe, which was mounted onto a syringe driver set to deliver 5 ml/hr. Though the exact placements of the various electrospinning components differed between runs and required a bit of trial and error for the optimal positioning of the two grounded posts, generally the air gap between

posts was set between 3 to 5 cm and the assembly containing the posts was placed no more than 20 cm away from the nozzle.

Chondroitinase ABC Bioassay

To test the extent to which ChABC remains bioactive when the enzyme is electrospun into matrix directly, a stripe bioassay was employed. Aggrecan, a CSPG known to inhibit axonal growth (Lemons et al., 2003), was deposited in stripe lane fashion via a micropipette onto poly-L-lysine-coated Thermanox cover slips. Upon the drying of the aggrecan, DRGs were pinned onto the cover slips between the CSPG lanes and the cover slips were placed in Petri dishes containing NGF-added DRG culture media (formula described previously). ChABC (0.5 U per matrix) was mixed into the PDS spinning solution and matrices were fabricated. After spinning, these matrices were cut into small pieces such that each piece contained enough ChABC to supply a concentration of 0.05 U/ml in culture conditions. After sterilizing in 70% ethanol, a piece of the cut ChABC-containing matrix was placed in each experimental dish while a piece of the cut BSA-containing matrix was placed in each control dish. A schematic of the experimental setup is shown in Figure 3.5. This assay was performed three times per animal with populations of E16 rat DRGs from four different animals.

To visualize the DRGs and aggrecan lanes, the cultures were first fixed in 4% paraformaldehyde and subsequently immunolabeled for the β-tubulin neuronal marker TuJ1 (Covance) and the CSPG marker CS-56 (Sigma). In addition to the staining steps

outlined in Chapter 2, a denaturing step utilizing 2-M hydrochloric acid is included before blocking.

Results

Once we established that electrospinning can be used to generate a biocompatible bridge that provides directionality to axonal regrowth (Chapter 2), we next sought to establish the extent to which proteins that facilitate regeneration can be incorporated into the bridging matrix. First, we sought to supplement the matrices with a neurotrophin, namely NGF, via the use of an alginate delivery vehicle. NGF-containing alginate microspheres of uniform diameter were produced via electrospraying (Figure 3.2). To test the effectiveness of using alginate to deliver NGF and the extent to which the neurotrophin remains bioactive, DRGs, which are a clusters of neurons that convey sensory information through the spinal cord and require NGF for their survival, were cultured in wells of a 48-well plate under the following conditions: in the absence of NGF in the media, in the presence of NGF in the media, in the presence of BSA-containing microspheres, and in the presence of NGF-containing microspheres. Following 3 d of incubation, DRG neurites displayed predictably scant outgrowth in the absence of NGF (Figure 3.3B). In the presence of NGF in the culture media, neuritic outgrowth was also unsurprisingly evident (Figure 3.3D). However, the NGF-induced neuritic outgrowth was even more pronounced in cultures where DRGs were exposed to NGF-containing alginate microspheres (Figure 3.3F). The readily apparent difference in the extent of outgrowth between NGF in media and NGF supplied by the alginate is

likely the result of the gradual increase in concentration of NGF in the media with time. To quantify the extent of outgrowth exhibited by the DRG cultures, the area occupied by the neuritic processes of each DRG was measured by counting pixels of digital images. The group means of the estimated area occupied by a DRG are shown in Figure 3.4. Finally, electrospun PDS matrices containing NGF-incorporated alginate microspheres were fabricated and tested on DRG cultures and similar results were obtained (data not shown).

We next sought to investigate the extent to which we can incorporate other proteins of interest into the matrix that could facilitate axonal regeneration. Specifically, as mentioned previously, ChABC has been shown in numerous occasions its ability to elicit improved axonal regrowth and in some cases functional recovery following SCI by neutralizing the inhibitory nature of CSPGs. In view of its success, we sought to incorporate ChABC into electrospun matrices as another means of making the post-SCI microenvironment more growth permissive. Since reactive astrogliosis and gliotic scar formation have a longer time horizon, there needs to be a somewhat delayed yet sustained release in order for ChABC to be useful. Accordingly, it was decided that ChABC be incorporated directly into the PDS matrix during the electrospinning process. To test the extent to which enzyme remains bioactive in the matrix, DRG neurons were cultured between lanes of aggrecan, a known CNS CSPG, and an appropriately sized piece of matrix incorporated with or without ChABC was placed in each culture. Following 7 d of incubation, in the absence of the enzyme, DRG neurites avoided the aggrecan lanes thereby demonstrating the extent to which CSPGs can inhibit axonal growth (Figure

3.5B). In contrast, DRGs grown in the presence of the enzyme, which is released from the matrix, displayed no inhibition and readily grew across the aggrecan lanes (Figure 3.5D). These results demonstrate that the enzyme is released from the matrix in a bioactive form and neutralizes the axon growth-inhibitory properties of CSPG.

Collectively, these studies point toward a novel approach by which a biocompatible scaffold can be implanted into the fluid-filled cyst post-SCI, providing regenerating axons with a directional path across the lesion site as well as trophic and inhibitor-neutralizing support in a single package.

Discussion

One of the many pathologic obstacles of spinal cord repair following contusive trauma is the formation of a fluid-filled cyst across which regenerating axons have to traverse in order to reinnervate their distal targets. To this end, in Chapter 2, we examined and demonstrated the potential use of electrospinning to engineer an implantable directional matrix for axonal guidance. In view of the recognition that successful SCI therapies require a multifaceted tactic, we proposed a novel approach of incorporating into electrospun guidance matrices pharmacologic agents that can promote neuronal survival and neutralize inhibitory molecules associated with the gliotic scar. Specifically, NGF was encapsulated into electrospun alginate microspheres and the extent to which this protein remains bioactive was assessed with DRG bioassays. These microspheres were placed in Transwell membrane inserts over the ganglia so as to provide the only source of NGF in the culture. Their presence supported vigorous

neuritic outgrowth in contrast to control microspheres containing only albumin. The bioactivity of NGF was similarly preserved when NGF-containing microspheres were incorporated into electrospun matrices. We next sought to investigate the incorporation of ChABC into the matrix as it has been previously shown that this enzyme can reduce the axonal growth-inhibition of various CSPG. Stripes of aggrecan, a CSPG found in the CNS, were placed on cover slips with DRGs pinned in between the inhibitory lanes. In control cultures, DRG neurites did not extend onto aggrecan lanes. However, upon exposure of the cultures to ChABC-incorporated matrices, the growth-inhibitory nature of aggrecan was neutralized and neurites grew extensively across the stripes. Collectively, these experiments point toward a novel SCI therapeutic approach of generating electrospun scaffolds that can directionally guide axons across the lesion site while providing trophic and inhibitor-neutralizing support.

A remarkable observation that was made in the present study was the dramatic difference in the outgrowth pattern of DRGs when cultures were exposed to NGF in the media versus NGF in the alginate microspheres. When DRGs were exposed to NGF in the culture media, the DRG displayed a growth that was prototypical—neurites grew radially and linearly outward from the ganglion and producing a round, spokes-of-a-wheel appearance. When DRGs were exposed to the alginate microspheres containing the NGF, the neurites similarly grew outward radially from the ganglion. However, the appearance of the neuritic processes in this experimental perturbation was not linear, but highly branched. In these cultures, nearly all the neuritic processes were seen to crisscross and overlap over and over at almost all locations occupied by the DRGs. Thus,

in view of our attempt to measure the area occupied by the neuritic processes by way of counting pixels in high resolution digital images and our subsequent detection of quantitative differences in the amount of growth between experimental groups, we surmised that we probably still underestimated the extent of growth in the culture exposed to the alginate microspheres. Since the amount of microspheres that was initially deposited in these experimental cultures was determined assuming a 50% collection estimate after electrospinning, it was first suggested that the dramatic outgrowth seen was perhaps due to a much higher concentration of NGF, which could have potentially reached at much as six times the level used in the positive control culture if the NGF was release all at once from the alginate. As introduced in the first chapter, the low-affinity p75 neurotrophin receptor (p75NTR) may act as a sink for the excess NGF and synergizes with the tropomyosin receptor kinase (Trk) receptor, specifically TrkA, to produce the extraordinary branched pattern of DRG process outgrowth seen. However, in a side experiment where DRGs were exposed to 10μg/ml of NGF (ten times the normally used concentration), the branched pattern of outgrowth was not observed. A second explanation is that perhaps the alginate may have some synergistic effect with the NGF. Though no known mechanism would suggest that this would occur, we nevertheless tested this hypothesis in yet another side experiment where DRGs were exposed to NGF in the culture media while blank alginate microspheres were deposited in the cultures. Again, only the typical radially linear outgrowth pattern was seen. A third possibility that may cause the dramatic branching is that perhaps the neurons respond to a gradual increase in NGF concentration in the media from the alginate

release. Such an increase of neurotrophin may result in a temporal shift of the cellular profile of activated receptors. The p75NTR, having low affinity to the neurotrophins, would not bind the NGF early on during the experiment but would bind later when the NGF concentration in the media increased. Though we did not attempt to prove this hypothesis, this explanation can be established with a simple experiment where DRGs would be exposed to a gradually increasing concentration of NGF.

Another notable observation involves the ChABC-CSPG stripe bioassays. Though DRG neurites undoubtedly grew over the aggrecan lanes when exposed to ChABC, the DRG processes displayed a webby fasciculated appearance. As mentioned in Chapter 2, it is well-known that neurites often fasciculate when elongating on a less than optimal substrate and that cell adhesion molecules and their interactions with the substrate play a significant role in this response (Acheson et al., 1991; Honig and Rutishauser, 1996; Tang et al., 1994). In an *in vitro* study, Snow et al. demonstrated how DRG neurites readily fasciculate upon contact with locales containing very low permissive concentrations of CSPGs, stayed fasciculated while elongating over such areas, and defasciculated upon leaving the CSPG zone (2003). While ChABC was not employed in the study completed by Snow et al., their results show that even a minute amount of an inhibitor, though not able to outright prevent outgrowth over the inhibitory areas, was able to cause neuritic fasciculation. In our study, ChABC cleaved the glycosaminoglycan chains on the aggrecan molecules, which is known to reduce the inhibitory nature of the CSPGs. However, though less understood, there are also direct protein core effects, which may partially explain the fasciculation seen in our cultures.

Hence, in our study, while the ChABC is able to reduce the inhibition of the aggrecan such that outgrowth is possible on the CSPG lanes, the reduction is not enough to cause defasciculated growth. Fasciculated growth is not necessary undesirable, as it has been suggested that fasciculation may promote axonal pathfinding and prevent deviant sprouting post-injury (Snow et al., 2003).

In the experiments outlined in this chapter, NGF was selected and tested in bioassays experiments. However, the presence of NGF in the microenvironment post-SCI has been shown to cause undesirable side effects such as autonomic dysreflexia and neuralgia caused by the aberrant spouting of certain neurons (Krenz et al., 1999). Autonomic dysreflexia is a condition characterized by an immense sympathetic discharge caused by noxious stimuli that results in increased blood pressure via widespread vasoconstriction. Neuralgia, also known as neuropathic pain, is pain that is not a result of pain receptor activation. Both of these adverse conditions are debilitating and potentially dangerous, with the former being a medical emergency. In view of this, we seek to incorporate other factors into our matrices that may be beneficial post-SCI. Since we have demonstrated that NGF can successfully be integrated into our matrices and delivered, other factors can be incorporated to aid in the survival and resprouting of other neuronal groups. Exogenous administration of brain-derived neurotrophic factor (BDNF) and neurotrophin-3 (NT-3) have been found to preserve the neuroplasticity of corticofugal fibers and in some cases led to functional recovery post-SCI (Namiki et al., 2000; Iarikov et al., 2007). Additionally, insulin-like growth factor-1 (IGF-1), a polypeptide with sequence homology to insulin released primarily by the liver in

response to growth hormone that affects human cells almost ubiquitously, has been shown to promote the growth of projecting axons and dendrites, synaptogenesis, and neuroprotection (Niblock et al., 2000; Cheng et al., 2003; Ozdinler and Macklis, 2006; Hung et al., 2007). Hence, these factors such as BDNF, NT-3, and IGF-1 can concomitantly be delivered via alginate microspheres by way of an electrospun matrix implant.

In other experiments outlined in this chapter, ChABC was selected to be incorporated into our electrospun matrices so as to neutralize the CSPGs seen after SCI. However, other axon growth-inhibitory molecules have also been identified. One notorious group of inhibitors is found to be associated with central myelin. Members of this group include Nogo-A, myelin-associated glycoprotein, and oligodendrocyte-myelin glycoprotein (McKerracher et al., 1994; Chen et al., 2000; Kottis et al., 2002). All three have been demonstrated through *in vitro* and *in vivo* studies to cause growth cone collapse by their binding to the Nogo-66 receptor (Liu et al., 2002; Xie and Zheng, 2008). In view of this, we seek to incorporate a compound into our matrices that can overcome the inhibitory effects of these myelin-associated proteins. One such compound of interest is bucladesine, which is a cell permeable cyclic adenosine monophosphate (cAMP) analog. Also known as dibutyryl cAMP, this cyclic nucleotide has been shown to alter the growth state of older neurons and induce axonal growth in the presence of myelin-associated inhibitors (Cai et al., 1999; Gao et al., 2003; Domeniconi and Filbin, 2005). Accordingly, bucladesine is an excellent candidate for incorporation.

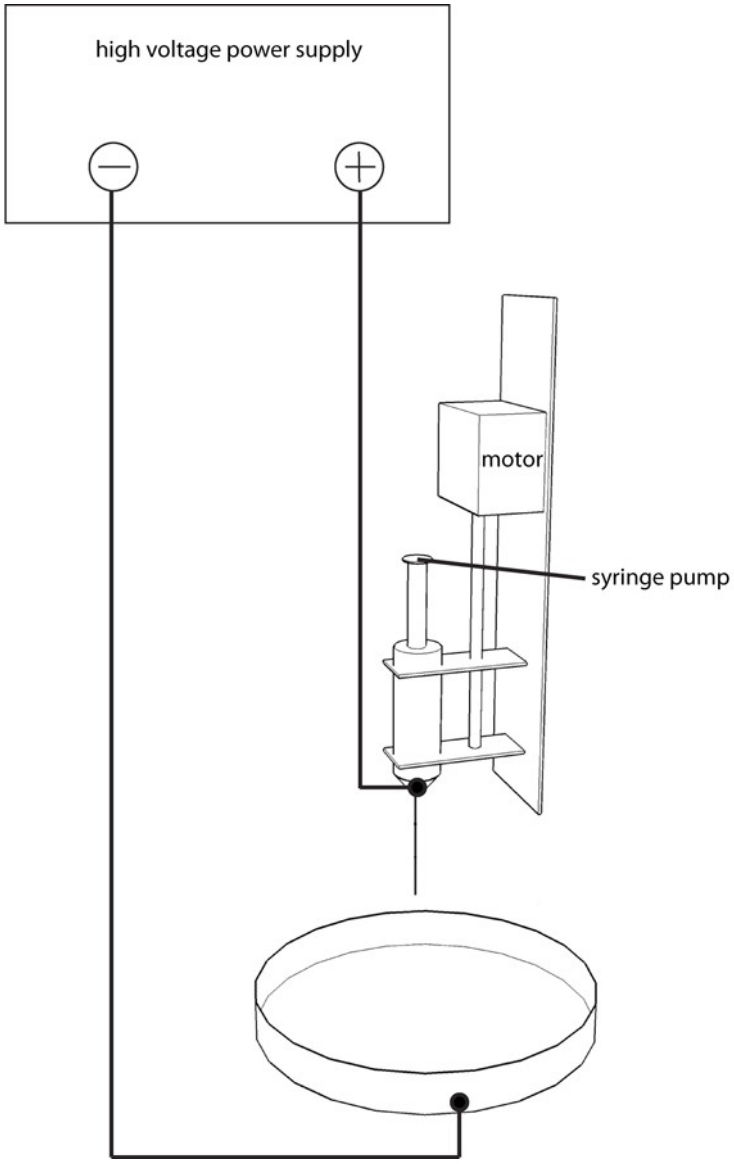

Figure 3.1. The electrospraying apparatus is very similar to the electrospinning apparatus. Key system components include a solution reservoir (syringe), nozzle (18-gauge, blunted, metallic needle), high-voltage DC power supply, and grounded target.

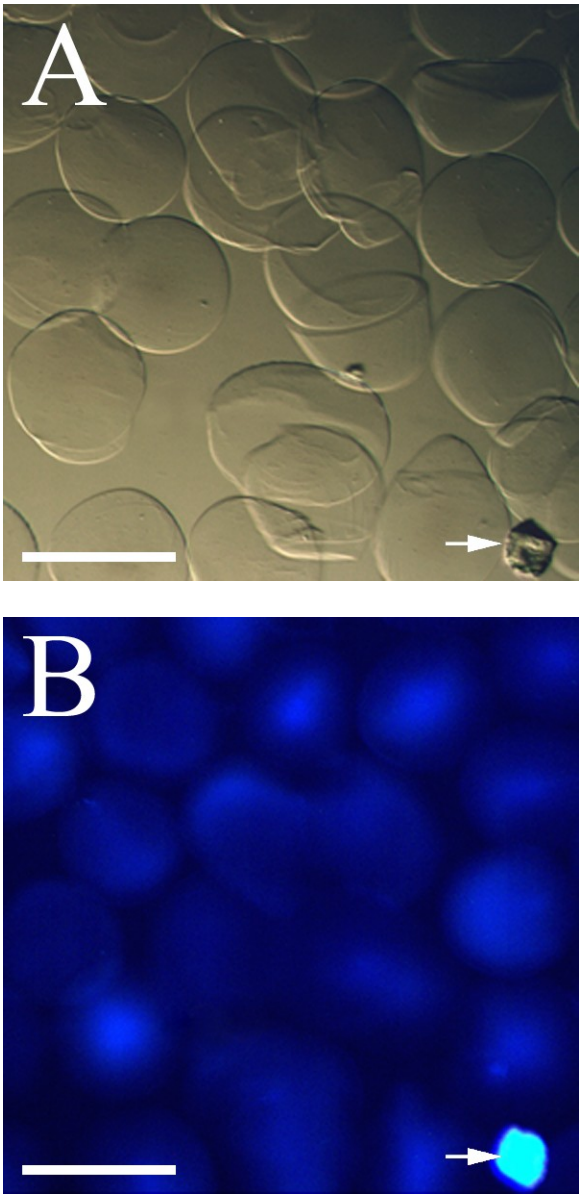

Figure 3.2. (A) A light microscopic image of alginate microspheres showing their uniform diameter. (B) A wide-field fluorescence image of the same microspheres showing the incorporation of a fluorescent protein. The white arrows point to the same piece of debris, indicating the same field of view in both images. Scale Bars (A and B) = 10 μm.

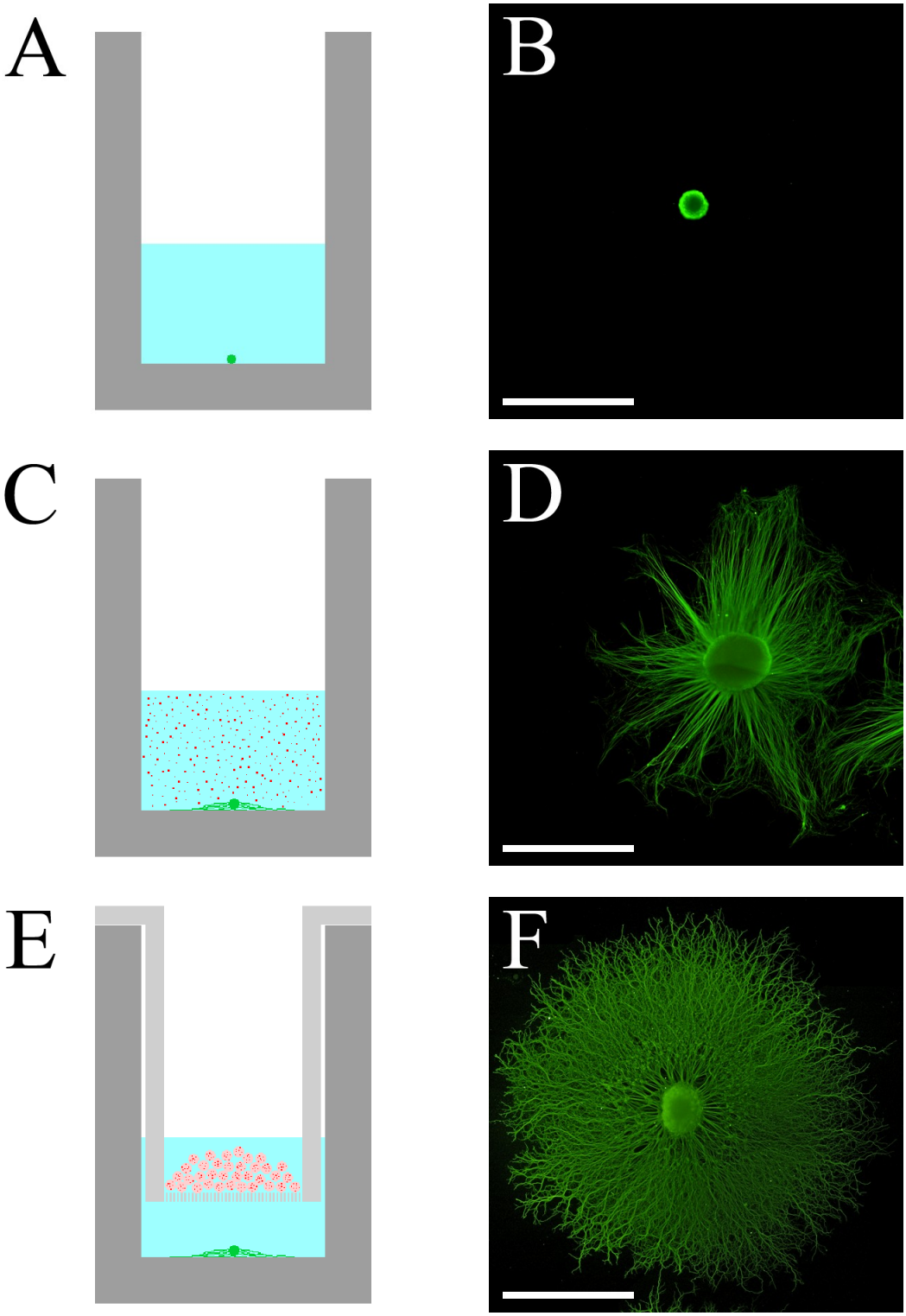

Figure 3.3. Bioassay assessing the bioactivity of NGF-incorporated alginate microspheres on DRG outgrowth. DRGs were isolated from E16 rat embryos and cultured in wells of a 48-well plate. Schematics (A, C, and E) of the experimental setup and their corresponding results (B, D, and F) are shown. In the absence of NGF in the media (A), predictably no outgrowth is seen (B). However in a positive control setup, specifically in the presence of NGF in the media (C), neuritic outgrowth is evident (D). Microspheres were deposited in a Transwell insert and placed into wells (E). Neuritic processes of DRGs exposed to NGF-incorporated alginate microspheres showed exuberant outgrowth as compared with the positive control (F). Scale Bars (B, D, and F) = 500 μm.

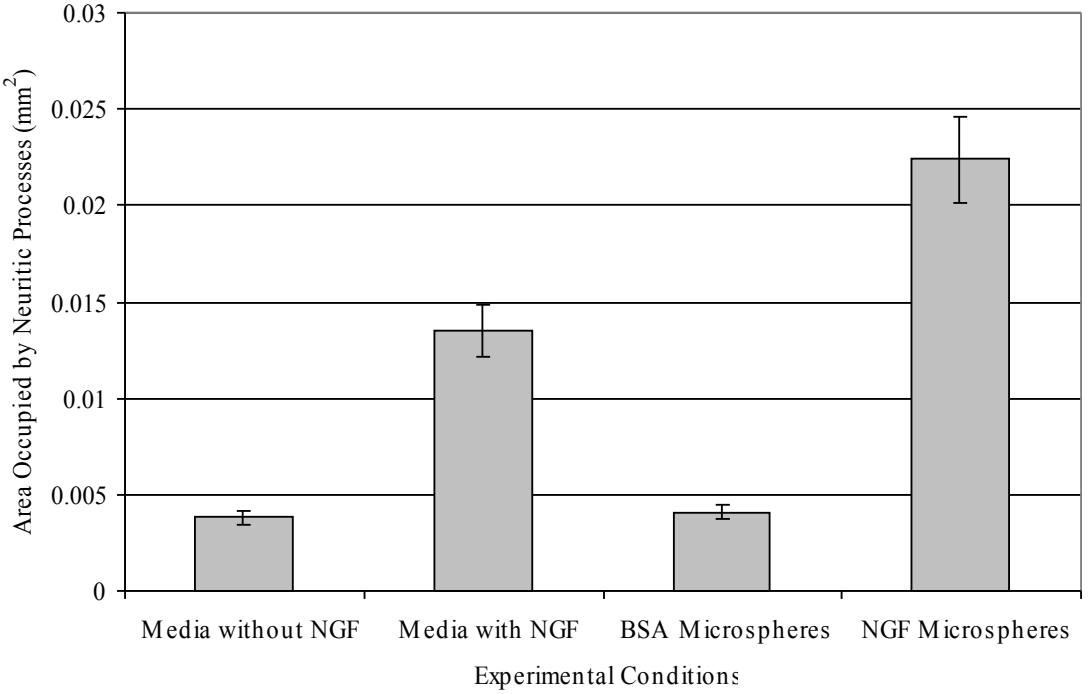

Figure 3.4. The extent of outgrowth exhibited by the DRG cultures when exposed to various sources of NGF (in media or alginate microspheres) was quantified and shown here. The difference in the extent of outgrowth between NGF in media and NGF supplied by the alginate is likely the result of the gradual increase in concentration of NGF in the media with time.

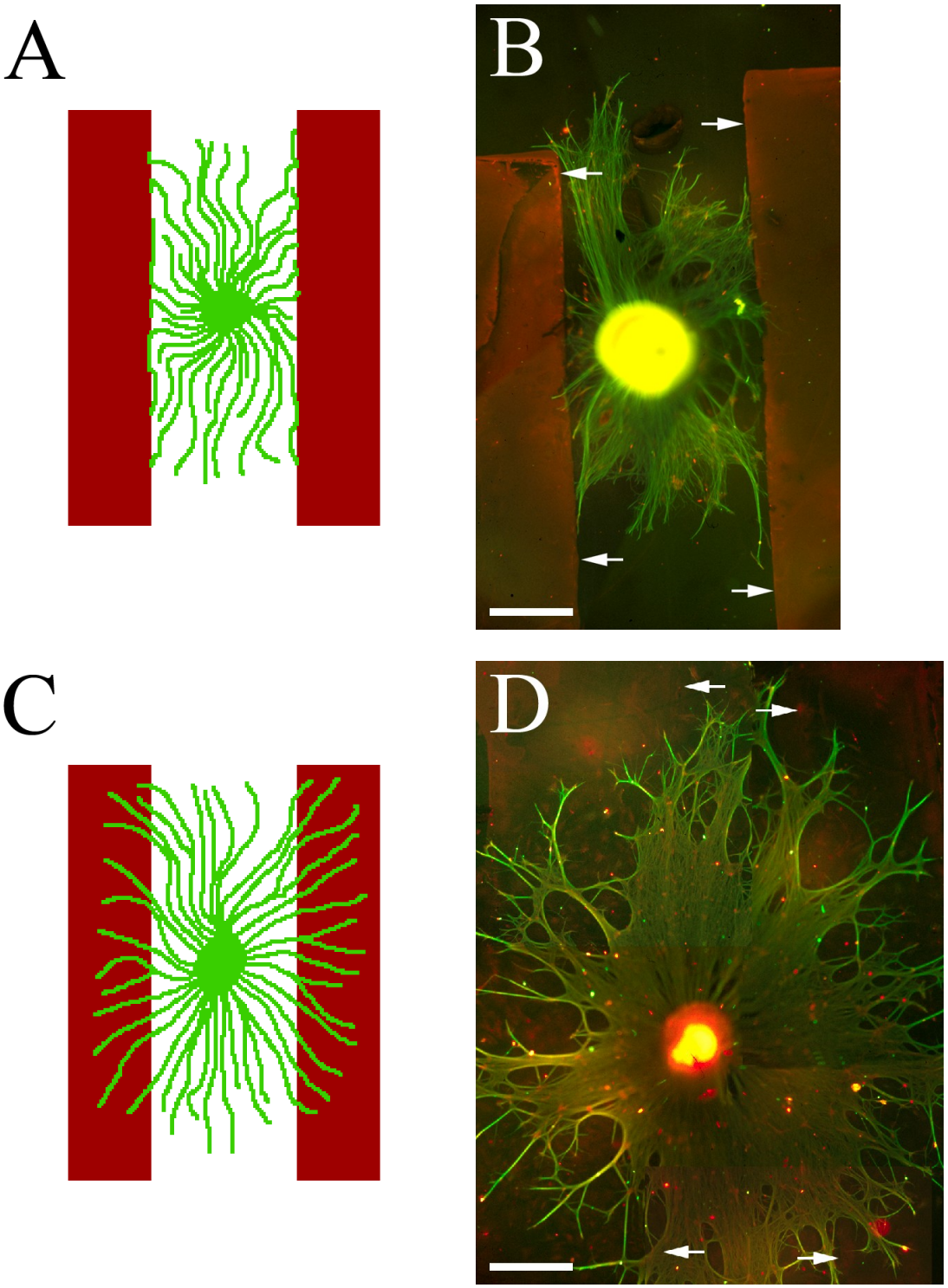

Figure 3.5. Stripe bioassay of dorsal root ganglia (green) grown between aggrecan lanes (red) for 7 d in culture. Aggrecan, a CSPG, is a known inhibitor of axonal regrowth following SCI. Schematics of the stripe bioassays are shown with or without incorporating ChABC into the matrix (A and C) and their corresponding results (B and D). In the absence of ChABC, DRG neurites were inhibited from growing on aggrecan lanes (A and B). In contrast, in the presence of a ChABC-incorporated matrix, the growth-inhibitory nature of aggrecan was neutralized. Aggrecan lane boundaries marked by arrows. Scale Bars (B and D) = 500 μm.

Chapter 4

Preliminary Tests of Implanting Electrospun Matrices in a Rat Spinal Cord Transection Model

Introduction

In Chapter 2, we presented data demonstrating the successful use of electrospinning to generate biocompatible, implantable matrices that are able to direct neuritic outgrowth. And in Chapter 3, we showed how these matrices can be enhanced to address the two specific therapeutic obstacles of neurotrophic support and increased chondroitin sulfate proteoglycan (CSPG) expression after spinal cord injuries (SCI) by supplementing the matrices with a growth factor and an enzyme that neutralizes the axon growth-inhibitory activity of CSPGs. In view of these successes, we next sought to examine the extent to which these matrices perform when implanted into a rat model of SCI. In this brief chapter, we present a bit of preliminary results showing some initial successes of this *in vivo* study.

Materials and Methods

Electrospinning

Air-gap electrospinning was similarly employed in order to fabricate cylindrical conduits of aligned fibers as described previously in Chapter 3 and the suture material polydioxanone (PDS) was again used. Briefly, for each matrix, a PDS filament was dissolved in the solvent HFIP at a concentration of 125 mg/ml and the solution was deposited in a syringe, which was mounted onto a syringe driver set to deliver 5 ml/hr. Though the exact placements of the various electrospinning components differed between runs and required a bit of trial and error for the optimal positioning of the two grounded posts, generally the air gap between posts was set between 3 to 5 cm and the assembly containing the posts was placed no more than 20 cm away from the nozzle. To match the size of the thoracic cord in a rat, spinning continued until a diameter target of 2 mm was reached during the fabrication process.

Animal Model and Surgical Procedures

Adult Long Evans Hooded rats aged approximately 70 days were used for this study. Owing to extensive experience with the rat percussive SCI model, we learned that the presentations of cystic cavities that formed post-injury were highly inconsistent. Furthermore, the extent of white matter sparing was equally variable. Therefore, in this study, we elected not to use the percussive SCI model. Though we hope that these electrospun matrices would in the future be used to bridge the fluid-filled cyst after contusion SCIs in humans, we wanted an experimental animal model that would present

consistent complete injuries so that our testing conditions of these electrospun matrix implants would be as uniform as possible from animal to animal. Accordingly, a transection SCI model was selected instead.

Adult Long Evans Hooded rats aged approximately 70 d were used for the transection SCI protocols. All surgical and postoperative care procedures were performed in accordance with the Virginia Commonwealth University Institutional Animal Care and Use Committee. Animals were placed in a closed container, sedated with 5% isoflurane, endotracheally intubated, and maintained under 2.5% isoflurane during surgical procedure. Depth of anesthesia was assessed periodically during the surgical procedures by tail pinch and watching for reflexive movements. Body temperature was kept normothermic using a homeothermic blanket placed under the animal. Employing sterile techniques, a dorsal midline incision was made over the mid-thoracic spine and a standard thoracic level 8 (T8) laminectomy was performed on the animal to expose the spinal cord (Figure 4.1A). A 2-mm segment of the cord was then completely removed via transection by iridectomy scissors, leaving a similarly sized gap (Figure 4.1B). Thrombin-soaked foam pieces were placed in and around the created gap to hasten hemostasis. After bleeding slowed (usually after about 15 to 20 min post-transection), an electrospun PDS matrix conduit was custom-fitted into the gap and approximated to the cut cord stubs such that the fiber grain of the matrix ran longitudinally with the cord (Figure 4.1C). The wound was closed in layers with silk sutures and skin incision closed with surgical staple clips. Animals were subsequently allowed to recover in a separate area containing a warming blanket.

All animals received prophylactic gentamicin (5 mg/kg) before surgery and daily thereafter for 7 d. Post-operatively, all animals were given easy access to food and water and housed two per cage. Analgesic medication (acetaminophen oral suspension, 2 mg/ml) was mixed into the drinking water and administered for the first 3 d post-injury. Manual bladder expression was performed three times daily for the first week after surgery and two times daily thereafter until spontaneous micturation was reestablished. Due to the severe nature of transection cord injuries, spontaneous micturation generally did not occur in animals until the eighth week post-surgery.

Preliminary Results

At the end of week 1 and week 6 post-surgery, animals were sacrificed and their spinal cord containing the electrospun implant was isolated. Grossly, the implant was well integrated into the cord with excellent implant-stub adherence (Figure 4.2A). These cords were cryosectioned longitudinally and the sections were labeled with the cell nuclear fluorescent stain DAPI (4',6-diamidino-2-phenylindole). At the end of week 1 post-surgery, growing tissue has enveloped the implant and cells are seen infiltrating the implant from all sides (Figure 4.2B). By week 6 post-surgery, the matrix implant is almost packed full of cells (Figure 4.2C). These results demonstrate the biocompatibility and the capacity of the electrospun matrix conduit to facilitate cellular infiltration, an important step in the bridging of gaps and cysts post-SCI. We are currently carrying out other histological and behavioral assessment experiments to determine the extent of

implant penetration by regrowing axons and recovery of motor functions. For these experiments, enhanced matrices such as those described in Chapter 3 are being tested.

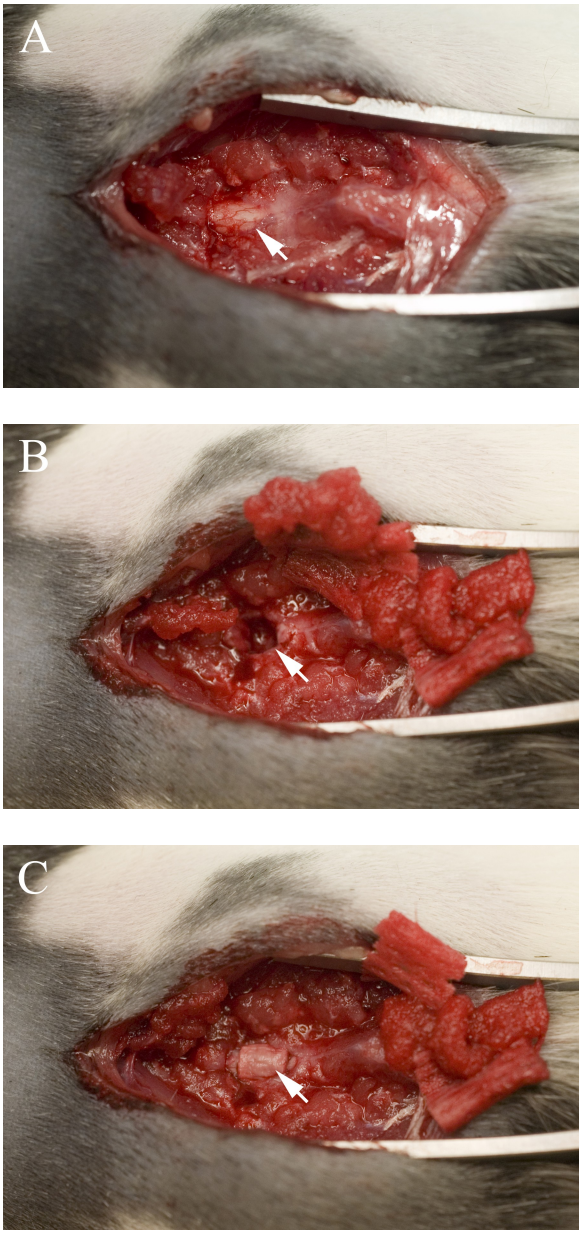

Figure 4.1. Photographs showing the matrix implantation portion of the surgical procedure. (A) The spinal cord (arrow) is exposed after completing a laminectomy at the T8 level. (B) A gap (arrow) remains after 2 mm of the cord is removed via transection. (C) Placement of a similarly sized cylinder of electrospun matrix (arrow) into the gap.

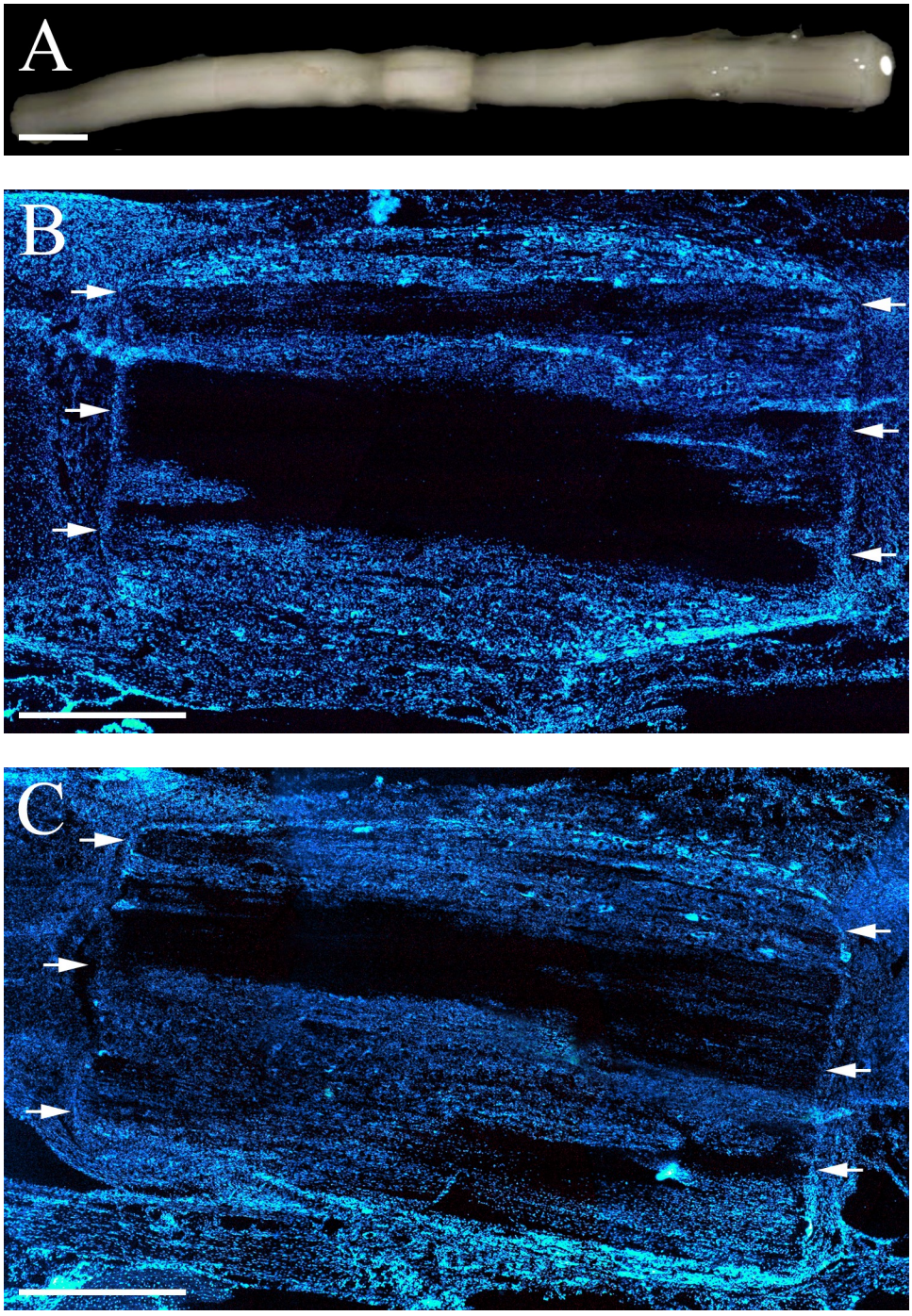

Figure 4.2. (A) Gross view at week 6 post-surgery of a transected cord implanted with an electrospun matrix conduit. (B) A representative longitudinal cord section labeled with a fluorescent cell nuclear marker DAPI showing excellent integration of the matrix (arrows) into the cord by the end of week 1 post-surgery. Cells are seen infiltrating the matrix from all sides. (C) By week 6 post-surgery, the matrix (arrows) is almost packed full of cells. Scale Bars (A) = 2 mm. Scale Bars (B and C) = 500 μm.

Chapter 5

Chronicling the Injury-Induced Proliferative Response at the Spinal Cord Injury Lesion Site and Attenuating the Response with X-Irradiation

Introduction

Traumatic injury to the spinal cord results in the proliferation of cells at the lesion site that mature into astrocytes, ultimately resulting in the formation of a gliotic scar. The cells within the scar, of which the majority are astroctyes, express factors that are known to inhibit axonal regeneration. In addition, as a result of the tight spatial cellular associations of the scar, regrowing axons are prevented from crossing the scar toward the opposite margin of the lesion. Consequently, the scar presents both a biochemical and to a lesser extent physical barrier to axonal regeneration following spinal cord injury (SCI). It is believed that the attenuation of this injury-induced cell population may be helpful in reducing the inhibitory nature of the scar so as to allow a greater extent of regeneration (Moon and Fawcett, 2001; Woerly et al., 2004; Tian et al., 2006). Furthermore, gliotic scar attenuation may be a necessary adjuvant treatment to the implantation of a bridging

scaffold since the scar represents on-ramp and off-ramp barriers to axonal regrowth onto and off of the bridge. The attenuation of cellular proliferation needs not be extreme, since, as previously noted, the gliotic scar features a number of important beneficial effects, such as the isolation of damaged tissue from viable tissue and its notable role in providing a substrate for angiogenesis.

Accordingly, using a rat percussive cord injury model and employing immunohistochemical and flow cytometric methods by means of various cellular proliferation and glial cell markers, we first identified the injury-induced cell populations in and around the SCI lesion site and subsequently chronicled their initial periods of proliferation. Once this information was obtained, we next sought to demonstrate the extent to which this proliferative response can be attenuated with methods that target dividing cells. Specifically, as previously shown by this laboratory and others, cellular proliferation can be attenuated by appropriate levels of ionizing irradiation, a very similar procedure which has been applied for decades to control malignant cells in cancer therapy. Irradiation therapy possesses a number of desirable characteristics in that it is non-invasive, reproducible, and accurate in its targeting. The use of irradiation as an adjunctive therapy for SCI is not entirely novel. A very small number of published studies have previously demonstrated mixed results in attenuating scar formation and improving motor function (Kalderon et al., 2001; Pinjuh and Bedi, 2003; Ridet et al., 2000; Zeman et al., 2001; Zhang et al., 2005). A reason for the inconclusiveness of these studies perhaps may be attributable to the irradiation dosing, which was sometimes orders

of magnitude apart between studies. Furthermore, the timing and frequency of doses given often varied greatly between methodologies.

In view of these apparent deficiencies, a serial series of related experiments was completed systematically so that the best timing and dose can be determined. As previously stated, a chronicling of the injury-induced proliferative response after SCI was first accomplished. This was done to establish the timing component. Before initiating the irradiation experiments, exhaustive dosimetry was completed with the assistance of the Division of Radiation Physics and Biology in the Department of Radiology. In order to obtain dosing response and efficacy in neural tissue, the irradiation method was first tested on a model of normal cellular proliferation in neural tissue, namely the subventricular zone (SVZ) of neonatal rats, which contains a large number of dividing cells. Later, the paradigm was further tested on an injury-induced cellular population in a cortical stab injury rat model before ultimately tested on a contusion SCI rat model.

Materials and Methods

Mixed Glia Isolation and Culture

Before proceeding to *in vivo* experimentation, the reliability of employing flow cytometry to count glial cells required confirmation. In view of this, unpurified glial cultures were first used to test the flow cytometric methodology. In accordance with the Virginia Commonwealth University Institutional Animal Care and Use Committee, glial cells were isolated using similar methods described previously (McCarthy and de Vellis, 1980). Briefly, isolated postnatal-day 3 rat cortices were minced and dissociated

mechanically and enzymatically. Cells were seeded into T-75 poly-L-lysine-coated tissue culture flasks that contained Dulbecco's modified Eagle medium/Ham's F-12 medium with 10% fetal bovine serum and 1% antibiotic-antimycotic agent, and allowed to proliferate until the population reached confluency. During this time, culture media changes were made every 3 to 4 d. Cultures were ready for use after splitting.

Flow Cytometry

Flow cytometric methods were carried out using similar procedures described previously (Bilsland et al., 2006). Glial cultures were trypsinized, resuspended, fixed with 4% paraformaldehyde, and permeabilized with Cytoperm (BD Biosciences). Cells were first labeled with 7-aminoactinomycin D (7-AAD) to identify cells from debris and subsequently labeled with fluorochrome-conjugated antibodies for the thymidine analog and marker of proliferating cells bromodeoxyuridine (BrdU) and for the glial markers vimentin and glial fibrillary acidic protein (GFAP). Negative control antibodies were used to facilitate the setting of quadrant gates.

Animal Model and Surgical Procedures

Adult Long Evans Hooded rats aged approximately 70 d were used for the contusion SCI protocols. All surgical and postoperative care procedures were performed in accordance with the Virginia Commonwealth University Institutional Animal Care and Use Committee. Animals were endotracheally intubated and maintained under inhalation anesthesia (2.5 % isoflurane) during surgical procedure. Depth of anesthesia was

assessed during surgical procedures by tail pinch and observation for reflexive movements. Body temperature was kept normothermic using a homeothermic blanket. Employing sterile techniques, a dorsal midline incision was made over the mid-thoracic spine and a standard thoracic level 8 (T8) laminectomy was performed (Figure 5.1B). Animals were then placed in a spinal frame and the exposed spinal cord was contused with the Multicenter Animal Spinal Cord Injury Study (MASCIS) impactor using a 10-g weight dropped from a height of 25 mm (Figure 5.1A and 2.1C). Sham animals underwent laminectomy but did not receive spinal cord contusions. The reproducibility of the computer-driven MASCIS impactor can be assessed by examining the impact parameters acquired by the computer during each trial, which includes the trajectory of the falling rod, impact velocity, cord compression distance, and cord compression time. Animal injuries with unacceptable impact parameters were excluded entirely from the study. The wound was closed in layers with sutures and skin incision closed with surgical staple clips. Animals were subsequently allowed to recover in a separate area containing a warming blanket. For the irradiation studies, the impact site location was noted via a single exclusive suture tied through skin and muscle layers dorsal to the laminectomy site.

All animals received prophylactic gentamicin (5 mg/kg) before surgery and daily thereafter for 7 d. Post-operatively, all animals were given easy access to food and water and housed two per cage. Analgesic medication (acetaminophen oral suspension, 2 mg/ml) was mixed into the drinking water and administered for the first 3 d post-injury.

Manual bladder expression was performed three times daily for the first week after surgery and two times daily thereafter until spontaneous micturation was reestablished.

Chronicling the Glial Cell Proliferation at Lesion Site

To establish the time course of the injury-induced proliferative response after SCI and relate this to gliotic scar formation, animals were first divided into two groups of sham and injured. Subsequently, they were subdivided further (n = 3) as to the day post-injury (day 1, 2, 3, 4, 7, 10, and 14) an animal would receive two doses, 12 h apart, of BrdU (300 mg/kg body weight). On day 14 post-injury, animals were sacrificed with a lethal dose of pentobarbital and transcardially perfused with phosphate buffered saline (PBS). The 5-mm spinal cord segment containing the SCI lesion epicenter was harvested and the tissue was mechanically dissociated by passage though a 70-µm filter. The resulting cell suspension was washed with PBS and the unwanted erythrocytes were lysed with tris-buffered ammonium chloride. The cells were then prepared as described previously for flow cytometric analysis.

X-Irradiation

To assess the extent to which X-irradiation can attenuate the normal proliferative response in neural tissue, the SVZ of neonatal rats, which is an area in the brain containing large numbers of dividing cells, was unilaterally irradiated via a Faxitron 43855D X-ray irradiator with varying single doses (5, 10, 15, and 20 Gy). (Irradiator dosimetry was completed with film before experiments proceeded.) When it was

determined that 15 Gy was the lowest dose that can attenuate 80% of the proliferative response (data not shown) as compared to the SVZ of the control hemisphere, the use of irradiation was further explored in injury-induced cellular proliferation model, specifically in a cortical stab injury in rats.

After determining the peak period of proliferation via the chronicling experiment described above, another group of SCI animals (n = 3) received a single dose of irradiation administered on day 2 post-injury. To prepare the animal for the irradiation procedure, the rat was first anesthetized with a mild dose of ketamine/xylazine cocktail and placed in a small box. The dorsum of the animal was raised with a paper towel roll placed beneath its upper abdomen. To protect the other tissues for irradiation damage, a 2-mm thick solid lead plate containing a square opening of 2.5 cm by 2.5 cm was placed over the animal, with the center of the opening aligned with the laminectomy site as noted by an exclusive suture that was tied during the wound closure after surgery. The box containing the animal was then placed into the irradiator and a dose of 15 Gy as determined by the duration of exposure (about 14 min) administered. After the exposure, the animal was allowed to recover.

Results

Though the ultimate goal is to examine the approach of using X-irradiation to reduce gliotic scar formation after SCI, a series of experiment was planned to determine the appropriate dose and timing of the therapy. In order to establish the appropriate dose of the irradiation, various doses were first tested on a model of normal cellular

proliferation in neural tissue. Based on previous experience of the procedure in our laboratory (McGinn et al., 2008), four different doses of irradiation (5, 10, 15, and 20 Gy) were tested on the SVZ of neonatal rats, which contains a large number of dividing cells. It was found that 15 Gy sufficiently attenuated the proliferative response by 80% (data not shown). Subsequently, the use of irradiation was further tested on an injury-induced cellular proliferation model, specifically a cortical stab injury in rats. In this experiment, rats were given a needle stab injury to the cortex, inducing the cells in the vicinity to proliferate (Figure 5.2A). In contrast, rats that were then irradiated at the site of injury when cells began to proliferate at day 2 post-injury showed the presence of only few dividing cells (Figure 5.2B).

Now that the dosing of irradiation was established, we wished to explore when such a dose should be given to maximize its effect. In the next series of experiments, we sought to establish the time course of the injury-induced proliferative response in SCI and relate this to gliotic scar formation with the use of flow cytometry. In order to ascertain the validity of using flow cytometry to count cells of the central nervous system (CNS), a preliminary study using mixed glial cultures was first completed (Figure 5.3). When it was found that flow cytometry can reliably count vimentin+ and GFAP+ cells, the chronicling of the injury-induced proliferative response with *in vivo* experiments proceeded (Figure 5.4). For reactive astrocytes, which are labeled with vimentin, the peak period of proliferation lasts from day 2 to 5 post-injury (Figure 5.4G). We then found that a single targeted 15-Gy exposure of irradiation to the lesion site at day 2 post-injury reduced the proliferating cell population by over 50 % (Figure 5.4H).

Discussion

We hypothesized that irradiation treatment, when targeted to the site of spinal cord trauma, may reduce the injury-induced proliferative cell population. As this population contributes significantly to the formation of the gliotic scar, the reduction of this cell population would reduce scar formation and create a more favorable environment for axonal regeneration. However, since the gliotic scar contributes a number of important benefits, we merely want to "punch a few holes" such that regrowing axons can penetrate the physical barrier aspect of the scar while scar integrity can be preserved to prevent the spread of cellular destruction. To optimize the process, we completed several preliminary experiments in order to determine the lowest dose that can be used to maximally attenuate the injury-induced proliferative response as well as the best timeframe for administration.

In this study, though we showed how irradiation can attenuate the injury-induced proliferative response post-SCI, we never proceeded to determine the extent to which irradiation can improve functional outcome. In the past several years, there has been increasingly strong evidence that the reactive astrogliotic process and subsequent gliotic scarring play an imperative role in neuroprotection during the early acute phase of injury. As discussed previously, it has been known for some time that the scar possesses a beneficial role, especially in the establishment of a new glia limitans around the lesion. However, mounting evidence as to the scar being inhibitory to regeneration has led to the common general perception that it is something that should aggressively be removed or at least reduced in size even though earlier evidence has shown scar ablation to drastically

increase lesion volume and promote neuronal and oligodendrocyte cell death (Bush et al., 1999; Fauklner et al., 2004). In view of the many recent studies that show how the gliotic scar goes beyond just isolating the lesion post-injury, specifically the roles of sealing the blood-brain barrier, preventing overwhelming inflammatory infiltration, supplying various growth factors, and even promoting axonal sprouting (Okada et al., 2006; Renault-Mihara et al. 2008; Rolls et al., 2009), the overall perception of the scar being unfavorable post-SCI is slowly changing.

Though it is still true that the scar represents a barrier to regeneration, both physically and biochemically, this recent paradigm shift of regarding gliotic scar formation as almost necessary during the immediate and acute phases of injury leads us to reconsider the advantages of attenuating the injury-induced cellular proliferation so early on post-SCI. However, once the SCI lesion is stabilized and the process of gliosis occurred to such an extent that the scar causes more harm than benefits, we believe the continuing injury-induced proliferation, despite having peaked earlier, can still be attenuated by way of irradiation to facilitate a more efficient penetration of regrowing axons into and beyond the gliotic scar.

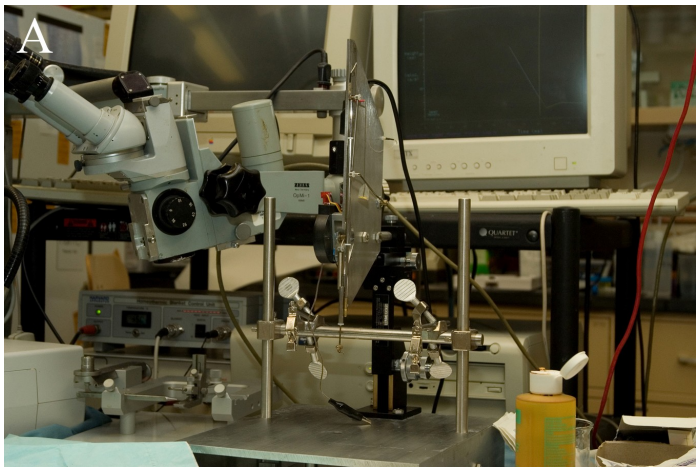

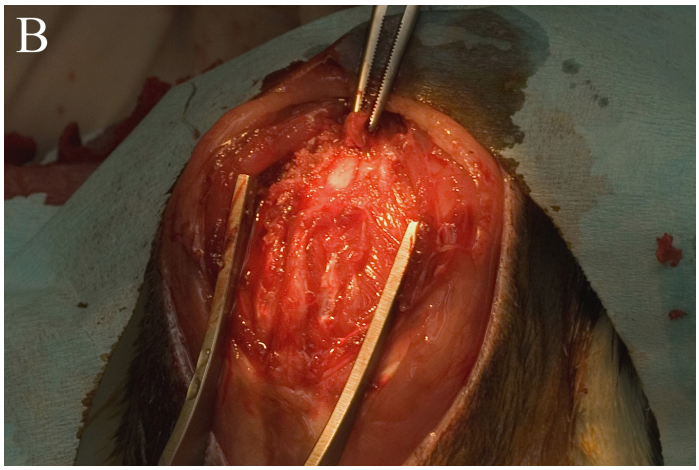

Figure 5.1. (A) The MASCIS Impactor, developed in 1991 by Drs. John Gruner, Carl Mason, and Wise Young, is a device used to deliver reproducible spinal cord contusions in rats. A 10-g rod can be dropped onto an exposed rodent spinal cord from a distance of 12.5, 25, or 50 mm, which equate approximately to a mild, moderate, or severe contusion SCI respectively. (B) The white spinal cord is exposed after completing a laminectomy at the vertebral level T8. (C) The spinal frame holds the animal via two spinous processes adjacent to the laminectomy so that the exposed segment of the cord is aligned directly beneath the rod.

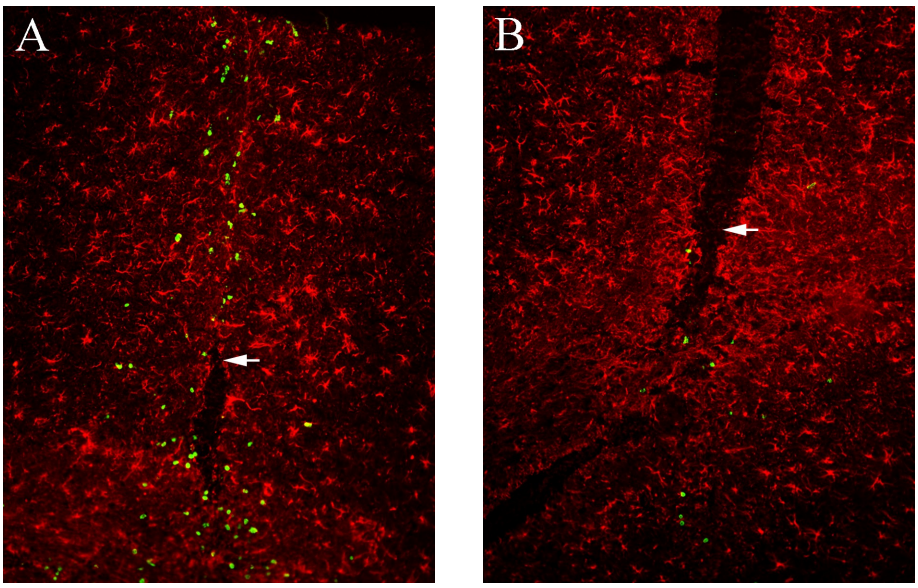

Figure 5.2. A single dose of irradiation can drastically reduce the number of proliferating cells in the injured cortex. (A) Sections immunolabeled with BrdU (green) and GFAP (red) showing the injury-induced proliferative response 4 d following a cortical stab wound (arrow). (B) The reduction of this response as a result of a single dose of irradiation directed locally at the wound site 2 d post-injury.

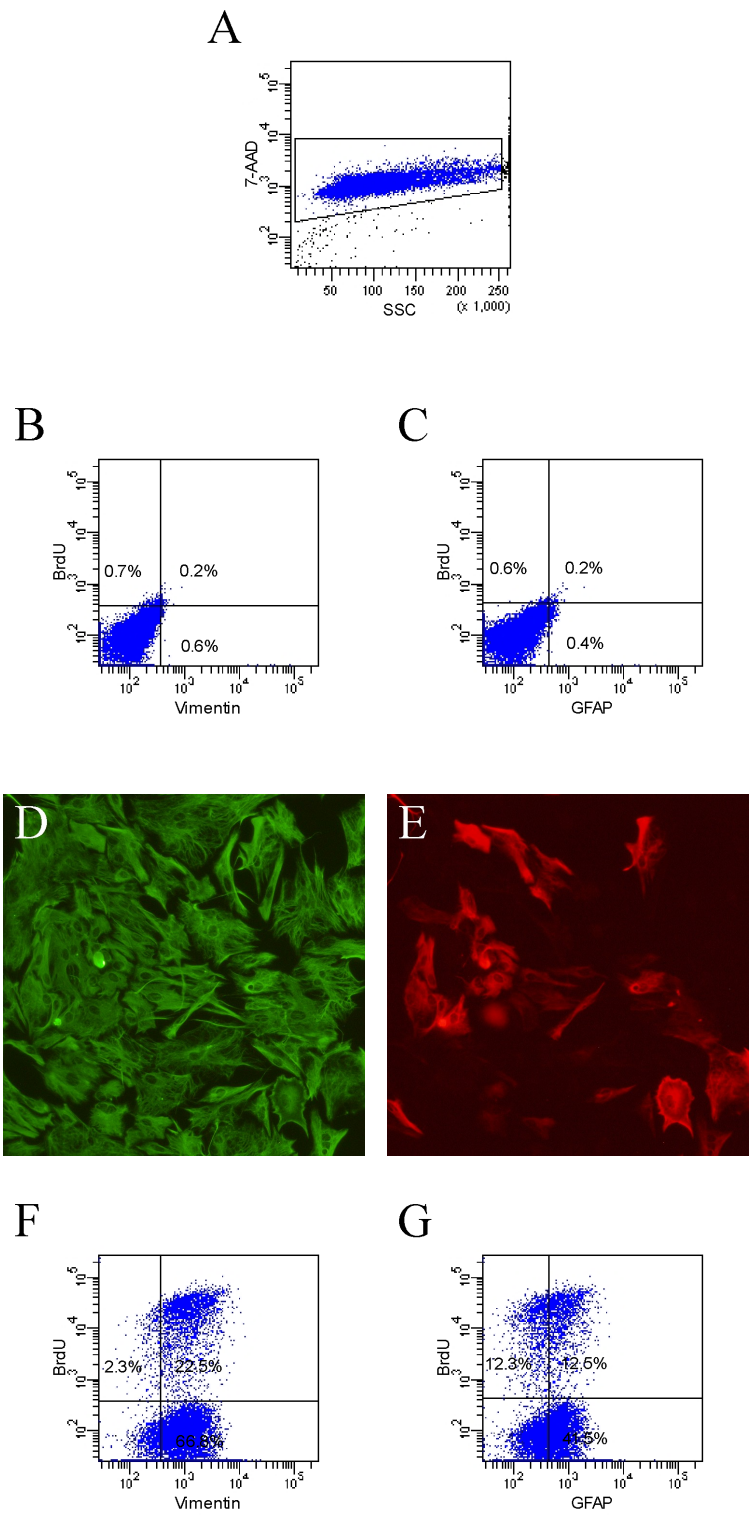

Figure 5.3. Flow cytometry can reliably count vimentin+ and GFAP+ cells. Unpurified glial cultures were trypsinized, resuspended, fixed, and permeabilized. Cells were first labeled with 7-AAD to identify cells from debris (A) and subsequently labeled with fluorochrome-conjugated antibodies for BrdU, vimentin, and GFAP. Negative control antibodies were used to facilitate the setting of quadrant gates for the BrdU-vimentin analysis (B) and BrdU-GFAP analysis (C). Flow cytometric counts (F and G) were comparable to that of actual counts done on immunolabeled cultures (D and E). A similar study was also completed using glioblastoma cells and cell counts using all three markers were equally comparable between flow cytometric and manual immunocytochemical counts (Data not shown).

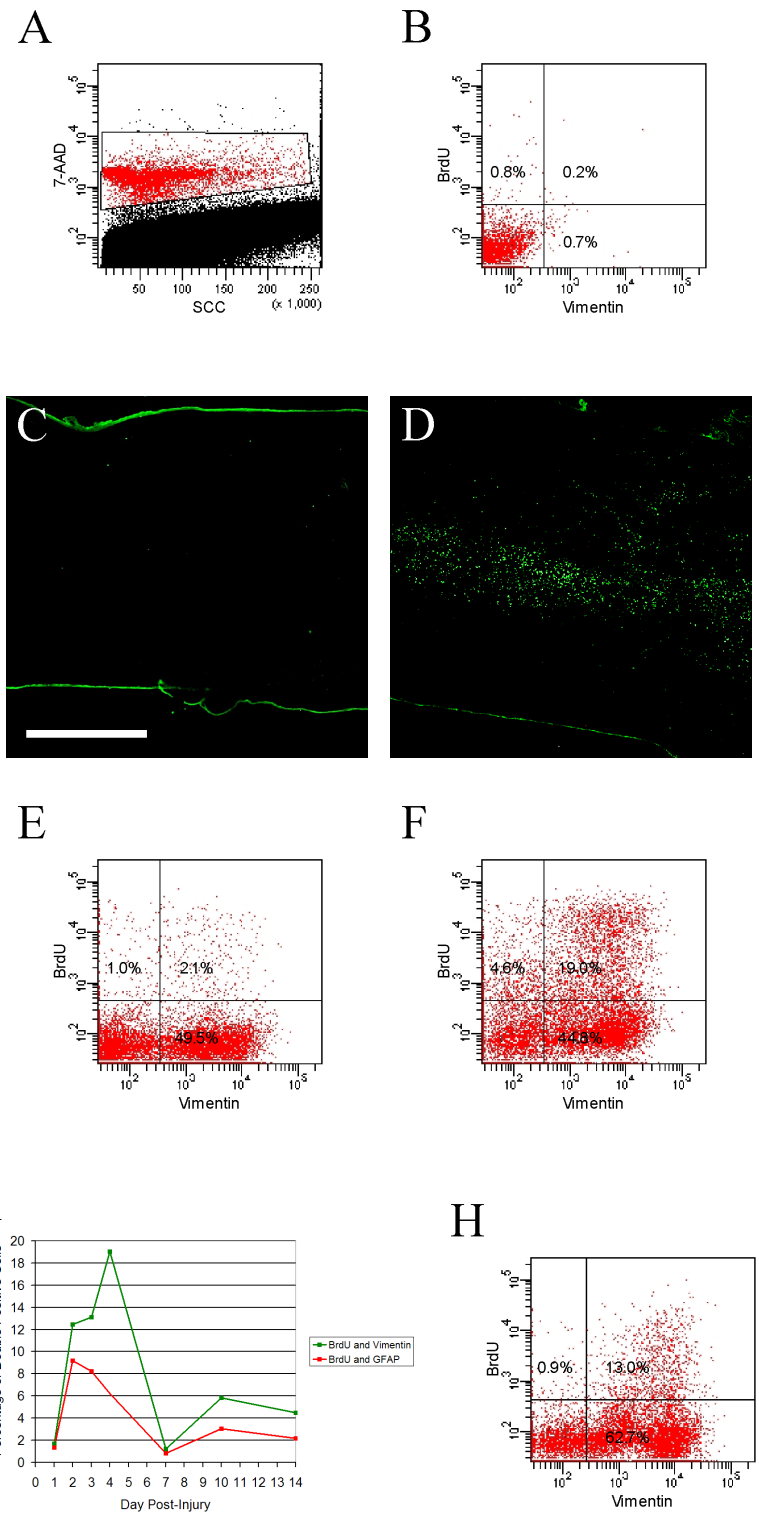

Figure 5.4. Spinal cords of rats were percussively injured by a 10-g weight drop from 25 mm. To obtain the flow cytometric dataset displayed here, on day 4 post-injury, animals were given two doses of BrdU. On day 14 post-injury, the 5-mm spinal cord segments containing the lesion epicenter from three experimental groups of rat (sham, injured, and injured with irradiation) were mechanically dissociated into a cell suspension, fixed, and permeabilized. Cells were first labeled with 7-AAD to identify cells from debris (A) and subsequently labeled with fluorochrome-conjugated antibodies for BrdU and vimentin. To facilitate the setting of quadrant gates for the analysis, cells from the spinal cord of a non-BrdU treated sham animal were used (B). In sham animals, very little proliferation was seen as shown by BrdU immunohistochemistry (C) and as indicated by low flow cytometric counts of BrdU+ events in the top two quadrants (1.0% + 2.1%) (E). In contrast, in injured animals, there is a massive increase of cell proliferation as shown by BrdU immunohistochemistry (D) and flow cytometry (4.6% + 19.0%) (F). Moreover, a large number of these proliferating cells are vimentin+ (19.0%). The above described process was repeated with BrdU being administered at different time points and a graph depicting the chronicling of the proliferative response of vimentin- and GFAP+ cells was generated (G). A single dose of irradiation administered at the beginning of the peak period of proliferation (day 2 post-injury) was able to attenuate the injury-induced proliferative response as indicated by flow cytometry (H). Scale Bar (C) = 1 mm.

Chapter 6

Concluding Statement

Traumatic spinal cord injury (SCI) is a debilitating, costly, and emotionally devastating condition that is characterized by marked neuropathology and limited recovery of function. While the initial insult rapidly disrupts neural tracts and kills cells, an insidious, complex secondary cascade of cellular and biochemical events soon follows. Glial cells such as astrocytes react to the injury by proliferating and hypertrophying, which results in the development of a gliotic scar that partitions the lesion epicenter from viable tissue. Although this process aids to prevent the spread of uncontrolled tissue damage, the scar nevertheless acts as a physical barrier to axonal regeneration. Furthermore, the scar and the cells within are a major source of axon growth-inhibitory molecules such as chondroitin sulfate proteoglycans (CSPG) and thus concomitantly acts as a biochemical barrier. Concurrently, inflammatory cells infiltrate the cord parenchyma and through immunologic activation, possess the capacity to exacerbate damage by propelling viable cells into apoptosis. Additionally, the severing of axons results in the interference of neurotrophic support, making neuronal survival precarious. Finally, the pathology culminates in the formation of a fluid-filled cyst,

which puts in place yet another insuperable hurdle for regrowing axons to overcome. Collectively, these pathological processes perhaps partially explain the lack of effective central nervous system (CNS) recovery seen following SCI.

Up until the recent decades, there was little hope for the successful treatment of SCI. But despite our incomplete understanding of the mechanisms that control these pathological processes, we now know that they are amenable to therapeutic interventions that may promote neuroplasticity and the regeneration of axons, leading to improved functional outcomes. Moreover, it has been demonstrated numerous times that adult CNS neurons retains the ability of regrowing functional axons (Richardson et al., 1980; von Meyenburg et al., 1998; Chuckowree et al., 2004). In view of this, when provided with a permissive microenvironment, the notion of severed axons regenerating is indeed a very valid possibility.

In this dissertation, we introduced a few of our own strategies to overcome the aforementioned therapeutic challenges post-SCI. We employed electrospinning to generate a biocompatible matrix implant that can bridge and direct axonal elongation across the fluid-filled cyst. Given the complex array and scope of pathological sequelae post-SCI, it is generally recognized that successful treatment requires a multifaceted approach. In view of this, we presented novel approaches by which successful tried and true therapeutic strategies are combined. To facilitate the delayed but necessary long-term release of an enzyme capable of neutralizing the axon growth-inhibitory activity of CSPGs, chondroitinase ABC was incorporated directly into our electrospun matrices and tested. And to ensure an immediate replacement source of neurotrophic support during

the acute phase of the injury, we tested the use of an alginate microsphere vehicle that can also be incorporated into our electrospun matrices to deliver growth factors and other potential neuroprotective and growth-promoting agents. To address the injury-induced proliferative response, which represents an on-ramp off-ramp obstacle that prevents axonal regeneration onto our matrix implant, we showed how X-irradiation can moderate the the injury-induced proliferative glial response so as to facilitate a more efficient penetration of regrowing axons into and beyond the gliotic scar. And finally, FTY720 was utilized as a pharmacologic intervention to prevent lymphocytic egress from lymphoid tissues and reducing the infiltration of lymphocytes into the cord parenchyma post-SCI, which resulted in improved hindlimb motor recovery.

Although many of the ideas presented have been assessed in animal studies and these experiments have produced results that demonstrated potential and optimism, these strategies may not translate easily into human SCIs without additional effort. As mentioned previously, the presentation of cysts formed post-SCI is highly variable in both its time of emergence and spatial dimensions. While the timeframes of the many cellular and molecular events have been chronicled in the rodent models of SCI, researchers have only a rudimentary understanding of such details in human cases of SCIs due to the sparse availability of study specimens. A determination of the appropriate time to implant our or any other experimental scaffold bridges post-SCI in humans will be required to optimize regeneration. Additionally, while cavities formed post-injury in human SCIs are inherently larger than those of rat SCIs, fitting, aligning, and implanting our bridging matrices into these narrow cysts may not be trivial.

Although extreme, some have suggested transecting and removing the damaged cord segment in contusion SCI patients that have absolute complete cord injuries and replacing the segment with a bridge in a process similar to our animal trials. There is some merit with this radical procedure since much of the inhibition and barrier effects are removed instantly. Additionally, a laceration of the cord, such as this method, has been shown to produce little gliotic scarring, which would enable the cord stubs to act as a more permissive on-ramp off-ramp zone after bridge implantation. Naturally, this approach would not be a therapeutic solution for incomplete SCI patients with cords that have some level of white matter sparing.

Another notion of interest is the use of our electrospun matrix implants during the chronic phase of human SCI, which generally begins six months to a year after the initial traumatic insult. Although research targeting the chronic phase of the injury is sorely lacking, what is known is rather discouraging. In a longstanding injury, the diminished regenerative capacity of the neurons and the increasing rigid scar barriers at and beyond the lesion site make functional recovery even more of a challenge. Potential therapies that have shown promise when applied acutely, have almost all shown to fail when employed to injuries older than four weeks in animal models of SCI (Houle and Tessler, 2003). At this point with our current understanding, it is most likely that the best therapeutic time window will reside during the early stages of the injury's pathological progression.

Table 6.1 displays a general but almost exhaustive list of therapeutic obstacles arranged by the timeframes in which they occur after traumatic SCI. Each of these

phases presents a number of known therapeutic aims. A combination of treatments that target in a serial fashion the listed objectives during the appropriate timeframe would probably give SCI patients the best chance at regenerating axotomized neurons and recovering lost physiological functions. Despite this well-recognized point of view, very few combinatory strategies have been documented in the literature. This is not surprising given the difficulty of the problem and the enormous amount of resources required to carry out experiments based on a combinatory approach. Nevertheless, in the short span of four years, we came up with a few novel ideas, tested them experimentally, and have started to combine some of these potential treatment strategies. As discussed in Chapter 5, we have now obtained some promising preliminary results from our matrix implant trials in animals. Though more *in vivo* runs are required to show conclusively that our electrospun matrix is able to bring about functional improvements post-SCI, we plan to combine our other treatment approaches as well as other outside strategies that have been proven to be successful.

Collectively, the ideas presented in this manuscript and the results from experimentally testing these ideas represent a new body of knowledge that, if perhaps only incrementally, advance the pathological understanding as well as the treatment of traumatic SCI.

SCI phases, timeframe of phases, key events, and therapeutic aims within each phase

Phases	Immediate Phase	Acute Phase	Subacute Phase	Intermediate Phase	Chronic Phase
Approximate Timeframe in Human Injuries	Immediately to Hours after injury	Hours to days after injury	Days to weeks after injury	Weeks to months after injury	Months to years after injury
Events and Potential Therapeutic Obstacles	▪ Primary mechanical insult ▪ Severing of axons ▪ Hyperemia ▪ Blood vessel damage and hemorrhage ▪ Microglial activation	▪ Edema ▪ Ischemia and hypoxia ▪ Hemorrhagic necrosis ▪ Excitotoxicity ▪ Blood-spinal cord barrier degradation ▪ Demyelination ▪ Inflammatory infiltration	▪ Reactive astrogliosis	▪ Gliotic scarring ▪ Cyst formation	▪ Wallerian degeneration
Major Therapeutic Goals Within Phase		▪ Neuroprotection and promotion of neuronal survival ▪ Immune modulation	▪ Modulation of injury-induced proliferation ▪ Promotion of regeneration ▪ Remyelination ▪ Neutralization of myelin debris and proteins ▪ Neutralization of proteoglycans	▪ Cyst bridging	▪ Physical Rehabilitation

Table 6.1. The aftermath of SCI is divided into five phases: the immediate phase, acute phase, subacute phase, intermediate phase, and chronic phase.

Appendix

FTY720 Reduces Inflammation and Promotes Functional Recovery after Spinal Cord Injury

Introduction

The pathophysiology of spinal cord injury (SCI) has classically been partitioned into primary and secondary injury processes. As described previously, after the initial primary injury, secondary injury encompasses an insidious cascade of cellular and biochemical events, the magnitude of which is rivaled only by its complexity. Within this milieu of events, inflammation has been identified as an important component of secondary injury and numerous cell populations have been implicated as mediators of inflammation. Among these cells, lymphocytes have generated interest for their key involvement in the concept of trauma induced autoimmunity (Popovich et al., 1996; Gonzalez et al., 2003; Ankeny et al., 2006). This concept is based on the hypothesis that traumatic injury results in the release of neural self-antigens and subsequent immunologic activation. In support of this possibility, injection into naïve animals of T cells isolated

from rats subjected to SCI resulted in central nervous system (CNS) tissue injury and neurological deficit (Popovich et al., 1996).

Many of these studies in SCI and autoimmunity have drawn on parallels from our current knowledge of multiple sclerosis (MS) and the animal model experimental autoimmune encephalomyelitis (EAE). In both of these processes, T cells are known to infiltrate the CNS, resulting in demyelination and neurologic dysfunction. Targeted therapies for MS have therefore focused on immunomodulation, specifically in the T cell population.

Fingolimod administration is one of the newest immunomodulatory therapies for MS and is currently undergoing phase III clinical trials as a monotherapy. Fingolimod, commonly known as FTY720, is a chemical derivative of the fungal metabolite myriocin and in its phosphorylated form, acts as a spingosine-1-phosphate (S1P) mimetic and agonist of the S1P receptor (Brinkmann et al., 2002). Several groups have shown that administration of FTY720 results in a significant reduction in peripheral lymphocyte counts (Chiba et al., 1998; Brinkmann et al., 2000; Pinschewer et al., 2000). It has been postulated that FTY720 induces this lymphopenia by preventing lymphocyte egress from peripheral lymphoid organs. Once FTY720 binds to the S1P receptor, internalization and subsequent degradation of the receptor occurs (Matloubian et al., 2004). This degradation thereby eliminates the necessary S1P signal for lymphocyte egress and prevents recirculation into the CNS (Brinkmann et al., 2002; Mandala et. al., 2002; Matloubian et al., 2004).

Independent of this ability to prevent lymphocyte migration, FTY720 has also been shown to have other cytoprotective capabilities. Studies have shown that FTY720 can prevent apoptosis in neural cells and act on endothelial cells to preserve vascular integrity (Fujino et al., 2003; Brinkmann et al., 2004; Coelho et al., 2007). The exact mechanisms of these effects are still under investigation.

In the series of experiments presented in this chapter, we examined the efficacy of FTY720 in a moderate to severe contusion model of SCI. We hypothesized that administration of FTY720 would reduce infiltration of T cells to the spinal cord lesion site and enhance functional recovery after SCI. Our results indeed demonstrate the efficacy of FTY720 in a model of CNS trauma and show that administration enhances tissue preservation and functional outcome after SCI.

Materials and Methods

Animal Model and Surgical Procedures

Adult Long Evans Hooded rats aged approximately 70 days were used for the contusion SCI protocols. The surgical procedure employed in this study was identical to that used in the previously discussed study of Chapter 5 and details of the method can be found in that chapter.

Immediately after injury, animals were randomized to receive an intraperitoneal injection of FTY720 (1 mg/kg body weight) (Cayman Chemical, Ann Arbor, MI) solubilized in 0.1% dimethyl sulfoxide (DMSO), vehicle (0.1% DMSO), or no injection

(injury only). Animals were then allowed to recover in a separate area with a warming blanket.

All animals received prophylactic gentamicin (5 mg/kg body weight) before surgery and daily thereafter for 7 d. Manual bladder expression was performed three times daily for the first week after surgery and two times daily thereafter until spontaneous micturation was reestablished. Urine volumes were recorded at each collection and spontaneous micturation was defined as established when daily volumes collected were less than 2 ml total for 3 consecutive days. Expressed urine was also monitored for evidence of urinary tract infection (UTI) by the presence of elevated urine pH or leukocytes and treated with a 5-d course of gentamicin if diagnosed.

Flow Cytometry

For flow cytometry, injured animals received daily intraperitoneal injections of either FTY720 (n = 5) or vehicle (n = 5) until sacrificed. On the first, fourth, and seventh days post-injury, animals were sacrificed with a lethal dose of pentobarbital and perfused transcardially with phosphate buffered saline (PBS). A 1-cm section of the cord centered to the impact site as well as the spleen was then harvested. Both the cord and spleen tissue were individually dissociated by passage through a 70-µm filter and washed twice with PBS. Erythrocytes were lysed with tris-buffered ammonium chloride. Leukocytes were identified as round, phase-bright entities with a diameter of approximately 10 µm that excluded trypan blue and were enumerated on a hemocytometer. Antibodies used for phenotypic analysis were anti-CD3, -CD4, -CD8α, -CD11b, and -His48 and were

biotinylated or conjugated to R-phycoerythrin or fluorescein isothiocyanate (BD Biosciences). Streptavidin conjugated to allophycocyanin was used for the detection of biotinylated antibodies. Approximately 1×10^6 cells were stained with 0.5 µg of each monoclonal antibody as previously described (Graf et al., 2001). Cells were then fixed with Cytofix (BD Biosciences), permeablized with Cytoperm (BD Biosciences), washed with PBS, and stained with the DNA-specific dye 7-aminoactinomycin (7-AAD) at a concentration of 10 µg/ml. Three-color fluorometric analysis was performed using a FACSCanto flow cytometer (BD Biosciences). Cells were identified as 7-AAD+ events on a FL3 verses side scatter histogram as described by Lipton et al. (2005) and 10,000 7-AAD+ events were analyzed. T cell subsets were identified as CD3+/CD4+ or CD3+/CD8+ double-positive cells. Monocytes and granulocytes were identified as CD11b+ and His48+ cells, respectively.

Behavioral Outcome Assessment

All animals were gentled in an open field twice a day for 7 consecutive days prior to injury. Animals randomized to the treated group (n = 11) received daily intraperitoneal injections of FTY720 for 4 weeks. Vehicle group animals (n = 10) received daily intraperitoneal injections of 0.1% DMSO for the same time period. The injury only group (n = 9) received no injections. Laminectomies were performed on sham animals (n = 2) but no cord injuries were performed and no injections administered. At day 2 and 7 post-injury and once weekly thereafter for a total of 6 weeks, rats were placed in the open field and observed for 4 min (Figure A.1A). Two researchers blinded

to treatment groups observed the animals in open field testing. Gross locomotor recovery after SCI was assessed using the Basso-Beattie-Bresnahan (BBB) locomotor rating scale as shown in Table 3.1 (Basso et al., 1995). Observations for each hind limb were scored and averaged to provide a single score for each animal per session. All data were collected within the 4 min period. Once a plateau in locomotor recovery was evident (generally after day 28 post-injury), a frequency analysis of plantar stepping and coordination was performed across all groups.

All animals were also tested on the inclined plane task (Figure A.1B). This task evaluates the animal's ability to maintain a horizontal body position on an inclined board. The angle of the board is incrementally raised until the animal is no longer able to maintain the horizontal position. Performance on the inclined plane correlates with the integrity of the rubrospinal tract (as well as other non-pyramidal pathways) after SCI. During testing, animals were placed in the right and left side up positions. The maximum angle at which the animal was able to maintain position on the board for 10 s was recorded for each side. Data were recorded as the average of the two sides to obtain a single score for each animal per session.

Analysis of Myelin Sparing

At week 6 post-injury, animals were sacrificed with a lethal dose of pentobarbital and perfused transcardially with PBS followed by 4% paraformaldehyde. Spinal cords were harvested and postfixed for 2 h in the same fixative before being immersed in PBS overnight. The fixed cords were then cryoprotected in 30% sucrose for 48 h. FTY720-

treated (n = 9) and vehicle (n = 8) cords were blocked and embedded together in optimal cutting temperature compound and sectioned at a thickness of 20 µm. A complete series of axial sections spanning the injury site was collected and stained with eriochrome cyanine (EC) to assess for myelin sparing. Also, axial sections peripheral to the injury epicenter were collected at 0.5-mm intervals and stained with EC. For each spinal cord, the lesion epicenter was qualitatively defined by a blinded researcher as the section containing the least amount of intact tissue. This section and sections located 100 µm rostral and caudal were chosen to quantify the area of spared myelin at the epicenter. Light microscopy at 25 × magnification was used to visualize the sections and images were captured with an Olympus DP12 camera. These images were then imported into ImageJ, an open architecture image processing program developed at the National Institutes of Health, and white matter sparing analysis was performed by a blinded observer. Percent myelin spared was calculated by manually outlining the spared white matter regions which then generated an area as denoted by the number of pixels. This area was then divided by the total cross-sectional area of the axial section. The average of the three sections was used to denote the percent myelin spared at the injury epicenter. In the same fashion as described above, sections rostral and caudal to the epicenter at 0.5-mm intervals were analyzed for white matter sparing.

Statistical Analysis

The data presented here in this chapter is reported as means ± standard error of the mean. All statistical analyses were performed using the statistical software package

SPSS. Open field, inclined plane, and urine volumes data were analyzed by repeated measures two-way analysis of variance (ANOVA) with post hoc pairwise comparison test. Days to spontaneous voiding data was analyzed by one-way ANOVA with post hoc Tukey analysis. The Fisher's exact test was used for hematuria incidence and locomotor frequency analysis. Flow cytometry and myelin sparing analysis data were compared using Student's *t*-test. Differences with a p value less than 0.05 were considered statistically significant.

Results

FTY720 reduces T cell infiltration to the spinal cord lesion site after injury.

FTY720 is known to be a potent immunomodulator and numerous reports have shown that administration reduces peripheral lymphocyte circulation (Chiba et al., 1998; Brinkmann et al., 2000; Pinschewer et al., 2000). In order to establish the efficacy of FTY720 treatment in a model of SCI, we quantified inflammatory cell infiltration into injured spinal cord using flow cytometry. Data from this analysis showed that FTY720 administration significantly reduced the infiltration of CD4+ T helper cells to the spinal cord lesion site as compared to vehicle administration at day 4 post-injury (7.56 ± 0.25 vs. 3.80 ± 0.5, $p < 0.001$) (Figure A.2D). This response was similar to the reduction seen in the CD8+ cytotoxic T cell population (7.80 ± 1.01 vs. 3.68 ± 1.31, $p = 0.008$). At day 7 post-injury, a similar reduction was seen in the CD4+ T helper cells (10.01 ± 1.40 vs. 6.40 ± 0.72, $p = 0.048$) and in the CD8+ cytotoxic T cell population (8.51 ± 0.51 vs. 6.01 ± 0.40, $p = 0.009$). However, there was no difference noted in either cell population at

day 1 post-injury. For all time points, no statistical difference was noted between vehicle and FTY720 administration in the spleen tissue.

In order to evaluate for other inflammatory cell populations infiltrating the spinal cord after injury, antibody labeling for His48 (granulocytes) and CD11b (monocytes) was performed (data not shown). A slight trend towards reduction was observed with FTY720 administration in the His48+ (24 ± 2.4 vs. 20.2 ± 1.9, $p = 0.29$) and the CD11b+ cell populations (40.3 ± 1.47 vs. 32.8 ± 7.5, $p = 0.38$). However neither of these differences was statistically significant, suggesting that FTY720 specifically inhibits T cell infiltration.

FTY720 promotes hind limb recovery after spinal cord injury.

Once we established the efficacy of FTY720 in a model of SCI, our next step was to determine the extent to which administration would impact functional recovery. Hind limb function was therefore evaluated for 6 weeks after injury using the open field and inclined plane tests. During the acute and intermediate recovery stages, no differences in BBB locomotor scores were noted among groups (Figure A.3A). However, by day 21 post-injury the mean BBB score in the FTY720-treated animals surpassed those of the vehicle animals by 1.4 (11.5 vs. 10.1, $p = 0.02$). Moreover, this difference was sustained throughout the remainder of the analysis even after drug treatment was discontinued at day 28 post-injury. By the end of the analysis, the mean difference between treated and vehicle groups was 1.5 (12.5 vs. 11.0, $p = 0.001$). No differences were noted between vehicle and injury only groups at any time point.

A frequency analysis of the open field data is shown in Table 3.2 and reflects differences in locomotor milestones between the groups once recovery reached a plateau. For each time point analyzed, a significantly greater proportion of animals were consistently plantar stepping (BBB ≥ 11) or stepping with occasional coordination (BBB ≥ 12) in the FTY720-treated group as compared to vehicle and injury only groups. By day 42 post-injury, all animals in the FTY720-treated group were consistently plantar stepping and 81.8% exhibited at least occasional coordination. In contrast, only 80% of animals in the vehicle group exhibited consistent plantar stepping and only 20% were at least occasionally coordinated.

Performance on the inclined plane mirrored open field testing performance with the exception that differences were noted at earlier times along the study (Figure A.3B). By day 14 post-injury, the mean difference between treated and vehicle groups was 6.5° (35.5 vs. 29, $p < 0.0001$). Average angles were consistently higher in the treated group for the duration of the study and at day 42 post-injury the mean difference between treated and vehicle groups was 8.6° (43.9 vs. 35.3, $p < 0.0001$)

For both the open field and inclined plane tests, no significant difference in scores was detectable at any time point between vehicle and injury only control groups. Linear regression analysis revealed a very strong correlation ($r = 0.87$) between the BBB and inclined plane scores for all time points (Figure A.3C).

FTY720 improves bladder function after spinal cord injury.

A well-known consequence of SCI in both animals and humans is bladder dysfunction. Using an animal model of SCI, Wrathall et al. (2006) showed that injury severity could be directly correlated with degree of bladder dysfunction, which was reflected in the volume of urine collected during manual expression. We therefore sought to utilize bladder function as another measure of functional recovery. Figure A.4A shows that all animals had impaired bladder function immediately after SCI. However, animals in the treated group had significantly lower mean urine volumes expressed as compared to vehicle and injury only groups ($n = 10$ for each group, $p < 0.0001$). Post hoc analysis also revealed no statistical difference between vehicle and injury only groups in terms of daily urine volumes collected.

For all animals, daily bladder expressions were performed until total daily volume collected was less than 2 ml for 3 consecutive days, indicating return of spontaneous bladder function. Inter-group comparison of the number of days required to reach this milestone revealed that animals in the treated group required fewer days as compared to vehicle and injury only groups (Figure A.4B) (6.2 ± 0.4 vs. 10.3 ± 0.6 and 9.8 ± 0.74, $p < 0.0001$). No statistical difference was noted between vehicle and injury only groups.

For each urine collection, urine color was recorded. Retrospective analysis of the incidence of gross hematuria revealed that FTY720 treatment significantly reduced the incidence of gross hematuria as compared to vehicle and injury only groups (Figure A.4C) (45.5% vs. 90% and 100%, $p = 0.002$). No difference was noted when comparing vehicle and injury only groups with each other.

FTY720 and Body Weight

One important aspect of assessing the utility of an immunosuppressant drug is determining whether the drug has an unacceptable level of toxicity. Many immunomodulators, although useful in their ability to reduce inflammation, are limited by their toxicity profile. Animal body weight was used as an indicator of general toxicity and monitored throughout the course of the study. Decreases in body weight can indicate failure to thrive which would then imply drug toxicity. However, no significant differences in percent change in body weight were noted among the three treatment groups studied (Figure A.5).

Locomotor recovery correlates with myelin sparing.

In order to correlate locomotor recovery results with histological findings, we performed myelin sparing analysis of the lesion epicenter. Animals were sacrificed at the end of the final open field testing and spinal cords were harvested for EC staining. Due to the lack of differences detected in behavioral outcome between the vehicle and injury only groups, we confined our analysis to the treated ($n = 9$) and vehicle groups ($n = 8$) for comparison. The data showed that FTY720 treatment resulted in a significant increase in the percentage of myelin spared (Figure A.6C) (28.5 ±1.6 vs. 20.8 ± 1.7, $p = 0.004$). By linear regression analysis, final BBB scores also had a very strong correlation with percentage of myelin spared at the epicenter (Figure A.6D, $r = 0.75$).

Discussion

The data presented in this study demonstrate that FTY720 administered after SCI dramatically reduces T cell infiltration into the spinal cord. Furthermore, the results of behavioral outcome analyses revealed that treatment with FTY720 was effective in enhancing hind limb and bladder recovery. Interestingly, the effect of FTY720 on hind limb function was evident during the chronic phase of recovery in contrast to its effect on bladder function which was noted during the acute recovery phase. Results from morphometric analysis also provided support for the neuroprotective capacity of FTY720 and revealed that white matter preservation is enhanced with treatment.

Our initial step in establishing the efficacy of FTY720 in SCI was to determine whether treatment would affect lymphocyte infiltration into the spinal cord after injury. Analysis by flow cytometry revealed that treatment with FTY720 after SCI significantly reduced T cell infiltration into the spinal cord whereas granulocyte and monocyte populations were relatively unaltered. These data are in agreement with previously reported studies that showed that FTY720 had differential effects on CD4+ and CD8+ T cells and minimal effects on peripheral blood counts of granulocytes and monocytes (Quesniaux et al., 1999; Budde et al., 2003; Kahan et al., 2003; Bohler et al., 2004). The degree of lymphocyte reduction has been shown to be dose-dependent but previously reported reduction ranges of 30 to 70% (Quesniaux et al., 1999; Bohler et al., 2004) are in good agreement with the data reported in this study of 50 to 59%.

Our flow cytometry results clearly demonstrated the efficacy of FTY720 as an immunomodulator in post-SCI inflammatory response. However, the question remained

as to whether this would have a beneficial or detrimental effect on functional recovery. Although inflammation is a well-established sequela of CNS trauma, its role in recovery has been somewhat controversial. Both beneficial and detrimental effects have been associated with the inflammatory process. Through the release of cytokines and other factors, inflammatory cell populations such as neutrophils and macrophages have long been associated with CNS toxicity (Chao et al., 1992; Bao et al., 2002; Shamash et al., 2002; Donnelly et al., 2008). Various groups have further demonstrated that attenuation of these inflammatory mediators is beneficial and promotes neurologic recovery (Giulian et al., 1990; Blight, 1994; Popovich et al., 1999; Gris et al., 2004; Pannu et al., 2005; Beril et al., 2007). However, it has also been suggested that inflammation may play a dual role in neural recovery and may have significant beneficial aspects. As surveyors of the CNS, microglia have been hypothesized to have a clearing mechanism after spinal cord injury, eliminating debris and reducing the presence of any factors that might play an inhibitory role in CNS repair. These cells are known for their cytotoxic capabilities but they have also been shown to secrete trophic factors for both neurons and glia (Banati and Graeber, 1994; Kreutzberg, 1996). There is also evidence that macrophages may have a neuroprotective role in the CNS (Rimaniol et al., 2000; Yin et al., 2006).

The concept of protective autoimmunity has been championed by some with the implication that enhancement rather than attenuation of the immune response is necessary to promote CNS recovery (Schwartz and Kipnis, 2001, 2002; Yoles et al., 2001). Experimental data revealed that augmentation of the immune response via passive or active immunization with myelin basic protein limited secondary degeneration and

improved functional recovery after SCI (Hauben et al., 2000, 2001). As a result, efforts have been made to design vaccines for various neurodegenerative diseases as well as for CNS trauma (Schwartz, 2001). However, the concept of protective autoimmunity also runs counter to the classic concept of T cells as pathologic entities. Using T cells isolated from spinal injured rats, Popovich et al. (1996) demonstrated that injection into naïve rats resulted in neurological deficit and pathology reminiscent of EAE. Subsequent studies using transgenic mice and athymic nude rats also support the traditional view of the T cell as a pathogenic entity (Jones et al., 2002; Potas et al., 2006). Interestingly, independent efforts to replicate the original experimental vaccine protocols of Hauben et al. (2000, 2001) failed to demonstrate any benefit and in fact revealed that functional recovery was impaired with vaccination (Jones et al., 2004). This has raised some questions regarding the safety and utility of intentionally activating CNS-reactive T cells (Popovich and Jones, 2003; Jones et al., 2004).

It is clear therefore that the only conclusion that can be made regarding the inflammatory response is that it is quite complex and these studies only bolster the notion that the role of inflammation cannot be succinctly distilled as either beneficial or detrimental. In this present study we showed that administration of FTY720 dramatically reduced T cell infiltration into the spinal cord lesion site and enhanced locomotor recovery as well as tissue preservation after SCI. Although the locomotor enhancement observed in the open field and inclined plane tests was modest, frequency analysis of the open field data highlighted the differences between treatment groups. By the end of the study, the vast majority of animals in the treated group exhibited at least occasional

coordination whereas only a minority of animals in the vehicle group exhibited this milestone. Previously reported studies by Gonzales et al. (2003) using a mouse spinal hemisection model, also showed similar results after T cell infiltration was inhibited using a neutralizing antibody to a T cell chemoattractant chemokine. Similarly, Ibarra et al. (2003) showed that pharmacologic inhibition of T cell responses to spinal cord antigens using cyclosporine improved functional recovery after SCI.

The results from this present study would then imply that the T cells attenuated by FTY720 are deleterious in the process of recovery. Since FTY720 is not specific for all inflammatory cell populations, it may be that treatment is inhibitory to pathologic lymphocytic populations only and not to that subset which may have a beneficial role. However, it is clear that the mechanism of action of FTY720 is not solely limited to immunomodulation. *In vitro* studies have shown that FTY720 directly protects oligodendrocyte progenitor cells (OPC) from apoptosis (Coelho et al., 2007). Studies have also shown that FTY720 acts on endothelial cells and helps to preserve vascular integrity and barrier function (Brinkmann et al., 2004). It is therefore possible that these actions of FTY720 on vascular integrity and OPC cytoprotection could also play a role in the observed effects of the drug treatment.

Another observation that was made in our present study was the effect of FTY720 on bladder function. Drug treatment dramatically reduced post-void residuals immediately after SCI and reduced the number of days required to regain spontaneous bladder function. This observation suggests a direct drug effect on bladder function independent of spinal cord recovery. A link between FTY720 and bladder function is

supported by *in vitro* studies on rabbit bladder smooth muscle which showed that FTY720 can regulate detrusor muscle tone (Watterson et al., 2007). We also noted a dramatic reduction in the incidence of hemorrhagic cystitis after SCI. This phenomenon is known to occur after experimental SCI but the mechanism of this process has yet to be well characterized. Experimental studies have linked inflammatory changes in the spinal cord with disruption of bladder epithelium and hemorrhage (Doggweiler et al., 1998; Apodaca et al., 2003). Interestingly, studies have shown that FTY720 can act on endothelial cells and help to preserve vascular integrity and barrier function (Brinkmann et al., 2004). Thus, it is possible that this preservation of vascular integrity is responsible for the reduced incidence of hemorrhagic cystitis observed in this study.

The effect of FTY720 on bladder function, although dramatic, represented a possible confounder and limitation of this study. Overall, fewer UTIs were diagnosed in the treated as compared to vehicle group which was reflected in the number of antibiotic courses administered (6 vs. 14). This difference is hypothesized to be due to the robust effect of treatment on bladder function. Animals that were able to void more efficiently would retain less urine and therefore be at lower risk for UTI. Theoretically, this could then confound our analysis since improved overall systemic status could result in improved clinical scores in the open-field and inclined plane. However, there is a notable disparity in the time frame in which the effects of FTY720 on locomotor scores and bladder function are noted. If the above conjecture were true, then no disparity should be present and locomotor improvement should be noted coincident with bladder function improvement. Furthermore, there were no differences noted among treatment groups in

terms of body weight change, suggesting that overall systemic status was similar among the groups. Finally, morphometric analysis also supports the neuroprotective capabilities of FTY720 as improved bladder function would presumably not result in enhanced tissue preservation in the spinal cord. Taken together this leads us to conclude that administration of FTY720 enhances locomotor function independent of bladder function and systemic status.

Our results suggest that treatment with FTY720 not only reduces the adaptive immune response but also affords neuroprotection and enhances bladder function after injury. Given the complexity of the posttraumatic inflammatory cascade, the results of this study do not clarify the role of T cells in CNS recovery. However, these results do reinforce the growing body of knowledge suggesting immunomoduation as a possible therapeutic strategy in SCI.

Figure A.1. (A) Weekly hind limb evaluations were completed by putting the animals one at a time on an open field for 4 min. (B) In addition, assessment of functional recovery included an inclined plane task.

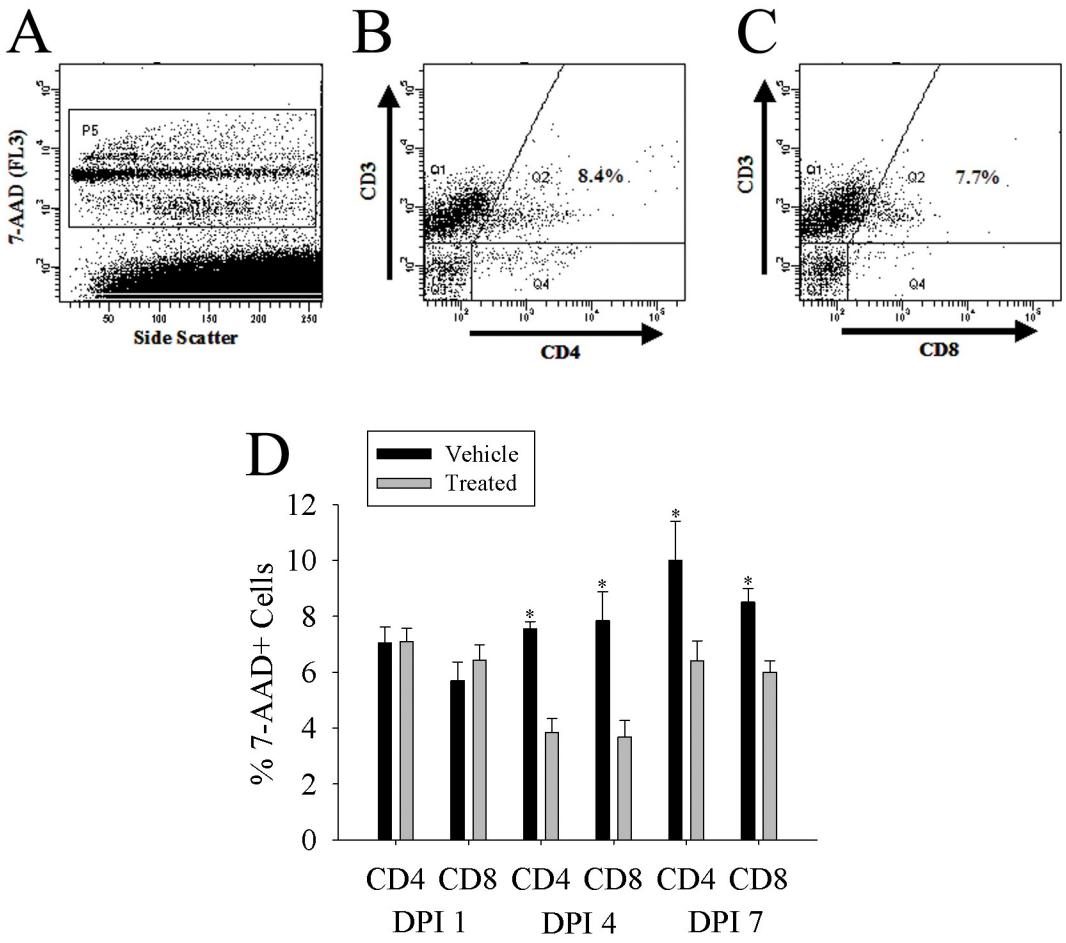

Figure A.2. FTY720 treatment reduces T cell infiltration into the spinal cord after injury. After SCI, animals were injected with either vehicle or FTY720 for 1, 4, or 7 d. A 1-cm segment of the cord centered on the impact site was then harvested from each animal and prepared for flow cytometry. (A) Representative dot blots of the injury site of a vehicle injected animal showing the 7-AAD+ population used for analysis (Gate P5). (B) Representative dot blots of the injury site of a vehicle injected animal showing the percentages of CD3+/CD4+ double-positive cells (Gate Q2) and of (C) CD3+/CD8+ double-positive cells (Gate Q2) within the 7-AAD+ gate. (D) A graphical summary of the mean percentages of 7-AAD+ events that were CD3+/CD4+ and CD3+/CD8+ for treated and vehicle animals at the various days post-injury (DPI). As shown by this flow cytometric paradigm, FTY720 treatment reduces infiltration of both CD3+/CD4+ helper and CD3+/CD8+ cytotoxic T-cell populations into the cord after SCI. $*p < 0.05$ compared with vehicle treated rats.

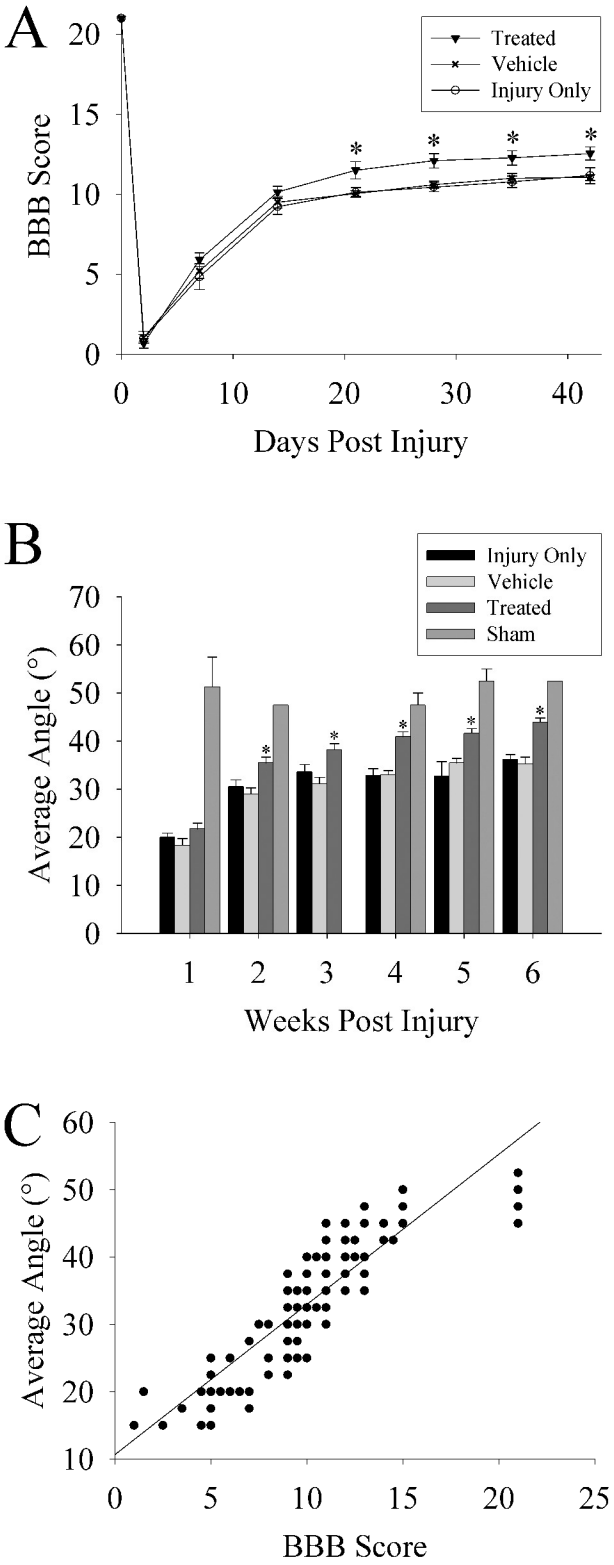

Figure A.3. FTY720 promotes hind limb recovery after spinal cord injury. After SCI, animals were randomly placed into one of three groups: injury only, vehicle, and FTY720-treated. Functional assessments were performed weekly for 6 weeks. (A) Open field assessment of hind limb locomotor function using the BBB scale. Starting at week 3, treated rats as a group performed significantly better than the control groups. No significant differences were noted between vehicle and injury only groups at any time point. (B) The inclined plane test. Treated animals outperformed members of the control groups starting at week 2 and continued to do so for the duration of the study. (C) For all time points, linear regression analysis revealed a very strong correlation between the BBB and inclined plane scores ($r = 0.87$). $*p < 0.05$ compared with injury only and vehicle treated rats.

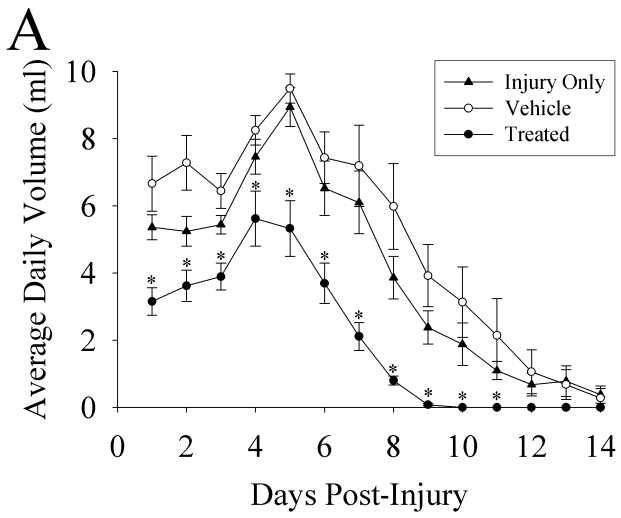

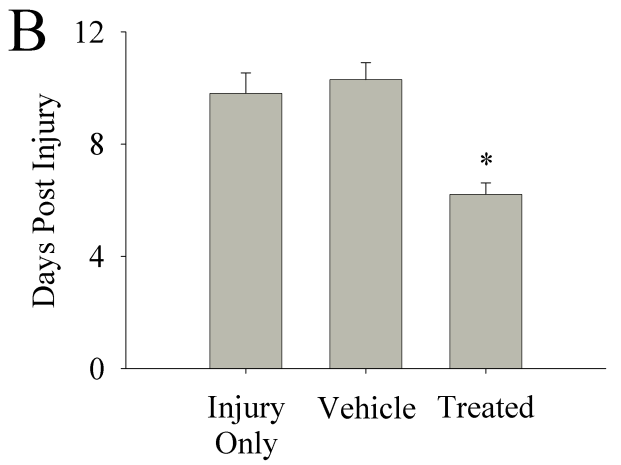

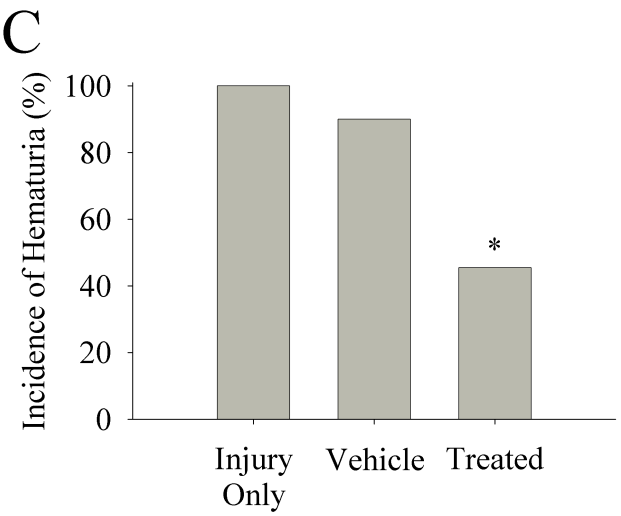

Figure A.4. FTY720 improves bladder function after spinal cord injury. Manual bladder expression was performed three times daily for the first week after SCI and two times daily thereafter until spontaneous micturation was reestablished. The residual urine volumes of each animal were measured and recorded during each expression session to provide an average daily urine volume for the first 2 weeks post-SCI. Furthermore, during urine collection, gross hematuria was noted when observed. (A) The mean residual urine volumes of treated rats were consistently and significantly lower than that of the control groups. (B) Days required until spontaneous micturation was reestablished as defined by an average daily volume of less than 2 ml for 3 consecutive days. Treated animals did not require extended assistance in expelling urine and regained spontaneous bladder function by day 6. Control animals did not reach such a milestone until day 10. (C) FTY720 treatment significantly reduced the incidence of gross hematuria as compared to control groups. *$p < 0.05$ compared with injury only and vehicle treated rats.

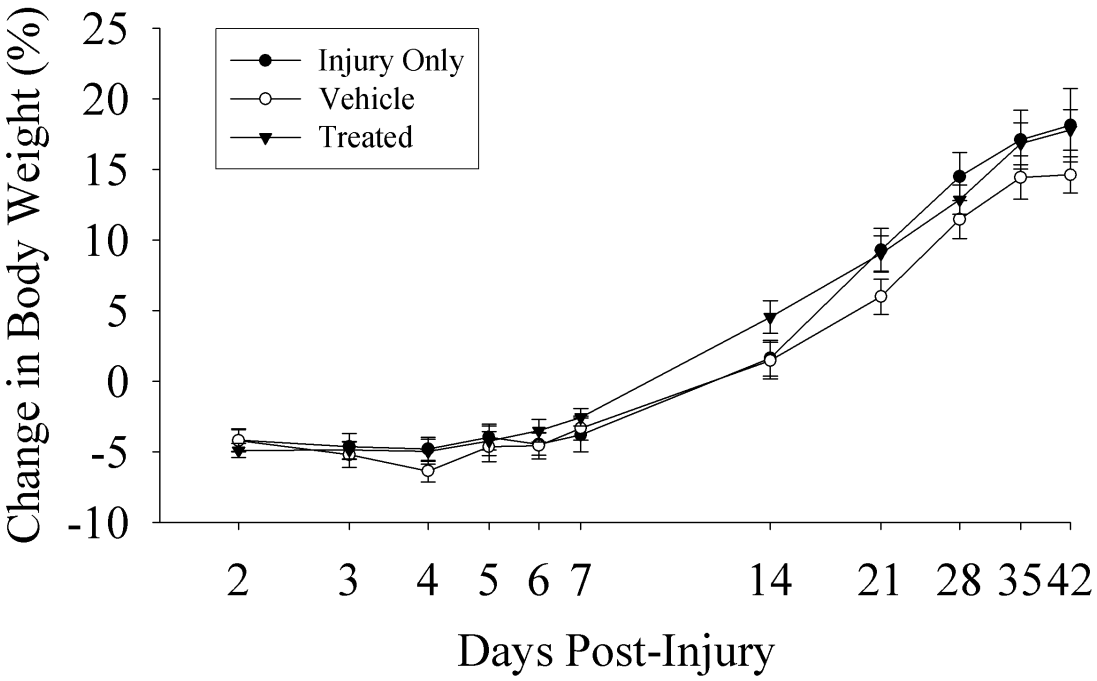

Figure A.5. FTY720 treatment does not adversely affect body weight. Animal body weights were measured and recorded throughout the duration of the behavioral outcome study. Treatment with FTY720 did not affect body weight following SCI. (The horizontal axis is presented on a logarithmic scale.)

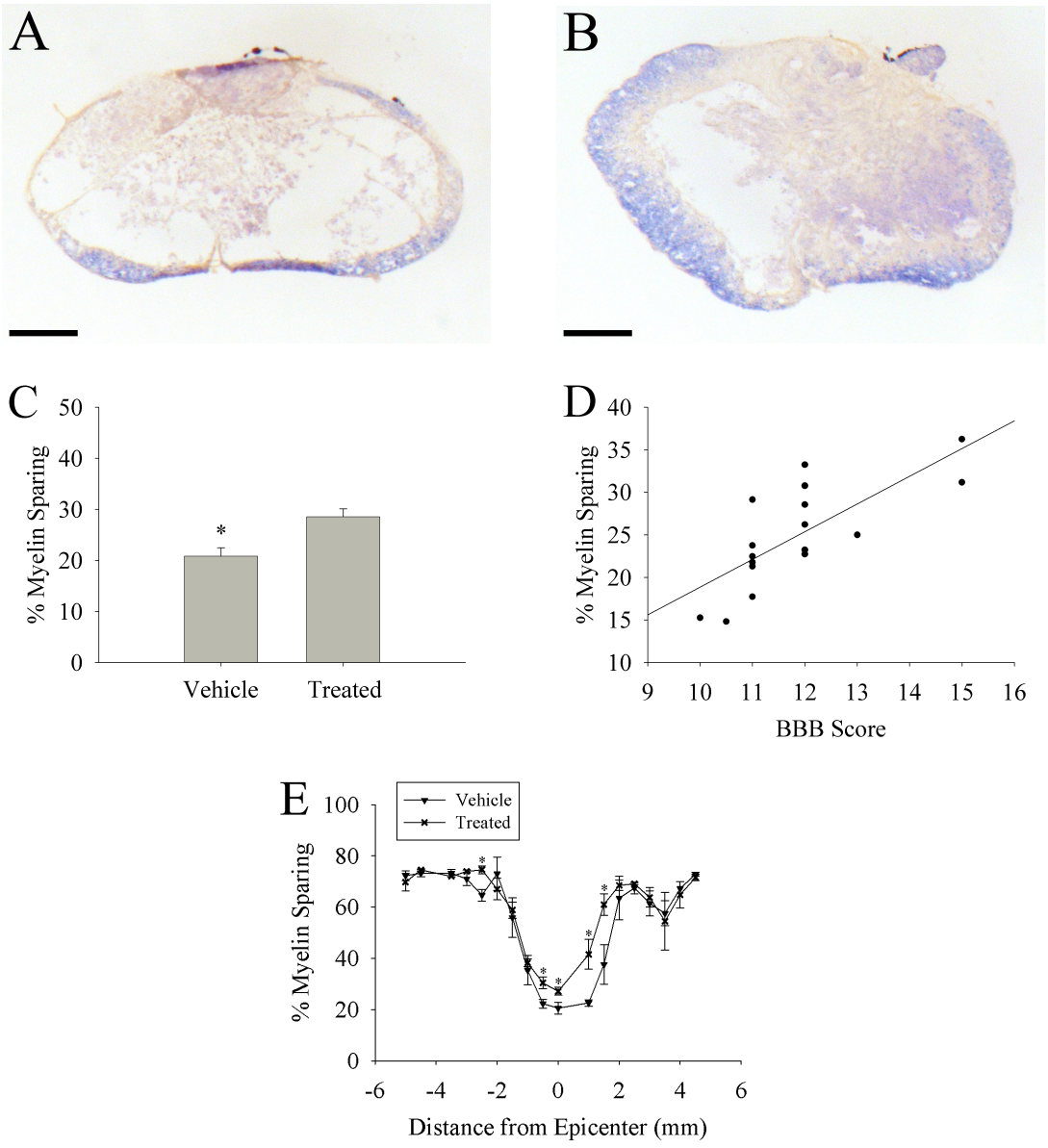

Figure A.6. Myelin sparing correlates with locomotor recovery. At the conclusion of the behavioral outcome study (6 weeks post-SCI), animals were sacrificed and cords were harvested and cryosectioned. Sections at the level of the SCI epicenter were stained with EC to determine the extent of white matter sparing. (A) A representative EC-stained cross-section at the level of the SCI epicenter from a vehicle animal. (B) A comparable section from a FTY720-treated animal. (C) At the level of the SCI epicenter, FTY720 treatment resulted in a significant increase in the percentage of spared myelin as compared to vehicle treatment. (D) A linear regression analysis of the final BBB locomotor scores and spared myelin percentages at the epicenter exhibited a very strong correlation ($r = 0.75$). (E) In addition to the myelin sparing analysis completed at the injury epicenter, adjacent cord sections of every 0.5 mm up to 5 mm away from the epicenter were similarly processed and analyzed. This analysis revealed that FTY720 treatment resulted in a significant increase in the percentage of spared myelin as compared to vehicle treatment in adjacent areas of the injury epicenter, especially regions caudal. (Negative distances on horizontal axis denote rostral direction whereas positive denote caudal direction.) Scale bars (A and B) = 300 μm. $*p < 0.05$ compared with vehicle treated rats.

BBB Locomotor Rating Scale

0	No observable hind limb movement
1	Slight movement of one or two joints, usually the hip and/or knee
2	Extensive movement of one joint or extensive movement of one joint and slight movement of one other joint
3	Extensive movement of two joints
4	Slight movement of all three joints of the hind limb
5	Slight movement of two joints and extensive movement of the third
6	Extensive movement of two joints and slight movement of the third
7	Extensive movement of all three joints of the hind limb
8	Sweeping with no weight support or plantar placement of the paw with no weight support
9	Plantar placement of the paw with weight support in stance only (i.e., when stationary) or occasional, frequent, or consistent weight supported dorsal stepping and no plantar stepping
10	Occasional weight supported plantar steps, no forelimb-hind limb coordination
11	Frequent to consistent weight supported plantar steps and no forelimb-hind limb coordination
12	Frequent to consistent weight supported plantar steps and occasional forelimb-hind limb coordination
13	Frequent to consistent weight supported plantar steps and frequent forelimb-hind limb coordination
14	Consistent weight supported plantar steps, consistent forelimb-hind limb coordination; and predominant paw position during locomotion is rotated (internally or externally) when it makes initial contact with the surface as well as just before it is lifted off at the end of stance or frequent plantar stepping, consistent forelimb-hind limb coordination, and occasional dorsal stepping
15	Consistent plantar stepping and consistent forelimb-hind limb coordination; and no toe clearance or occasional toe clearance during forward limb advancement; predominant paw position is parallel to the body at initial contact
16	Consistent plantar stepping and consistent forelimb-hind limb coordination during gait; and toe clearance occurs frequently during forward limb advancement; predominant paw position is parallel at initial contact and rotated at lift off
17	Consistent plantar stepping and consistent forelimb-hind limb coordination during gait; and toe clearance occurs frequently during forward limb advancement; predominant paw position is parallel at initial contact and lift off
18	Consistent plantar stepping and consistent forelimb-hind limb coordination during gait; and toe clearance occurs consistently during forward limb advancement; predominant paw position is parallel at initial contact and rotated at lift off
19	Consistent plantar stepping and consistent forelimb-hind limb coordination during gait; and toe clearance occurs consistently during forward limb advancement; predominant paw position is parallel at initial contact and lift off; and tail is down part or all of the time
20	Consistent plantar stepping and consistent coordinated gait; consistent toe clearance; predominant paw position is parallel at initial contact and lift off; tail consistently up; and trunk instability
21	Consistent plantar stepping and coordinated gait, consistent toe clearance, predominant paw position is parallel throughout stance, consistent trunk stability, tail consistently up

Terms and Operational Definitions

Slight	partial joint movement through less than half the range of joint motion
Extensive	movement through more than half of the range of joint motion
Sweeping	rhythmic movement of hind limb in which all three joints are extended, then fully flex and extend again; animal is usually lying on its side, the plantar surface of paw may or may not contact the ground; no weight support across the hind limb is evident
No Weight Support	no contraction of the extensor muscles of the hind limb during plantar placement of the paw; or no elevation of the hindquarter
Weight Support	contraction of the extensor muscles of the hind limb during plantar placement of the paw, or elevation of the hindquarter
Plantar Stepping	paw is in plantar contact with weight support then the hind limb is advanced forward and plantar contact with weight support is reestablished
Dorsal Stepping	weight is supported through the dorsal surface of the paw at some point in the step cycle
forelimb-hind limb Coordination	for every forelimb step an hind limb step is taken and the hind limbs alternate
Occasional	less than or equal to half; <50%
Frequent	more than half but not always; 51-94%
Consistent	nearly always or always; 95-100%
Trunk Instability	lateral weight shifts that cause waddling from side to side or a partial collapse of the trunk

Table A.1. The 21-point BBB locomotor scale used to rate functional recovery after SCI. (Adapted from Basso et al., 1995)

Percentage of Animals within Each Group Reaching Locomotor Milestones

	Day 28 Post-Injury		Day 35 Post-Injury		Day 42 Post-Injury	
	PS	C	PS	C	PS	C
Injury Only	44.4% (4/9)	11.1% (1/9)	55.6% (5/9)	11.1% (1/9)	66.7% (6/9)	33.3% (3/9)
Vehicle	50% (5/10)	10% (1/10)	70% (7/10)	20% (2/10)	80% (8/10)	20% (2/10)
FTY 720	81.8% (9/11)*	63.6% (7/11)**	100% (11/11)*	63.6% (7/11)**	100% (11/11)*	81.8% (9/11)**

Table A.2. Animals treated with FTY720 are more likely to reach locomotor milestones. Frequency analysis of rats achieving consistent plantar stepping (PS) or occasional coordination (C) between 4 and 6 weeks after injury. *$p < 0.05$ compared with injury only and vehicle treated rats. **$p < 0.005$ compared with injury only and vehicle treated rats.

References

Acheson A, Sunshine JL, Rutishauser U. NCAM polysialic acid can regulate both cell-cell and cell-substrate interactions. J Cell Biol. 1991 Jul;114(1):143-53.

Acosta CG, Fábrega AR, Mascó DH, López HS. A sensory neuron subpopulation with unique sequential survival dependence on nerve growth factor and basic fibroblast growth factor during development. J Neurosci. 2001 Nov 15;21(22):8873-85.

Akiyama Y, Radtke C, Kocsis JD. Remyelination of the rat spinal cord by transplantation of identified bone marrow stromal cells. J Neurosci. 2002 Aug 1;22(15):6623-30.

Alexander JK, Fuss B, Colello RJ. Electric field-induced astrocyte alignment directs neurite outgrowth. Neuron Glia Biol. 2006 May;2(2):93-103.

Anderson DK, Demediuk P, Saunders RD, Dugan LL, Means ED, Horrocks LA. Spinal cord injury and protection. Ann Emerg Med. 1985 Aug;14(8):816-21.

Ankeny DP, Lucin KM, Sanders VM, McGaughy VM, Popovich PG. Spinal cord injury triggers systemic autoimmunity: evidence for chronic B lymphocyte activation and lupus-like autoantibody synthesis. J Neurochem. 2006 Nov;99(4):1073-87.

Apodaca G, Kiss S, Ruiz W, Meyers S, Zeidel M, Birder L. Disruption of bladder epithelium barrier function after spinal cord injury. Am J Physiol Renal Physiol. 2003 May;284(5):F966-76.

Asher RA, Morgenstern DA, Fidler PS, Adcock KH, Oohira A, Braistead JE, Levine JM, Margolis RU, Rogers JH, Fawcett JW. Neurocan is upregulated in injured brain and in cytokine-treated astrocytes. J Neurosci. 2000 Apr 1;20(7):2427-38.

Asher RA, Morgenstern DA, Shearer MC, Adcock KH, Pesheva P, Fawcett JW. Versican is upregulated in CNS injury and is a product of oligodendrocyte lineage cells. J Neurosci. 2002 Mar 15;22(6):2225-36.

Ayres CE, Bowlin GL, Henderson SC, Taylor L, Shultz J, Alexander J, Telemeco TA, Simpson DG. Modulation of anisotropy in electrospun tissue-engineering scaffolds: Analysis of fiber alignment by the fast Fourier transform. Biomaterials. 2006 Nov;27(32):5524-34.

Ayres CE, Jha BS, Meredith H, Bowman JR, Bowlin GL, Henderson SC, Simpson DG. Measuring fiber alignment in electrospun scaffolds: a user's guide to the 2D fast Fourier transform approach. J Biomater Sci Polym Ed. 2008;19(5):603-21.

Balentine JD. Pathology of experimental spinal cord trauma. I. The necrotic lesion as a function of vascular injury. Lab Invest. 1978 Sep;39(3):236-53.

Banati RB, Graeber MB. Surveillance, intervention and cytotoxicity: is there a protective role of microglia? Dev Neurosci. 1994;16(3-4):114-27.

Bao F, Liu D. Peroxynitrite generated in the rat spinal cord induces neuron death and neurological deficits. Neuroscience. 2002;115(3):839-49.

Barbacid M. The Trk family of neurotrophin receptors. J Neurobiol. 1994 Nov;25(11):1386-403.

Basso DM, Beattie MS, Bresnahan JC. A sensitive and reliable locomotor rating scale for open field testing in rats. J Neurotrauma. 1995 Feb;12(1):1-21.

Beril Gok H, Solaroglu I, Okutan O, Cimen B, Kaptanoglu E, Palaoglu S. Metoprolol treatment decreases tissue myeloperoxidase activity after spinal cord injury in rats. J Clin Neurosci. 2007 Feb;14(2):138-42.

Berkowitz M, O'Leary P, Kruse D, Harvey C. Spinal cord injury: an analysis of medical and social costs. Demos Medical Publishing Inc., 1998.

Bilsland JG, Haldon C, Goddard J, Oliver K, Murray F, Wheeldon A, Cumberbatch J, McAllister G, Munoz-Sanjuan I. A rapid method for the quantification of mouse hippocampal neurogenesis *in vivo* by flow cytometry. Validation with conventional and enhanced immunohistochemical methods. J Neurosci Methods. 2006 Oct 15;157(1):54-63.

Blesch A, Tuszynski MH. Transient growth factor delivery sustains regenerated axons after spinal cord injury. J Neurosci. 2007 Sep 26;27(39):10535-45.

Blight AR. Effects of silica on the outcome from experimental spinal cord injury: implication of macrophages in secondary tissue damage. Neuroscience. 1994 May;60(1):263-73.

Blight AR. Macrophages and inflammatory damage in spinal cord injury. J Neurotrauma. 1992 Mar;9 Suppl 1:S83-91.

Blight AR, Cohen TI, Saito K, Heyes MP. Quinolinic acid accumulation and functional deficits following experimental spinal cord injury. Brain. 1995 Jun;118 (Pt 3):735-52.

Böhler T, Waiser J, Schuetz M, Neumayer HH, Budde K. FTY720 exerts differential effects on CD4+ and CD8+ T-lymphocyte subpopulations expressing chemokine and adhesion receptors. Nephrol Dial Transplant. 2004 Mar;19(3):702-13.

Boland ED, Coleman BD, Barnes CP, Simpson DG, Wnek GE, Bowlin GL. Electrospinning polydioxanone for biomedical applications. Acta Biomater. 2005 Jan;1(1):115-23.

Boland ED, Matthews JA, Pawlowski KJ, Simpson DG, Wnek GE, Bowlin GL. Electrospinning collagen and elastin: preliminary vascular tissue engineering. Front Biosci. 2004 May 1;9:1422-32.

Bouslama-Oueghlani L, Wehrlé R, Sotelo C, Dusart I. Heterogeneity of NG2-expressing cells in the newborn mouse cerebellum. Dev Biol. 2005 Sep 15;285(2):409-21.

Bowlin G.L., Pawlowski K.J., Stitzel J.D., Boland E.D., Simpson D.G., Fenn J.B. et al. (2002) Electrospinning of polymer scaffolds for tissue engineering. In Lewandrowski K., Wise D., Trantolo D., Gresser J., Yaszemski M. ad Altobelli D. (eds) Tissue engineering and biodegradable equivalents: scientific and clinical applications. Marcel Dekker, pp.165-178.

Bradbury EJ, Moon LD, Popat RJ, King VR, Bennett GS, Patel PN, Fawcett JW, McMahon SB. Chondroitinase ABC promotes functional recovery after spinal cord injury. Nature. 2002 Apr 11;416(6881):636-40.

Bregman BS, McAtee M, Dai HN, Kuhn PL. Neurotrophic factors increase axonal growth after spinal cord injury and transplantation in the adult rat. Exp Neurol. 1997 Dec;148(2):475-94.

Bresnahan JC, Beattie MS, Stokes BT, Conway KM. Three-dimensional computer-assisted analysis of graded contusion lesions in the spinal cord of the rat. J Neurotrauma. 1991 Summer;8(2):91-101.

Brinkmann V, Cyster JG, Hla T. FTY720: sphingosine 1-phosphate receptor-1 in the control of lymphocyte egress and endothelial barrier function. Am J Transplant. 2004 Jul;4(7):1019-25.

Brinkmann V, Davis MD, Heise CE, Albert R, Cottens S, Hof R, Bruns C, Prieschl E, Baumruker T, Hiestand P, Foster CA, Zollinger M, Lynch KR. The immune

modulator FTY720 targets sphingosine 1-phosphate receptors. J Biol Chem. 2002 Jun 14;277(24):21453-7.

Brinkmann V, Pinschewer D, Chiba K, Feng L. FTY720: a novel transplantation drug that modulates lymphocyte traffic rather than activation. Trends Pharmacol Sci. 2000 Feb;21(2):49-52.

Brittis PA, Canning DR, Silver J. Chondroitin sulfate as a regulator of neuronal patterning in the retina. Science. 1992 Feb 7;255(5045):733-6.

Budde K, L Schmouder R, Nashan B, Brunkhorst R, W Lücker P, Mayer T, Brookman L, Nedelman J, Skerjanec A, Böhler T, Neumayer HH. Pharmacodynamics of single doses of the novel immunosuppressant FTY720 in stable renal transplant patients. Am J Transplant. 2003 Jul;3(7):846-54.

Bullock R, Maxwell WL, Graham DI, Teasdale GM, Adams JH. Glial swelling following human cerebral contusion: an ultrastructural study. J Neurol Neurosurg Psychiatry. 1991 May;54(5):427-34.

Bunge RP, Puckett WR, Becerra JL, Marcillo A, Quencer RM. Observations on the pathology of human spinal cord injury. A review and classification of 22 new cases with details from a case of chronic cord compression with extensive focal demyelination. Adv Neurol. 1993;59:75-89.

Bush TG, Puvanachandra N, Horner CH, Polito A, Ostenfeld T, Svendsen CN, Mucke L, Johnson MH, Sofroniew MV. Leukocyte infiltration, neuronal degeneration, and neurite outgrowth after ablation of scar-forming, reactive astrocytes in adult transgenic mice. Neuron. 1999 Jun;23(2):297-308.

Caggiano AO, Zimber MP, Ganguly A, Blight AR, Gruskin EA. Chondroitinase ABCI improves locomotion and bladder function following contusion injury of the rat spinal cord. J Neurotrauma. 2005 Feb;22(2):226-39.

Cai D, Shen Y, De Bellard M, Tang S, Filbin MT. Prior exposure to neurotrophins blocks inhibition of axonal regeneration by MAG and myelin via a cAMP-dependent mechanism. Neuron. 1999 Jan;22(1):89-101.

Cai Z, Pang Y, Lin S, Rhodes PG. Differential roles of tumor necrosis factor-alpha and interleukin-1 beta in lipopolysaccharide-induced brain injury in the neonatal rat. Brain Res. 2003 Jun 13;975(1-2):37-47.

Canning DR, Höke A, Malemud CJ, Silver J. A potent inhibitor of neurite outgrowth that predominates in the extracellular matrix of reactive astrocytes. Int J Dev Neurosci. 1996 Jun;14(3):153-75.

Carlson SL, Parrish ME, Springer JE, Doty K, Dossett L. Acute inflammatory response in spinal cord following impact injury. Exp Neurol. 1998 May;151(1):77-88.

Chao CC, Hu S, Molitor TW, Shaskan EG, Peterson PK. Activated microglia mediate neuronal cell injury via a nitric oxide mechanism. J Immunol. 1992 Oct 15;149(8):2736-41.

Chen C, Zhou XF, Rush RA. Neurotrophin-3 and trkC-immunoreactive neurons in rat dorsal root ganglia correlate by distribution and morphology. Neurochem Res. 1996 Jul;21(7):809-14.

Chen MS, Huber AB, van der Haar ME, Frank M, Schnell L, Spillmann AA, Christ F, Schwab ME. Nogo-A is a myelin-associated neurite outgrowth inhibitor and an antigen for monoclonal antibody IN-1. Nature. 2000 Jan 27;403(6768):434-9.

Cheng CM, Mervis RF, Niu SL, Salem N Jr, Witters LA, Tseng V, Reinhardt R, Bondy CA. Insulin-like growth factor 1 is essential for normal dendritic growth. J Neurosci Res. 2003 Jul 1;73(1):1-9.

Chiba K, Yanagawa Y, Masubuchi Y, Kataoka H, Kawaguchi T, Ohtsuki M, Hoshino Y. FTY720, a novel immunosuppressant, induces sequestration of circulating mature lymphocytes by acceleration of lymphocyte homing in rats. I. FTY720 selectively decreases the number of circulating mature lymphocytes by acceleration of lymphocyte homing. J Immunol. 1998 May 15;160(10):5037-44.

Chuckowree JA, Dickson TC, Vickers JC. Intrinsic regenerative ability of mature CNS neurons. Neuroscientist. 2004 Aug;10(4):280-5.

Coelho RP, Payne SG, Bittman R, Spiegel S, Sato-Bigbee C. The immunomodulator FTY720 has a direct cytoprotective effect in oligodendrocyte progenitors. J Pharmacol Exp Ther. 2007 Nov;323(2):626-35.

Cortes M, Baria AT, Schwartz NB. Sulfation of chondroitin sulfate proteoglycans is necessary for proper Indian hedgehog signaling in the developing growth plate. Development. 2009 May;136(10):1697-706.

Davies JE, Huang C, Proschel C, Noble M, Mayer-Proschel M, Davies SJ. Astrocytes derived from glial-restricted precursors promote spinal cord repair. J Biol. 2006;5(3):7.

Doggweiler R, Jasmin L, Schmidt RA. Neurogenically mediated cystitis in rats: an animal model. J Urol. 1998 Oct;160(4):1551-6.

Domeniconi M, Filbin MT. Overcoming inhibitors in myelin to promote axonal regeneration. J Neurol Sci. 2005 Jun 15;233(1-2):43-7.

Donnelly DJ, Popovich PG. Inflammation and its role in neuroprotection, axonal regeneration and functional recovery after spinal cord injury. Exp Neurol. 2008 Feb;209(2):378-88.

Dougherty KD, Dreyfus CF, Black IB. Brain-derived neurotrophic factor in astrocytes, oligodendrocytes, and microglia/macrophages after spinal cord injury. Neurobiol Dis. 2000 Dec;7(6 Pt B):574-85.

Dusart I, Schwab ME. Secondary cell death and the inflammatory reaction after dorsal hemisection of the rat spinal cord. Eur J Neurosci. 1994 May 1;6(5):712-24.

Esposito D, Patel P, Stephens RM, Perez P, Chao MV, Kaplan DR, Hempstead BL. The cytoplasmic and transmembrane domains of the p75 and Trk A receptors regulate high affinity binding to nerve growth factor. J Biol Chem. 2001 Aug 31;276(35):32687-95.

Faulkner JR, Herrmann JE, Woo MJ, Tansey KE, Doan NB, Sofroniew MV. Reactive astrocytes protect tissue and preserve function after spinal cord injury. J Neurosci. 2004 Mar 3;24(9):2143-55.

Fitch MT, Silver J. CNS injury, glial scars, and inflammation: Inhibitory extracellular matrices and regeneration failure. Exp Neurol. 2008 Feb;209(2):294-301.

Fridrikh SV, Yu JH, Brenner MP, Rutledge GC. Controlling the fiber diameter during electrospinning. Phys Rev Lett. 2003 Apr 11;90(14):144502.

Fujino M, Funeshima N, Kitazawa Y, Kimura H, Amemiya H, Suzuki S, Li XK. Amelioration of experimental autoimmune encephalomyelitis in Lewis rats by FTY720 treatment. J Pharmacol Exp Ther. 2003 Apr;305(1):70-7.

Gallo G, Lefcort FB, Letourneau PC. The trkA receptor mediates growth cone turning toward a localized source of nerve growth factor. J Neurosci. 1997 Jul 15;17(14):5445-54.

Gao Y, Nikulina E, Mellado W, Filbin MT. Neurotrophins elevate cAMP to reach a threshold required to overcome inhibition by MAG through extracellular signal-regulated kinase-dependent inhibition of phosphodiesterase. J Neurosci. 2003 Dec 17;23(37):11770-7.

Gehler S, Shaw AE, Sarmiere PD, Bamburg JR, Letourneau PC. Brain-derived neurotrophic factor regulation of retinal growth cone filopodial dynamics is

mediated through actin depolymerizing factor/cofilin. J Neurosci. 2004 Nov 24;24(47):10741-9.

Genovese T, Mazzon E, Crisafulli C, Di Paola R, Muià C, Bramanti P, Cuzzocrea S. Immunomodulatory effects of etanercept in an experimental model of spinal cord injury. J Pharmacol Exp Ther. 2006 Mar;316(3):1006-16.

Giulian D, Robertson C. Inhibition of mononuclear phagocytes reduces ischemic injury in the spinal cord. Ann Neurol. 1990 Jan;27(1):33-42.

Glaser J, Gonzalez R, Perreau VM, Cotman CW, Keirstead HS. Neutralization of the chemokine CXCL10 enhances tissue sparing and angiogenesis following spinal cord injury. J Neurosci Res. 2004 Sep 1;77(5):701-8.

Gonzalez R, Glaser J, Liu MT, Lane TE, Keirstead HS. Reducing inflammation decreases secondary degeneration and functional deficit after spinal cord injury. Exp Neurol. 2003 Nov;184(1):456-63.

Gopalakrishnan SM, Teusch N, Imhof C, Bakker MH, Schurdak M, Burns DJ, Warrior U. Role of Rho kinase pathway in chondroitin sulfate proteoglycan-mediated inhibition of neurite outgrowth in PC12 cells. J Neurosci Res. 2008 Aug 1;86(10):2214-26.

Graf MR, Prins RM, Merchant RE. IL-6 secretion by a rat T9 glioma clone induces a neutrophil-dependent antitumor response with resultant cellular, antiglioma immunity. J Immunol. 2001 Jan 1;166(1):121-9.

Gris D, Marsh DR, Oatway MA, Chen Y, Hamilton EF, Dekaban GA, Weaver LC. Transient blockade of the CD11d/CD18 integrin reduces secondary damage after spinal cord injury, improving sensory, autonomic, and motor function. J Neurosci. 2004 Apr 21;24(16):4043-51.

Hauben E, Agranov E, Gothilf A, Nevo U, Cohen A, Smirnov I, Steinman L, Schwartz M. Posttraumatic therapeutic vaccination with modified myelin self-antigen prevents complete paralysis while avoiding autoimmune disease. J Clin Invest. 2001 Aug;108(4):591-9.

Hauben E, Butovsky O, Nevo U, Yoles E, Moalem G, Agranov E, Mor F, Leibowitz-Amit R, Pevsner E, Akselrod S, Neeman M, Cohen IR, Schwartz M. Passive or active immunization with myelin basic protein promotes recovery from spinal cord contusion. J Neurosci. 2000 Sep 1;20(17):6421-30.

Hermann GE, Rogers RC, Bresnahan JC, Beattie MS. Tumor necrosis factor-alpha induces cFOS and strongly potentiates glutamate-mediated cell death in the rat spinal cord. Neurobiol Dis. 2001 Aug;8(4):590-9.

Honig MG, Rutishauser US. Changes in the segmental pattern of sensory neuron projections in the chick hindlimb under conditions of altered cell adhesion molecule function. Dev Biol. 1996 May 1;175(2):325-37.

Houle JD, Tom VJ, Mayes D, Wagoner G, Phillips N, Silver J. Combining an autologous peripheral nervous system "bridge" and matrix modification by chondroitinase allows robust, functional regeneration beyond a hemisection lesion of the adult rat spinal cord. J Neurosci. 2006 Jul 12;26(28):7405-15.

Huang WC, Kuo WC, Cherng JH, Hsu SH, Chen PR, Huang SH, Huang MC, Liu JC, Cheng H. Chondroitinase ABC promotes axonal re-growth and behavior recovery in spinal cord injury. Biochem Biophys Res Commun. 2006 Oct 27;349(3):963-8.

Hung KS, Tsai SH, Lee TC, Lin JW, Chang CK, Chiu WT. Gene transfer of insulin-like growth factor-I providing neuroprotection after spinal cord injury in rats. J Neurosurg Spine. 2007 Jan;6(1):35-46.

Iaci JF, Vecchione AM, Zimber MP, Caggiano AO. Chondroitin sulfate proteoglycans in spinal cord contusion injury and the effects of chondroitinase treatment. J Neurotrauma. 2007 Nov;24(11):1743-59.

Iarikov DE, Kim BG, Dai HN, McAtee M, Kuhn PL, Bregman BS. Delayed transplantation with exogenous neurotrophin administration enhances plasticity of corticofugal projections after spinal cord injury. J Neurotrauma. 2007 Apr;24(4):690-702.

Ibarra A, Correa D, Willms K, Merchant MT, Guizar-Sahagún G, Grijalva I, Madrazo I. Effects of cyclosporin-A on immune response, tissue protection and motor function of rats subjected to spinal cord injury. Brain Res. 2003 Jul 25;979(1-2):165-78.

Ito T, Oyanagi K, Wakabayashi K, Ikuta F. Traumatic spinal cord injury: a neuropathological study on the longitudinal spreading of the lesions. Acta Neuropathol. 1997 Jan;93(1):13-8.

Jacobson MD, Weil M, Raff MC. Programmed cell death in animal development. Cell. 1997 Feb 7;88(3):347-54.

Jones TB, Ankeny DP, Guan Z, McGaughy V, Fisher LC, Basso DM, Popovich PG. Passive or active immunization with myelin basic protein impairs neurological function and exacerbates neuropathology after spinal cord injury in rats. J Neurosci. 2004 Apr 14;24(15):3752-61.

Kahan BD, Karlix JL, Ferguson RM, Leichtman AB, Mulgaonkar S, Gonwa TA, Skerjanec A, Schmouder RL, Chodoff L. Pharmacodynamics, pharmacokinetics, and safety of multiple doses of FTY720 in stable renal transplant patients: a multicenter, randomized, placebo-controlled, phase I study. Transplantation. 2003 Oct 15;76(7):1079-84.

Kakulas BA. Pathology of spinal injuries. Cent Nerv Syst Trauma. 1984 Winter;1(2):117-29.

Kalderon N, Xu S, Koutcher JA, Fuks Z. Fractionated radiation facilitates repair and functional motor recovery after spinal cord transection in rat. Brain Res. 2001 Jun 22;904(2):199-207.

Kottis V, Thibault P, Mikol D, Xiao ZC, Zhang R, Dergham P, Braun PE. Oligodendrocyte-myelin glycoprotein (OMgp) is an inhibitor of neurite outgrowth. J Neurochem. 2002 Sep;82(6):1566-9.

Krenz NR, Meakin SO, Krassioukov AV, Weaver LC. Neutralizing intraspinal nerve growth factor blocks autonomic dysreflexia caused by spinal cord injury. J Neurosci. 1999 Sep 1;19(17):7405-14.

Krenz NR, Weaver LC. Nerve growth factor in glia and inflammatory cells of the injured rat spinal cord. J Neurochem. 2000 Feb;74(2):730-9.

Kreutzberg GW. Microglia: a sensor for pathological events in the CNS. Trends Neurosci. 1996 Aug;19(8):312-8.

Lee YB, Yune TY, Baik SY, Shin YH, Du S, Rhim H, Lee EB, Kim YC, Shin ML, Markelonis GJ, Oh TH. Role of tumor necrosis factor-alpha in neuronal and glial apoptosis after spinal cord injury. Exp Neurol. 2000 Nov;166(1):190-5.

Lemons ML, Howland DR, Anderson DK. Chondroitin sulfate proteoglycan immunoreactivity increases following spinal cord injury and transplantation. Exp Neurol. 1999 Nov;160(1):51-65.

Lemons ML, Sandy JD, Anderson DK, Howland DR. Intact aggrecan and chondroitin sulfate-depleted aggrecan core glycoprotein inhibit axon growth in the adult rat spinal cord. Exp Neurol. 2003 Dec;184(2):981-90.

Li Y, Field PM, Raisman G. Repair of adult rat corticospinal tract by transplants of olfactory ensheathing cells. Science. 1997 Sep 26;277(5334):2000-2.

Lipton HL, Kallio P, Jelachich ML. Simplified quantitative analysis of spinal cord cells from Theiler's virus-infected mice without the requirement for myelin debris removal. J Immunol Methods. 2005 Apr;299(1-2):107-15.

Liu BP, Fournier A, GrandPré T, Strittmatter SM. Myelin-associated glycoprotein as a functional ligand for the Nogo-66 receptor. Science. 2002 Aug 16;297(5584):1190-3.

Mandala S, Hajdu R, Bergstrom J, Quackenbush E, Xie J, Milligan J, Thornton R, Shei GJ, Card D, Keohane C, Rosenbach M, Hale J, Lynch CL, Rupprecht K, Parsons W, Rosen H. Alteration of lymphocyte trafficking by sphingosine-1-phosphate receptor agonists. Science. 2002 Apr 12;296(5566):346-9.

Marchand R, Woerly S, Bertrand L, Valdes N. Evaluation of two cross-linked collagen gels implanted in the transected spinal cord. Brain Res Bull. 1993;30(3-4):415-22.

Markus A, Patel TD, Snider WD. Neurotrophic factors and axonal growth. Curr Opin Neurobiol. 2002 Oct;12(5):523-31.

Marmarou A, Signoretti S, Aygok G, Fatouros P, Portella G. Traumatic brain edema in diffuse and focal injury: cellular or vasogenic? Acta Neurochir Suppl. 2006;96:24-9.

Massey JM, Amps J, Viapiano MS, Matthews RT, Wagoner MR, Whitaker CM, Alilain W, Yonkof AL, Khalyfa A, Cooper NG, Silver J, Onifer SM. Increased chondroitin sulfate proteoglycan expression in denervated brainstem targets following spinal cord injury creates a barrier to axonal regeneration overcome by chondroitinase ABC and neurotrophin-3. Exp Neurol. 2008 Feb;209(2):426-45.

Matloubian M, Lo CG, Cinamon G, Lesneski MJ, Xu Y, Brinkmann V, Allende ML, Proia RL, Cyster JG. Lymphocyte egress from thymus and peripheral lymphoid organs is dependent on S1P receptor 1. Nature. 2004 Jan 22;427(6972):355-60.

McCarthy KD, de Vellis J. Preparation of separate astroglial and oligodendroglial cell cultures from rat cerebral tissue. J Cell Biol. 1980 Jun;85(3):890-902.

McDonald JW, Liu XZ, Qu Y, Liu S, Mickey SK, Turetsky D, Gottlieb DI, Choi DW. Transplanted embryonic stem cells survive, differentiate and promote recovery in injured rat spinal cord. Nat Med. 1999 Dec;5(12):1410-2.

McGinn MJ, Sun D, Colello RJ. Utilizing X-irradiation to selectively eliminate neural stem/progenitor cells from neurogenic regions of the mammalian brain. J Neurosci Methods. 2008 May 15;170(1):9-15.

McKeon RJ, Höke A, Silver J. Injury-induced proteoglycans inhibit the potential for laminin-mediated axon growth on astrocytic scars. Exp Neurol. 1995 Nov;136(1):32-43.

McKeon RJ, Jurynec MJ, Buck CR. The chondroitin sulfate proteoglycans neurocan and phosphacan are expressed by reactive astrocytes in the chronic CNS glial scar. J Neurosci. 1999 Dec 15;19(24):10778-88.

McKerracher L, David S, Jackson DL, Kottis V, Dunn RJ, Braun PE. Identification of myelin-associated glycoprotein as a major myelin-derived inhibitor of neurite growth. Neuron. 1994 Oct;13(4):805-11.

Mitsui T, Fischer I, Shumsky JS, Murray M. Transplants of fibroblasts expressing BDNF and NT-3 promote recovery of bladder and hindlimb function following spinal contusion injury in rats. Exp Neurol. 2005 Aug;194(2):410-31.

Moon LD, Fawcett JW. Reduction in CNS scar formation without concomitant increase in axon regeneration following treatment of adult rat brain with a combination of antibodies to TGFbeta1 and beta2. Eur J Neurosci. 2001 Nov;14(10):1667-77.

Morgenstern DA, Asher RA, Fawcett JW. Chondroitin sulphate proteoglycans in the CNS injury response. Prog Brain Res. 2002;137:313-32.

Namiki J, Kojima A, Tator CH. Effect of brain-derived neurotrophic factor, nerve growth factor, and neurotrophin-3 on functional recovery and regeneration after spinal cord injury in adult rats. J Neurotrauma. 2000 Dec;17(12):1219-31.

Nesic O, Xu GY, McAdoo D, High KW, Hulsebosch C, Perez-Pol R. IL-1 receptor antagonist prevents apoptosis and caspase-3 activation after spinal cord injury. J Neurotrauma. 2001 Sep;18(9):947-56.

Niblock MM, Brunso-Bechtold JK, Riddle DR. Insulin-like growth factor I stimulates dendritic growth in primary somatosensory cortex. J Neurosci. 2000 Jun 1;20(11):4165-76.

Norenberg MD, Smith J, Marcillo A. The pathology of human spinal cord injury: defining the problems. J Neurotrauma. 2004 Apr;21(4):429-40.

Noushi F, Richardson RT, Hardman J, Clark G, O'Leary S. Delivery of neurotrophin-3 to the cochlea using alginate beads. Otol Neurotol. 2005 May;26(3):528-33.

Okada S, Nakamura M, Katoh H, Miyao T, Shimazaki T, Ishii K, Yamane J, Yoshimura A, Iwamoto Y, Toyama Y, Okano H. Conditional ablation of Stat3 or Socs3 discloses a dual role for reactive astrocytes after spinal cord injury. Nat Med. 2006 Jul;12(7):829-34.

Ozdinler PH, Macklis JD. IGF-I specifically enhances axon outgrowth of corticospinal motor neurons. Nat Neurosci. 2006 Nov;9(11):1371-81.

Pannu R, Barbosa E, Singh AK, Singh I. Attenuation of acute inflammatory response by atorvastatin after spinal cord injury in rats. J Neurosci Res. 2005 Feb 1;79(3):340-50.

Pinjuh D, Bedi KS. X-irradiation of adult spinal cord increases its capacity to support neurite regeneration *in vitro*. Int J Dev Neurosci. 2003 Nov;21(7):409-16.

Pinschewer DD, Ochsenbein AF, Odermatt B, Brinkmann V, Hengartner H, Zinkernagel RM. FTY720 immunosuppression impairs effector T cell peripheral homing without affecting induction, expansion, and memory. J Immunol. 2000 Jun 1;164(11):5761-70.

Popovich PG, Guan Z, Wei P, Huitinga I, van Rooijen N, Stokes BT. Depletion of hematogenous macrophages promotes partial hindlimb recovery and neuroanatomical repair after experimental spinal cord injury. Exp Neurol. 1999 Aug;158(2):351-65.

Popovich PG, Jones TB. Manipulating neuroinflammatory reactions in the injured spinal cord: back to basics. Trends Pharmacol Sci. 2003 Jan;24(1):13-7.

Popovich PG, Stokes BT, Whitacre CC. Concept of autoimmunity following spinal cord injury: possible roles for T lymphocytes in the traumatized central nervous system. J Neurosci Res. 1996 Aug 15;45(4):349-63.

Potas JR, Zheng Y, Moussa C, Venn M, Gorrie CA, Deng C, Waite PM. Augmented locomotor recovery after spinal cord injury in the athymic nude rat. J Neurotrauma. 2006 May;23(5):660-73.

Powell EM, Meiners S, DiProspero NA, Geller HM. Mechanisms of astrocyte-directed neurite guidance. Cell Tissue Res. 1997 Nov;290(2):385-93.

Quesniaux V, Fullard L, Arendse H, Davison G, Markgraaff N, Auer R, Ehrhart F, Kraus G, Schuurman HJ. A novel immunosuppressant, FTY720, induces peripheral lymphodepletion of both T- and B cells and immunosuppression in baboons. Transpl Immunol. 1999 Sep;7(3):149-57.

Ramón y Cajal. Degeneration and regeneration of the nervous system. Hafner, 1928.

Reier PJ, Bregman BS, Wujek JR. Intraspinal transplantation of embryonic spinal cord tissue in neonatal and adult rats. J Comp Neurol. 1986 May 15;247(3):275-96.

Renault-Mihara F, Okada S, Shibata S, Nakamura M, Toyama Y, Okano H. Spinal cord injury: emerging beneficial role of reactive astrocytes' migration. Int J Biochem Cell Biol. 2008;40(9):1649-53.

Richardson PM, McGuinness UM, Aguayo AJ. Axons from CNS neurons regenerate into PNS grafts. Nature. 1980 Mar 20;284(5753):264-5.

Ridet JL, Pencalet P, Belcram M, Giraudeau B, Chastang C, Philippon J, Mallet J, Privat A, Schwartz L. Effects of spinal cord X-irradiation on the recovery of paraplegic rats. Exp Neurol. 2000 Jan;161(1):1-14.

Rimaniol AC, Haïk S, Martin M, Le Grand R, Boussin FD, Dereuddre-Bosquet N, Gras G, Dormont D. Na+-dependent high-affinity glutamate transport in macrophages. J Immunol. 2000 May 15;164(10):5430-8.

Rolls A, Shechter R, Schwartz M. The bright side of the glial scar in CNS repair. Nat Rev Neurosci. 2009 Mar;10(3):235-41.

Schnell L, Fearn S, Klassen H, Schwab ME, Perry VH. Acute inflammatory responses to mechanical lesions in the CNS: differences between brain and spinal cord. Eur J Neurosci. 1999a Oct;11(10):3648-58.

Schnell L, Fearn S, Schwab ME, Perry VH, Anthony DC. Cytokine-induced acute inflammation in the brain and spinal cord. J Neuropathol Exp Neurol. 1999b Mar;58(3):245-54.

Schwartz M. Harnessing the immune system for neuroprotection: therapeutic vaccines for acute and chronic neurodegenerative disorders. Cell Mol Neurobiol. 2001 Dec;21(6):617-27.

Schwartz M, Kipnis J. Protective autoimmunity: regulation and prospects for vaccination after brain and spinal cord injuries. Trends Mol Med. 2001 Jun;7(6):252-8.

Schwartz M, Kipnis J. Multiple sclerosis as a by-product of the failure to sustain protective autoimmunity: a paradigm shift. Neuroscientist. 2002 Oct;8(5):405-13.

Shamash S, Reichert F, Rotshenker S. The cytokine network of Wallerian degeneration: tumor necrosis factor-alpha, interleukin-1alpha, and interleukin-1beta. J Neurosci. 2002 Apr 15;22(8):3052-60.

Sharma HS, Olsson Y, Cervós-Navarro J. Early perifocal cell changes and edema in traumatic injury of the spinal cord are reduced by indomethacin, an inhibitor of prostaglandin synthesis. Experimental study in the rat. Acta Neuropathol. 1993;85(2):145-53.

Sharma KV, Bigbee JW. Acetylcholinesterase antibody treatment results in neurite detachment and reduced outgrowth from cultured neurons: further evidence for a cell adhesive role for neuronal acetylcholinesterase. J Neurosci Res. 1998 Aug 15;53(4):454-64.

Sheng W, Wang G, Wang Y, Liang J, Wen J, Zheng PS, Wu Y, Lee V, Slingerland J, Dumont D, Yang BB. The roles of versican V1 and V2 isoforms in cell proliferation and apoptosis. Mol Biol Cell. 2005 Mar;16(3):1330-40.

Snow DM, Smith JD, Cunningham AT, McFarlin J, Goshorn EC. Neurite elongation on chondroitin sulfate proteoglycans is characterized by axonal fasciculation. Exp Neurol. 2003 Aug;182(2):310-21.

Stiefel MF, Tomita Y, Marmarou A. Secondary ischemia impairing the restoration of ion homeostasis following traumatic brain injury. J Neurosurg. 2005 Oct;103(4):707-14.

Stitzel JD, Pawlowski KJ, Wnek GE, Simpson DG, Bowlin GL. Arterial smooth muscle cell proliferation on a novel biomimicking, biodegradable vascular graft scaffold. J Biomater Appl. 2001 Jul;16(1):22-33.

Sun T, Mai S, Norton D, Haycock JW, Ryan AJ, MacNeil S. Self-organization of skin cells in three-dimensional electrospun polystyrene scaffolds. Tissue Eng. 2005 Jul-Aug;11(7-8):1023-33.

Tang J, Rutishauser U, Landmesser L. Polysialic acid regulates growth cone behavior during sorting of motor axons in the plexus region. Neuron. 1994 Aug;13(2):405-14.

Tang X, Davies JE, Davies SJ. Changes in distribution, cell associations, and protein expression levels of NG2, neurocan, phosphacan, brevican, versican V2, and tenascin-C during acute to chronic maturation of spinal cord scar tissue. J Neurosci Res. 2003 Feb 1;71(3):427-44.

Taylor, G. Disintegration of Water Drops in an Electric Field. Proceedings of the Royal Society of London A: Mathematical, Physical & Engineering Sciences. 1964;280, 383-397.

Telemeco TA, Ayres C, Bowlin GL, Wnek GE, Boland ED, Cohen N, Baumgarten CM, Mathews J, Simpson DG. Regulation of cellular infiltration into tissue engineering scaffolds composed of submicron diameter fibrils produced by electrospinning. Acta Biomater. 2005 Jul;1(4):377-85.

Teng HK, Teng KK, Lee R, Wright S, Tevar S, Almeida RD, Kermani P, Torkin R, Chen ZY, Lee FS, Kraemer RT, Nykjaer A, Hempstead BL. ProBDNF induces neuronal apoptosis via activation of a receptor complex of p75NTR and sortilin. J Neurosci. 2005 Jun 1;25(22):5455-63.

Tester NJ, Howland DR. Chondroitinase ABC improves basic and skilled locomotion in spinal cord injured cats. Exp Neurol. 2008 Feb;209(2):483-96.

Thoenen H, Barde YA. Physiology of nerve growth factor. Physiol Rev. 1980 Oct;60(4):1284-335.

Tian DS, Yu ZY, Xie MJ, Bu BT, Witte OW, Wang W. Suppression of astroglial scar formation and enhanced axonal regeneration associated with functional recovery in a spinal cord injury rat model by the cell cycle inhibitor olomoucine. J Neurosci Res. 2006 Oct;84(5):1053-63.

Trivedi A, Olivas AD, Noble-Haeusslein LJ. Inflammation and spinal cord injury: infiltrating leukocytes as determinants of injury and repair processes. Clin Neurosci Res. 2006 Dec;6(5):283-292.

Tsai EC, Dalton PD, Shoichet MS, Tator CH. Synthetic hydrogel guidance channels facilitate regeneration of adult rat brainstem motor axons after complete spinal cord transection. J Neurotrauma. 2004 Jun;21(6):789-804.

Tuszynski MH, Peterson DA, Ray J, Baird A, Nakahara Y, Gage FH. Fibroblasts genetically modified to produce nerve growth factor induce robust neuritic ingrowth after grafting to the spinal cord. Exp Neurol. 1994 Mar;126(1):1-14.

Tveten L. Spinal cord vascularity. IV. The spinal cord arteries in the rat. Acta Radiol Diagn (Stockh). 1976a Jul;17(4):385-98.

Tveten L. Spinal cord vascularity. V. The venous drainage of the spinal cord in the rat. Acta Radiol Diagn (Stockh). 1976b Sep;17(5B):653.

von Meyenburg J, Brösamle C, Metz GA, Schwab ME. Regeneration and sprouting of chronically injured corticospinal tract fibers in adult rats promoted by NT-3 and the mAb IN-1, which neutralizes myelin-associated neurite growth inhibitors. Exp Neurol. 1998 Dec;154(2):583-94.

von Wild KR, Brunelli GA. Restoration of locomotion in paraplegics with aid of autologous bypass grafts for direct neurotisation of muscles by upper motor neurons--the future: surgery of the spinal cord? Acta Neurochir Suppl. 2003;87:107-12.

Wang KC, Kim JA, Sivasankaran R, Segal R, He Z. P75 interacts with the Nogo receptor as a co-receptor for Nogo, MAG and OMgp. Nature. 2002 Nov 7;420(6911):74-8.

Watterson KR, Berg KM, Kapitonov D, Payne SG, Miner AS, Bittman R, Milstien S, Ratz PH, Spiegel S. Sphingosine-1-phosphate and the immunosuppressant, FTY720-phosphate, regulate detrusor muscle tone. FASEB J. 2007 Sep;21(11):2818-28.

Wen X, Tresco PA.Biomaterials. Fabrication and characterization of permeable degradable poly(DL-lactide-co-glycolide) (PLGA) hollow fiber phase inversion membranes for use as nerve tract guidance channels. 2006 Jul;27(20):3800-9.

White RE, Jakeman LB. Don't fence me in: harnessing the beneficial roles of astrocytes for spinal cord repair. Restor Neurol Neurosci. 2008;26(2-3):197-214.

Woerly S, Doan VD, Sosa N, de Vellis J, Espinosa-Jeffrey A. Prevention of gliotic scar formation by NeuroGel allows partial endogenous repair of transected cat spinal cord. J Neurosci Res. 2004 Jan 15;75(2):262-72.

Wong ST, Henley JR, Kanning KC, Huang KH, Bothwell M, Poo MM. A p75(NTR) and Nogo receptor complex mediates repulsive signaling by myelin-associated glycoprotein. Nat Neurosci. 2002 Dec;5(12):1302-8.

Wood PM. Separation of functional Schwann cells and neurons from normal peripheral nerve tissue. Brain Res. 1976 Oct 22;115(3):361-75.

Wozniewicz B, Filipowicz K, Swiderska SK, Deraka K. Pathophysiological mechanism of traumatic cavitation of the spinal cord. Paraplegia. 1983 Oct;21(5):312-7.

Wrathall JR, Emch GS. Effect of injury severity on lower urinary tract function after experimental spinal cord injury. Prog Brain Res. 2006;152:117-34.

Xie F, Zheng B. White matter inhibitors in CNS axon regeneration failure. Exp Neurol. 2008 Feb;209(2):302-12.

Xu XM, Guénard V, Kleitman N, Bunge MB. Axonal regeneration into Schwann cell-seeded guidance channels grafted into transected adult rat spinal cord. J Comp Neurol. 1995 Jan 2;351(1):145-60.

Yang F, Murugan R, Wang S, Ramakrishna S. Electrospinning of nano/micro scale poly(L-lactic acid) aligned fibers and their potential in neural tissue engineering. Biomaterials. 2005 May;26(15):2603-10.

Yang LJ, Schnaar RL. Axon regeneration inhibitors. Neurol Res. 2008 Dec;30(10):1047-52.

Yin Y, Henzl MT, Lorber B, Nakazawa T, Thomas TT, Jiang F, Langer R, Benowitz LI. Oncomodulin is a macrophage-derived signal for axon regeneration in retinal ganglion cells. Nat Neurosci. 2006 Jun;9(6):843-52.

Yoles E, Hauben E, Palgi O, Agranov E, Gothilf A, Cohen A, Kuchroo V, Cohen IR, Weiner H, Schwartz M. Protective autoimmunity is a physiological response to CNS trauma. J Neurosci. 2001 Jun 1;21(11):3740-8. Erratum in: J Neurosci 2001 Aug 1;21(15):1a.

Zeman RJ, Feng Y, Peng H, Visintainer PF, Moorthy CR, Couldwell WT, Etlinger JD. X-irradiation of the contusion site improves locomotor and histological outcomes in spinal cord-injured rats. Exp Neurol. 2001 Nov;172(1):228-34.

Zhang SX, Geddes JW, Owens JL, Holmberg EG. X-irradiation reduces lesion scarring at the contusion site of adult rat spinal cord. Histol Histopathol. 2005 Apr;20(2):519-30.

Zhou L, Baumgartner BJ, Hill-Felberg SJ, McGowen LR, Shine HD. Neurotrophin-3 expressed in situ induces axonal plasticity in the adult injured spinal cord. J Neurosci. 2003 Feb 15;23(4):1424-31.